CFENSS-SRS method for the uncertainty analysis of nuclear fuel and neutronics

Aapo Taavitsainen

School of Science

Thesis submitted for examination for the degree of Master of Science in Technology.

Espoo, 3rd of May 2016

Thesis supervisor:

Prof. Filip Tuomisto

Thesis advisor:

M.Sc. (Tech.) Risto Vanhanen

Aalto University
School of Science

AALTO UNIVERSITY
SCHOOL OF SCIENCE

ABSTRACT OF THE
MASTER'S THESIS

Author: Aapo Taavitsainen

Title: CFENSS-SRS method for the uncertainty analysis of nuclear fuel and neutronics

Date: 3rd of May 2016 Language: English Number of pages: 8+77

Department of Applied Physics

Professorship: F3005 – Engineering Physics

Supervisor: Prof. Filip Tuomisto

Advisor: M.Sc. (Tech.) Risto Vanhanen

Statistical uncertainty analysis has received much attention in the past decade. The impacts of both nuclear fuel and nuclear data uncertainties have been studied separately but not as a coupled system. The main research question of this Thesis was to confirm whether the uncertainties of fuel behaviour parameters and the nuclear data can be propagated separately. The secondary goals included comparing various statistical perturbation methods. The computations were performed close to the framework of the OECD/NEA UAM-LWR TMI-1 Pressurized Water Reactor benchmark, and more specifically, its pin cell exercise.

A novel CFENSS-SRS (**C**oupled **F**uel B**e**haviour and **N**eutronics **S**tochastic **S**ampling with **S**imple **R**andom **S**ampling) method is presented for the combined uncertainty analysis of nuclear fuel behaviour and neutronics. The method applies the statistical uncertainty analysis to univariate nuclear fuel parameters and correlated neutron cross sections. Truncated normal distribution is used as the objective distribution for drawing samples based on the Principle of Maximum Entropy. Due to practical difficulties in employing the distribution, the distribution parameters are approximated for the nuclear fuel parameters while a normal distribution is applied for the neutron cross sections. Negative values of inherently positive parameters are re-sampled to avoid distorting the distribution to a great extent.

The results support the hypothesis that the nuclear fuel parameters and the nuclear data can truly be treated as independent sources of uncertainty. Additionally, it was revealed that the details of the perturbation methodology, such as using relative covariance matrices rather than absolute ones, have a much smaller impact on the output uncertainty than neglecting some of the uncertainty data.

Keywords: Statistical, uncertainty and sensitivity analysis, nuclear fuel, neutronics, perturbation, uncertainty propagation

AALTO-YLIOPISTO
PERUSTIETEIDEN KORKEAKOULU

DIPLOMITYÖN
TIIVISTELMÄ

Tekijä: Aapo Taavitsainen

Työn nimi: CFENSS-SRS -menetelmä ydinpolttoaineen ja neutroniikan epävarmuusanalyysiin

Päivämäärä: 3. toukokuuta 2016 Kieli: Englanti Sivumäärä: 8+77

Teknillisen fysiikan laitos

Professuuri: F3005 – Teknillinen fysiikka

Työn valvoja: Prof. Filip Tuomisto

Työn ohjaaja: DI Risto Vanhanen

Tilastollisen epävarmuus- ja herkkyysanalyysin käyttö on lisääntynyt ydinenergia-alan tutkimuksessa kuluneen vuosikymmenen aikana. Ydinpolttoaineen ja ydinvakiotiedon epävarmuuksien vaikutuksia on tutkittu erikseen, mutta niitä ei ole käsitelty yhtenä kokonaisuutena. Tämän lopputyön tavoitteena oli selvittää, pystytäänkö näitä kahta tärkeää epävarmuuden lähdettä tarkastelemaan erikseen määritettäessä lopputuloksen kokonaisepävarmuutta. Tutkimuksen kuluessa tavoitteena oli myös vertailla erilaisia tilastollisia menetelmiä epävarmuuden liittämiseksi laskuihin.

Lopputyössä kehitettiin uusi CFENSS-SRS -menetelmä (engl. **C**oupled **F**uel B**e**haviour and **N**eutronics **S**tochastic **S**ampling with **S**imple **R**andom **S**ampling) yhdistettyyn epävarmuusanalyysiin. Työssä tutkittiin ydinvakiotiedon osalta vain mikroskooppisten vaikutusalojen epävarmuuksien vaikutusta. Maksimientropiaperiaatetta noudattaen tavoitteena oli käyttää katkaisua normaalijakaumaa epävarmojen muuttujien satunnaisarvonnassa. Käytännössä jakaumaa ei kuitenkaan ollut mahdollista soveltaa, sillä tällä hetkellä ei tunneta menetelmää sen parametrien laskemiseksi yleisessä tapauksessa. Ydinpolttoaineen kohdalla jakauman parametreja approksimoitiin normaalijakauman vastaavilla parametreilla, mutta vaikutusalojen osalta turvauduttiin kokonaan normaalijakaumaan. Positiiviseksi tunnettujen muuttujien satunnaisarvontaa toistettiin, kunnes normaalijakaumasta seuraavia negatiivisia arvoja ei ollut.

Tulokset tukevat oletusta, että epävarmuuslähteet voidaan käsitellä toisistaan riippumattomina. Menetelmää kehitettäessä puolestaan huomattiin, että kaikkien epävarmuuksien huomiointi on tärkeämpää kuin satunnaisarvonnan yksityiskohtien parantaminen. Tulokset vastasivat kirjallisuudesta löytyviä tuloksia niiltä osin kuin vastaavaa tutkimusta on tehty.

Avainsanat: Tilastollinen, epävarmuus- ja herkkyysanalyysi, ydinpolttoaine, neutroniikka, satunnaisarvonta

Preface

This Thesis is submitted in partial fulfilment for the requirements of the degree of Master of Science in Technology. The research was carried out between June 2015 and April 2016. The research was financed as a part of USVA project, a joint effort of Aalto University and VTT Technical Research Centre of Finland, and was conducted at the Department of Applied Physics of Aalto University School of Science.

I present a new method for the combined uncertainty analysis of nuclear fuel behaviour and neutronics. This is my original work and I am not aware of any similar methodology. The Thesis is aimed for an audience with a university level education in physics but not necessarily in nuclear engineering. The audience includes both graduates and undergraduates about to complete their degree. Differences to previously published methods have been described in detail to convince the more experienced researchers of the validity of the approach.

I have received plenty of support from the researchers of both VTT and Aalto University. I was a novice in nuclear engineering a year ago and I am grateful to my instructor Risto Vanhanen for his patience in tutoring me. I could not have hoped for a better guidance on my journey to the field of nuclear engineering. Your academic research on nuclear data covariances made this Thesis possible. I also want to thank Timo Ikonen for his instructions concerning the nuclear fuel uncertainties. I truly enjoyed using the FINIX code. Maria Pusa has helped me with the uncertainty analysis in general and in the Serpent Monte Carlo calculations I relied on Aarno Isotalo. My supervisor Filip Tuomisto I wish to credit for efficient bureaucracy and relaxed attitude. I was warmly welcomed to the research group. I thank you all for the encouragement, and a special thanks to everyone helping with the proof-reading of this Thesis.

Finally, I would like to express my gratitude to those dear to me. Hopefully, I will have now more time to enjoy your wonderful company. It is time to see the stars once again.

Otaniemi, 3rd of May 2016 Aapo Taavitsainen

Contents

Symbols, operators and abbreviations

Symbols

α	Population coverage (tolerance interval)
β	Confidence level (tolerance interval)
μ	Location parameter (of a continuous probability distribution)
ν	Total average number of emitted neutrons per fission
ρ_{ij}	Pearson's correlation coefficient
σ	Scale parameter (of a continuous probability distribution)
σ_{x}	Microscopic cross section of a reaction x
Σ_{x}	Macroscopic cross section of a reaction x
χ	Fission spectrum
χ^2	χ^2-distribution
$\mathcal{L}$	Lagrangian
$\mathbf{C}$	Correlation matrix
$E[X^k]$	kth algebraic population moment
f_X	Probability density function of a variable X
F_X	Cumulative distribution function of a variable X
H	Entropy
k_{eff}	Effective multiplication factor
$\ln N$	Log-normal distribution
m	Population mean (expectation value)
m^*	Unbiased estimator of an expectation value
$\bar{m}$	Arithmetic mean of a sample
N	Normal distribution
P	Probability
$\mathbf{Q}$	Eigenvector matrix
T_{c}	Cladding temperature
T_{f}	Nuclear fuel temperature
T_{g}	Gas gap temperature
T_{m}	Moderator/coolant temperature
TN	Truncated normal distribution
U	Uniform distribution
X	Continuous random variable
v	Standard deviation (population)
$\bar{v}$	Sample standard deviation
v^2	Variance (population)
v^{2*}	Unbiased estimator of a variance
$\mathbf{V}$	Covariance matrix
Z	Standardized random variable

Operators

$\mathbf{Q}^{\mathrm{T}}$	Matrix transpose of a matrix $\mathbf{Q}$
$\frac{\partial}{\partial r}$	Partial derivative with respect to variable r
$\prod_i$	Product over index i
$\int_a^b$	Riemann integral from a to b
$\sum_i$	Sum over index i

Abbreviations

BE	Best estimate
CDF	Cumulative distribution function
CFENSS	**C**oupled **F**uel B**e**haviour and **N**eutronics **S**tochastic **S**ampling
CLT	Central Limit Theorem
ECDF	Empirical cumulative distribution function
ECTS	Evolved Covariance Tool Set
ENDF	Evaluated Nuclear Data Format
ENDF/B	United States Evaluated Nuclear Data File
FINIX	**F**uel behaviour model and **in**terface for multiphys**ix**s applications
GENDF	Groupwise Evaluated Nuclear Data File
GRS	Gesellschaft für Anlagen- und Reaktorsicherheit
HFP	Hot full power (reactor conditions)
HZP	Hot zero power (reactor conditions)
IAEA	International Atomic Energy Agency
JEFF	Joint Evaluated Fission and Fusion file
JENDL	Japanese Evaluated Nuclear Data Library
KDE	Kernel density estimate
LHS	Latin Hypercube Sampling
LWR	Light Water Reactor
MC	Monte Carlo
MEPD	Maximum Entropy Probability Distribution
NDL	Nuclear Data Library
NEA	Nuclear Energy Agency
OECD	Organisation for Economic Co-operation and Development
PDF	Probability density function
PENDF	Pointwise Evaluated Nuclear Data File
PWR	Pressurized Water Reactor
SRS	Simple Random Sampling
S/U	Sensitivity/Uncertainty
TMI-1	Three Mile Island 1
UAM	Uncertainty Analysis in Modelling

1 Uncertainties in nuclear engineering

Safety of nuclear power is essential for the safe and economical design, construction, operation and decommissioning of nuclear power plants, not to mention gaining the public acceptance. The status of the nuclear power as a low carbon power source has been recognized and, with a considerable share of the current power generation, it can have a significant part in tackling the climate change. For the past decade the uncertainty and sensitivity analysis aiming for improved nuclear safety has received considerable attention in the field of nuclear engineering.

This Thesis presents a new stochastic uncertainty analysis methodology CFENSS-SRS (**C**oupled **F**uel B**e**haviour and **N**eutronics **S**tochastic **S**ampling with **S**imple **R**andom **S**ampling) for quantifying the combined uncertainty of fuel behaviour parameters and nuclear data. Both areas have been studied before independently but not as a coupled system. The main research question is whether the two uncertainty components can be handled separately as independent sources of uncertainty. The secondary tasks relate to comparing different methods and approaches to advance the stochastic uncertainty analysis in nuclear engineering.

The accuracy of both the nuclear data and fuel the behaviour parameters is continuously being improved but due to the nature of measurements the uncertainties cannot be completely eliminated. Best estimate (BE) codes are used to calculate the best estimates of different interesting output responses. The codes attempt to produce non-biased results following the best available knowledge and models. Technical limitations restrict the acceptable range, usually the upper limit, of the different parameters of a nuclear reactor, and safety limits have been imposed to avoid exceeding these technical constraints. Ensuring that a system operates within the safety limits cannot be based only on a single run of a BE code because, even if the modelling error is small, the results of the computer model are affected by the lack of knowledge of the input data. Applying realistic best estimate values in calculations yields the best estimates of the output parameters but the results may, and most likely will, differ from the reality due to the input data uncertainty.

International Atomic Energy Agency (IAEA) categorizes the uncertainties into five general classes: [1]

1. Code or model uncertainties due to approximations and uncertainties, for instance, in material properties or behaviour
2. Representation (discretization) uncertainty related to nodalization
3. Scaling uncertainty caused by scaling the results of experiments suitable for full scale systems
4. Plant uncertainty associated with the boundary and initial conditions, e.g. core power
5. User effect including user errors and different ways of applying the codes

These five classes, in turn, fall into two more general categories: aleatory and epistemic uncertainty. The former is irreducible stochastic uncertainty and an inherent property of the system while the latter is reducible subjective uncertainty arising from the lack

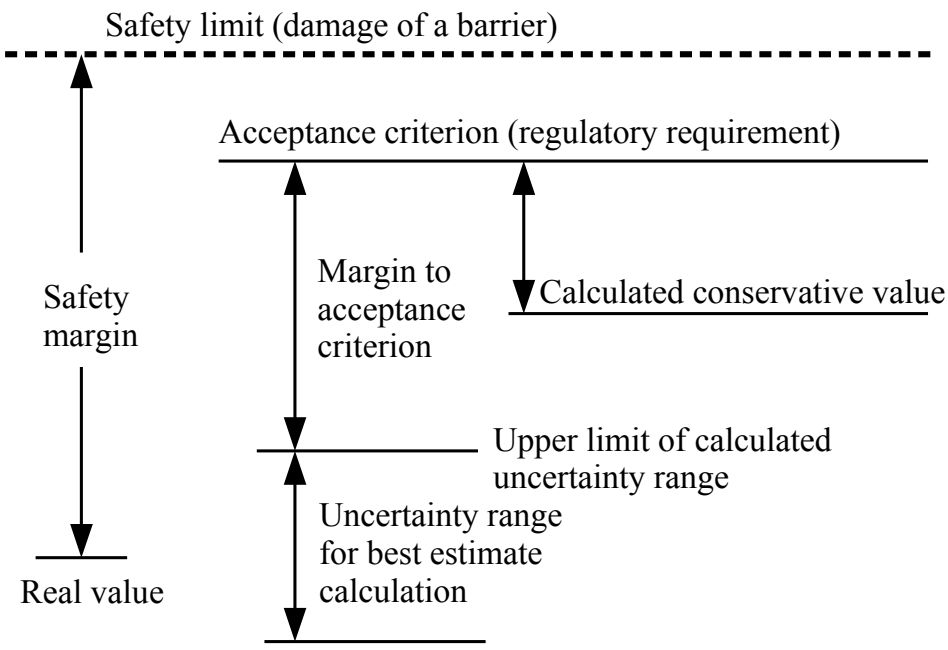

Figure 1: Illustration of a safety margin as defined by IAEA [1]

of knowledge such as insufficient sample size. [2] Uncertainty and sensitivity analysis aims first to map the epistemic uncertainty of the output (uncertainty analysis) and then to identify the major sources of the uncertainty (sensitivity analysis).

Currently the IAEA recognizes both a conservative and a best estimate approach when employing the best estimate codes. Both methods and the concept of a safety margin are illustrated in Fig. 1. In the former approach, conservative input data are used in the BE codes and the uncertainties of the results are evaluated. However, in complex systems the reliability of the conservative approach can be questioned as the correct "conservative" input values are possibly hard to determine. In the latter approach, statistical uncertainty analysis is applied to realistic best estimate input data to calculate an uncertainty range for the studied responses and determine with a convincing probability that the acceptance criterion is not exceeded. The statistical approach leads to more accurate safety margins with the price of a much higher computational cost. Moreover, it also removes the problem of defining the conservative input. Both methods should be accompanied with sensitivity studies. Neither of the methods leads to resolving the (always) unknown real value but they can nevertheless be used as a high-confidence assurance of safety. [1]

The developed CFENSS-SRS tool is based on a stochastic approach as opposed to conventional deterministic sensitivity/uncertainty (S/U) methods. The tool combines perturbing correlated nuclear data to a random sampling of univariate mutually independent fuel behaviour parameters. The decision on a suitable sampling distribution is based on the Principle of Maximum Entropy providing an objective distribution instead of a subjective choice. Fuel behaviour code FINIX (**F**uel behaviour model and **in**terface for multiphys**ix**s applications) [3] was used as the fuel behaviour code while a deterministic lattice code DRAGON [4] was employed for the neutronics calculations. The nuclear data and its

covariances were processed with a Nuclear Data Processing System NJOY [5] combined to an in-house ECTS (Evolved Covariance Tool Set) code.

OECD/NEA Uncertainty Analysis in Modelling (UAM) benchmark was launched in 2005 for developing uncertainty analysis methods for nuclear engineering simulations. The benchmark consists of steps or exercises ranging from steady-state pin cell neutronics to core transient multi-physics. As a demonstration the CFENSS-SRS tool was applied successfully to a Pressurized Water Reactor (PWR) pin cell exercise. The pin cell includes a fuel rod with enriched uranium oxide fuel, helium-filled gas gap, Zircaloy-4 cladding submerged in light water acting as a coolant and neutron moderator. On the nuclear data, only neutron cross sections were included to the uncertainty quantification, and for example average total fission neutron production and fission spectrum were left out. Ultimately, uncertainties were obtained for a collection of responses, and the respective shares of the fuel behaviour and the neutronics were studied.

The adopted approach is based on a so-called GRS method proposed by Gesellschaft für Anlagen- und Reaktorsicherheit [6]. In this method the responses are computed several times with perturbed input data yielding in practice a sample from a repeated indirect measurement. The input data are perturbed with some sampling method according to assigned probability distributions, and the responses are analysed statistically to extract the arising uncertainty ranges and sensitivities attributed to the total uncertainty of the input data. The subtasks of creating the CFENSS-SRS perturbation system included, *inter alia*, selecting the sampling distributions, obtaining relevant uncertainty and best estimate data, as well as both generating and analysing a sufficient number of samples.

We start Sec. 2 by covering the basic concepts of continuous probability distributions and the probabilistic approach in general followed by introductory reactor physics and the specialities of the nuclear fuel behaviour parameters. In reactor physics the focus is naturally on the neutron cross sections as they were the only parameters perturbed in the nuclear data. The details of the implemented CFENSS-SRS uncertainty quantification system are addressed in Sec. 3 along with the detailed settings of external codes used in the different subtasks. Sec. 4 covers the obtained response uncertainties and a rough sensitivity analysis along with results gathered for establishing the reliability of the code system. Discussion on the results is reserved for Sec. 5 while the conclusions and suggestions for future work are presented in Sec. 6.

2 Quantifying nuclear data and nuclear fuel behaviour uncertainties

The response uncertainty arising from the nuclear data and the nuclear fuel parameters can be obtained with either a stochastic (statistical) or a deterministic approach. For the deterministic methodology is suffices to say that the variances and the covariances of the system responses are computed with sensitivity coefficients related to the input parameters. The coefficients describe a local change in the responses caused by a change in the input. The statistical approach, on the other hand, draws samples of the input space from probability distributions assigned to the input parameters. The two methods have been summarized and compared, for example, in Ref. [7]. In this Thesis we shall discuss only the stochastic approach, and for this purpose we must begin with some basic notions of sampling continuous random variables and analysing the outcome. Only then we can understand the practical applications in nuclear engineering.

2.1 Introduction to continuous random variables

Physical parameters are often considered as random variables and the results of repeated measurements as random samples from the probability distributions of said variables. The random variables can be either discrete with a limited support of discrete values or continuous with a continuous support. The scope of this Thesis covers only the continuous random variables. First, a single random variable followed by a multidimensional set of random variables is considered.

Let X be a single continuous random variable with a probability density function (PDF) f_X. The probability density function describes the probability P of the random variable to take different values within an interval $[a, b]$ so that

$$\mathrm{P}[a \leq X \leq b] = \int_a^b f_X(x)dx, \tag{1}$$

and is subject to the normalization condition

$$\int f_X(x)dx = 1. \tag{2}$$

The integrated PDF describes the cumulative probability and is known as the cumulative distribution function or CDF in short:

$$\mathrm{P}[X \leq x] = F_X(x) = \int_{x_{\min}}^{x} f_X(x')dx', \tag{3}$$

with the properties $F(x_{\min}) = 0$ and $F(x_{\max}) = 1$. The kth algebraic *population* moment of the random variable is defined as

$$\mathrm{E}[X^k] = \int x^k f_X(x)dx, \tag{4}$$

with the expectation value or mean $\mathrm{E}[X] = m$ being the first moment. Variance

$$v^2 = \mathrm{Var}[X] = \mathrm{E}[(X - \mathrm{E}[X])^2] = \mathrm{E}[X^2] - (\mathrm{E}[X]^2) = \int (x-m)^2 f_X(x)dx, \quad (5)$$

is the second central moment from the general definition $\mathrm{E}[(X - \mathrm{E}[X])^k]$ with the standard deviation v being simply the square root of the variance. [8–10]

Consider next the multivariate case and a collection of distinct random variables $\mathbf{X} = (X_1, X_2, ..., X_n)$ with values $\mathbf{x} = (x_1, x_2, ..., x_n)$ and a joint density function $f(\mathbf{X})$. The mean and the variance of each random variable are given by

$$m_i = \mathrm{E}[X_i] = \int x_i f_{\mathbf{X}}(\mathbf{x})d\mathbf{x}, \quad (6)$$

$$v_i^2 = \mathrm{E}[(X_i - m_i)^2]. \quad (7)$$

The random variables are mutually independent if the joint density function can be written in a factorial form

$$f_{\mathbf{X}}(\mathbf{x}) = f_{(X_1,X_2,...,X_n)}(x_1, x_2, .., x_n) = f_{X_1}(x_1) f_{X_2}(x_2)...f_{X_n}(x_n). \quad (8)$$

Additional important concepts are the covariance

$$\mathrm{cov}(X_i, X_j) = \mathrm{E}[(X_i - m_i)(X_j - m_j)] = \mathrm{E}(X_i X_j) - \mathrm{E}(X_i)\mathrm{E}(X_j), \quad (9)$$

and Pearson's correlation coefficient

$$\mathrm{corr}(X_i, X_j) = \rho_{ij} = \frac{\mathrm{cov}(X_i, X_j)}{v_i v_j}, \ \rho_{ij} \in [-1, 1], \quad (10)$$

describing the connection between two random variables. The covariance depends on the scale (of the standard deviations) of the random variables but a normalization yields a scale-free measure, the correlation coefficient, for the connection's strength. The correlation coefficient represents the linear coupling between the variables. Two random variables with a zero correlation coefficient, such as the mutually independent variables, are said to be uncorrelated. [8–10]

The covariance and the correlation coefficient are limited to two-dimensional joint distributions but an $n \times n$ covariance matrix $\mathbf{V}$ and a correlation matrix $\mathbf{C}$ can be constructed for the collection of n random variables:

$$\mathbf{V} = \mathrm{cov}(\mathbf{X}) \begin{bmatrix} \mathrm{cov}(X_1, X_1) & \mathrm{cov}(X_1, X_2) & \dots & \mathrm{cov}(X_1, X_n) \\ \mathrm{cov}(X_2, X_1) & \mathrm{cov}(X_2, X_2) & \dots & \mathrm{cov}(X_2, X_n) \\ \dots & \dots & \dots & \dots \\ \mathrm{cov}(X_n, X_1) & \mathrm{cov}(X_n, X_2) & \dots & \mathrm{cov}(X_n, X_n) \end{bmatrix}, \quad (11)$$

$$\mathbf{C} = (\mathrm{diag}(\mathbf{V})^{-\frac{1}{2}})\mathbf{V}(\mathrm{diag}(\mathbf{V})^{-\frac{1}{2}}) = \begin{bmatrix} \rho_{11} & \rho_{12} & \dots & \rho_{1n} \\ \rho_{21} & \rho_{22} & \dots & \rho_{2n} \\ \dots & \dots & \dots & \dots \\ \rho_{n1} & \rho_{2n} & \dots & \rho_{nn} \end{bmatrix}. \quad (12)$$

In this Thesis diag($\mathbf{V}$) is a diagonal matrix with the main diagonal of the matrix $\mathbf{V}$ while the boldface symbols are reserved for vectors and matrices. The relative covariance matrix is related to the absolute covariance matrix $\mathbf{V}$ by

$$\mathrm{rcov}(\mathbf{X}) = (\mathrm{diag}(\mathbf{X}))^{-1}\mathbf{V}(\mathrm{diag}(\mathbf{X}))^{-1}. \tag{13}$$

Some important remarks must be made of the contents and properties of the two matrices. The main diagonal of the covariance matrix contains the variances of the random variables and thus the diagonal elements of the correlation matrix are all unity. Most importantly, both matrices are symmetric and positive-semidefinite. [8–10]

In practical applications the uncertainty data do not, in fact, always correspond to a valid covariance matrix. In some cases it may be that the data do not meet the condition of the positive-semidefinity or do not obey possible summation rules in case of redundant covariance data. Luckily, the data can be "corrected" by finding the nearest symmetric positive-semidefinite covariance matrix in the sense of the weighted Frobenius norm [11]. Furthermore, the Frobenius norm can be used also in computing the nearest matrix consistent with the possible summation rules [12].

2.1.1 Useful continuous probability distributions

Until now we have discussed only about a general continuous probability distribution. The population moments, however, are in statistical uncertainty analysis all but useless without a specific distribution to link them to. The statistical approach requires the ability to draw samples from the input distributions and this cannot be achieved without specifying the said distributions. There are several well-known and widely applied continuous probability distributions but here we shall restrict ourselves to the ones absolutely essential in understanding this study. Again, the univariate distributions are discussed first after which the corresponding multivariate distributions are presented, if necessary. The expectation values and the variances are denoted with m and v^2 as before while μ and σ are reserved for location and scale parameters, respectively. In the literature the distinction is not made often enough, as it is not always needed, but the practice can easily lead to a confusion.

We shall start with the continuous uniform distribution $U(a,b)$ and its PDF

$$f_{U(a,b)} = \begin{cases} \dfrac{1}{b-a}, & a \le x \le b \\ 0, & \text{elsewhere} \end{cases} \tag{14}$$

where a and b limit the support $x \in [a,b]$. For us this distribution is not especially interesting but it can be used as the first step in generating normally distributed random samples. For a random variable X the PDF of a normal distribution N with the location and scale parameters μ and σ^2 is defined as

$$f_{N(\mu,\sigma^2)}(x) = \frac{1}{\sigma\sqrt{2\pi}} \exp\left[-\frac{(x-\mu)^2}{2\sigma^2}\right], \quad -\infty < x < \infty, \tag{15a}$$

$$\mathrm{E}[X] = m = \mu, \quad -\infty < m < \infty, \tag{15b}$$

$$\mathrm{Var}[X] = v^2 = \sigma^2, \quad \sigma > 0, \tag{15c}$$

i.e., the location and the scale parameter equal the expectation value and the variance of the distribution. The general distribution $X \sim N(\mu, \sigma^2)$ can be standardized into a simpler, and therefore a tabulatable, case of $Z \sim N(0,1)$ with a formula

$$Z = \frac{X - \mu}{\sigma}, \tag{16}$$

where the standardized random variable Z follows the standard normal distribution

$$f_{N(0,1)}(z) = \frac{1}{\sqrt{2\pi}} \exp\left(-\frac{1}{2}z^2\right), \quad -\infty < z < \infty. \tag{17}$$

The joint PDF for a multivariate normal distribution of a random variable vector $\mathbf{X} = (X_1, X_2, ..., X_n)$ follows as

$$f_{N(\boldsymbol{\mu},\boldsymbol{\Sigma})}(\mathbf{x}) = \frac{1}{\sqrt{(2\pi)^n \det(\boldsymbol{\Sigma})}} \exp\left[-\frac{1}{2}(\mathbf{x} - \boldsymbol{\mu})^T \boldsymbol{\Sigma}^{-1} (\mathbf{x} - \boldsymbol{\mu})\right], \tag{18}$$

where $\mathrm{E}[\mathbf{X}] = \mathbf{m} = \boldsymbol{\mu}$ is now an n-dimensional real vector and the scale parameter $\boldsymbol{\Sigma} = \mathbf{V}$ an $n \times n$ matrix. [10]

The normal distribution is widely used which is explained at least partially by the Central Limit Theorem (CTL). The theorem states that the arithmetic mean of independent random variables $(X_1, X_2, ..., X_n)$ approaches, and can be approximated with, the normal distribution when the random variables have a common expectation value and variance. The normal distribution emerges even if the parent distribution of the random variables is not the normal distribution. The law of large numbers, in turn, states that the sample mean converges to the population mean as the sample size n approaches infinity. [8, 10]

A normally distributed random variable can take any real value. Confining the support to some interval leads to the truncated normal distribution. The PDF can be derived by starting from the general normal distribution, limiting the values to a truncation interval $[a, b]$ (a doubly truncated case) and renormalizing the probability mass to unity. All this yields the $TN(\mu, \sigma^2)$:

$$f_{TN(\mu,\sigma^2)}(x) = \begin{cases} \dfrac{\frac{1}{\sigma} f_{N(0,1)}\left(\frac{x-\mu}{\sigma}\right)}{F_{N(0,1)}\left(\frac{b-\mu}{\sigma}\right) - F_{N(0,1)}\left(\frac{a-\mu}{\sigma}\right)}, & a \le x \le b, \\ 0, \text{ elsewhere}, \end{cases} \tag{19}$$

where $f_{N(0,1)}$ and $F_{N(0,1)}$ are the PDF and the CDF of the standard normal distribution $N(0,1)$. It is important to understand that, although the parameters μ and σ are still the parameters of the corresponding normal distribution, they are no longer the mean (expectation value) or the variance of the truncated distribution. Via a moment generating function it can be derived

$$m = \mu - \sigma \frac{f_{N(0,1)}(\beta) - f_{N(0,1)}(\alpha)}{F_{N(0,1)}(\beta) - F_{N(0,1)}(\alpha)}, \tag{20}$$

and

$$v^2 = \sigma^2 \left\{ 1 - \frac{\beta f_{N(0,1)}(\beta) - \alpha f_{N(0,1)}(\alpha)}{F_{N(0,1)}(\beta) - F_{N(0,1)}(\alpha)} - \left[\frac{f_{N(0,1)}(\beta) - f_{N(0,1)}(\alpha)}{F_{N(0,1)}(\beta) - F_{N(0,1)}(\alpha)} \right]^2 \right\}, \tag{21}$$

where

$$\alpha = \frac{a-\mu}{\sigma},\ \beta = \frac{b-\mu}{\sigma}. \tag{22}$$

Finally, the n-variate truncated normal distribution is defined as

$$f_{TN(\boldsymbol{\mu},\boldsymbol{\Sigma})}(\mathbf{x}) = \frac{(2\pi)^{-n/2}(\det\boldsymbol{\Sigma})^{-\frac{1}{2}} \exp\left[-\frac{1}{2}(\mathbf{x}-\boldsymbol{\mu})^T \boldsymbol{\Sigma}^{-1}(\mathbf{x}-\boldsymbol{\mu}) \right]}{(2\pi)^{-n/2}(\det\boldsymbol{\Sigma})^{-\frac{1}{2}} \int_{\mathbf{a}}^{\mathbf{b}} \exp\left[-\frac{1}{2}(\mathbf{x}-\boldsymbol{\mu})^T \boldsymbol{\Sigma}^{-1}(\mathbf{x}-\boldsymbol{\mu}) \right]} \tag{23}$$

$$= \frac{\exp\left[-\frac{1}{2}(\mathbf{x}-\boldsymbol{\mu})^T \boldsymbol{\Sigma}^{-1}(\mathbf{x}-\boldsymbol{\mu}) \right]}{\int_{\mathbf{a}}^{\mathbf{b}} \exp\left[-\frac{1}{2}(\mathbf{x}-\boldsymbol{\mu})^T \boldsymbol{\Sigma}^{-1}(\mathbf{x}-\boldsymbol{\mu}) \right] d\mathbf{x}}, \tag{24}$$

where $\int_{\mathbf{a}}^{\mathbf{b}}$ is an n-dimensional Riemann integral from $\mathbf{a}$ to $\mathbf{b}$. [13]

For a log-normal random variable $X \sim \ln N(\mu, \sigma^2)$ with a distribution

$$f_{\ln N(\mu,\sigma^2)}(x) = \frac{1}{x\sigma\sqrt{2\pi}} \exp\left[-\frac{(\ln(x)-\mu)^2}{2\sigma^2} \right],\ \ x > 0, \tag{25a}$$

$$\mathrm{E}[X] = m = e^{\mu+\sigma^2/2}, \tag{25b}$$

$$\mathrm{Var}[X] = v^2 = e^{2\mu+\sigma^2}(e^{\sigma^2} - 1), \tag{25c}$$

the natural logarithm is normally distributed, i.e., $Y = \ln(X) \sim N(\mu, \sigma^2)$. Hence, the convenient result of the parameters matching the expectation value and the variance does not apply either for the log-normal distribution. The parameters μ and σ are the mean and the standard deviation of the normally distributed $\ln(X)$ in the "log-space" but not of the log-normally distributed X in the "x-space". [8, 10] The multivariate log-normal distribution, in turn, is given by [14]

$$f_{\ln N(\boldsymbol{\mu},\boldsymbol{\Sigma})}(\mathbf{x}) = \frac{1}{\sqrt{(2\pi)^n \det(\boldsymbol{\Sigma})}} \prod_{i=1}^{n} \frac{1}{x_i} \exp\left[-\frac{1}{2}(\ln(\mathbf{x})-\boldsymbol{\mu})^T \boldsymbol{\Sigma}^{-1}(\ln(\mathbf{x})-\boldsymbol{\mu}) \right]. \tag{26}$$

The parameters are related element-wise to the mean and the covariance matrix via

$$\begin{cases} \boldsymbol{\mu} = \ln\left(\frac{\mathbf{m}^2}{\sqrt{\mathrm{diag}(\mathbf{V}) + \mathbf{m}^2}} \right), & (27) \\ \mathbf{m} = \exp\left(\boldsymbol{\mu} + \frac{1}{2}\mathrm{diag}(\boldsymbol{\Sigma}) \right), & (28) \\ & (29) \end{cases}$$

and

$$\begin{cases} \mathbf{\Sigma} = \ln\left[(\mathrm{diag}(\mathbf{m}))^{-1}\mathbf{V}(\mathrm{diag}(\mathbf{m}))^{-1} + \mathbf{1}\right], & (30) \\ \mathbf{V} = \mathrm{diag}(\mathbf{m})\ (\exp(\mathbf{\Sigma}) - \mathbf{1})\ \mathrm{diag}(\mathbf{m}), & (31) \end{cases}$$

with '**1**' as a matrix of ones, *cf.* Eq. (13) [15].

The last relevant continuous distribution is the χ^2-distribution. A sum of squares of independent $N(0,1)$ distributed random variables follows this distribution with ν degrees of freedom. The parameter ν is the number of the squares to be summed. The PDF of the distribution $\chi^2(\nu)$ is given by

$$f_{\chi^2}(x) = \frac{1}{\Gamma(\nu/2)2^{\nu/2}} x^{\nu/2-1} e^{-x/2},\ x > 0,\ \nu > 0, \tag{32a}$$

$$\mathrm{E}[X] = \nu, \tag{32b}$$

$$\mathrm{Var}[X] = 2\nu, \tag{32c}$$

where Γ is the gamma function. Among other practical applications, the distribution is useful in estimating the goodness of fitting a theoretical distribution to data (see Sec. 2.2.7). [8, 10]

2.2 Statistical uncertainty analysis

There are several uncertainty analysis methods, some of which have been compared in Refs. [1, 16]. The uncertainty analysis can be performed, for example, by propagating input uncertainties or extrapolating output uncertainties. A statistical approach for the propagation of input uncertainties known as the GRS method [6] from Gesellschaft für Anlagen- und Reaktorsicherheit was utilized in this Thesis. The method, and the statistical approach in general, is illustrated in Fig. 2. It can be summarised as a repeated measurement of certain responses or parameters yielding data points from some unknown distribution. The response distributions can be handled as separate univariate distributions or as a joint multivariate distribution.

The propagation of the input uncertainties starts from a large group of input parameters. A subset $\mathbf{X} = (X_1, X_2, ..., X_j)$ of j variables is selected to be perturbed with random sampling according to probability distributions assigned to the parameters, see Sec. 2.2.1 and Sec. 2.2.2. Regarding the probability distribution from which to draw the samples, an objective choice can be made with the Maximum Entropy Principle of Sec. 2.2.3. In the GRS method a uniform distribution is used to express a full uncertainty about the distribution.

Presume that the subset is varied n times leading to n sets of input values $\mathbf{x}_i = (x_{i,1}, x_{i,2}, ..., x_{i,j})$. Each input is used in a possibly highly complicated model or a computer code which we shall describe here simply with a function f. The calculations, in turn, lead to n output vectors $\mathbf{y}_i = f(\mathbf{x}_i) = (y_{i,1}, y_{i,2}, ..., y_{i,k})$ with k output variables or responses. Re-grouping the output by responses yields k response vectors $\mathbf{r}_i$ with n elements in each. These vectors can be statistically analysed to extract, e.g., the sample moments and the distributions of the responses. The GRS method relies on the work of Wilks [17, 18] with non-parametric tolerance limits to determine the required sample size for sufficient

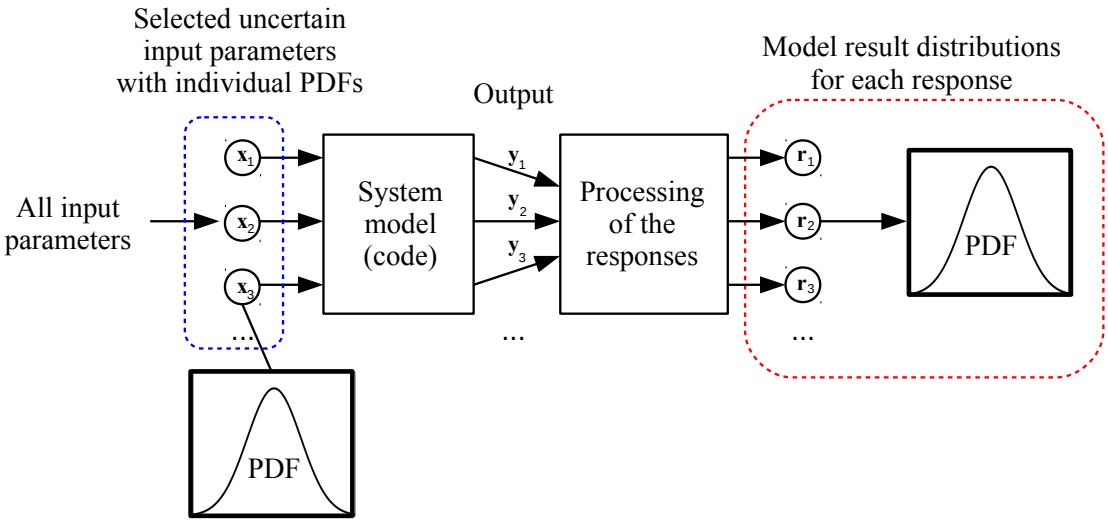

Figure 2: Propagation of input uncertainties in statistical uncertainty analysis

statistics and, therefore, confidence. The tolerance limits are discussed more in Sec. 2.2.6 along with confidence intervals.

The GRS method, or the stochastic approach in general, requires a sampling strategy for building the perturbed input decks. Three common sampling methods are simple random sampling (SRS), stratified sampling and its variant Latin Hybercube Sampling (LHS). Refer to Ref. [19] for a more detailed summary and comparison. In the simple random sampling the samples are generated drawing individual random numbers from a specified distribution. The SRS procedure is simple to implement but it has the drawback of not covering the input space efficiently. A high sample count is therefore required to achieve a good coverage for the input space, and hence a sufficient population coverage and convergence for the output space. Calculations with a high computational cost or a sample size may therefore require a more advanced method such as the LHS procedure.

In the stratified sampling, the sample space is partitioned into disjoint non-overlapping subgroups or strata. A simple random sample proportionate to the strata fraction is then sampled from each strata. This is an improvement over the SRS method but the LHS is an even more interesting choice for achieving a good input space coverage. Consider again the collection of perturbed inputs $\mathbf{x} = (\mathbf{x}_1, \mathbf{x}_2, .., \mathbf{x}_n)$. Now, each of the inputs consists of the same j input parameters $(x_{i,1}, x_{i,2}, ..., x_{i,j})$. In the LHS method the ranges of the parameters are divided into j equiprobable intervals. A random number is drawn from each of the intervals generating nj random numbers in total. The set of n perturbed inputs is then constructed by pairing the random numbers of the intervals so that each input has those j input parameters with values randomly selected from the intervals. Selecting a specific random number will exclude it from further random selections so that each of the intervals is covered in the final collection of inputs. This allows covering all subsets of the input space. [20] With certain monotonic conditions the variance of the estimated output mean resulting from the LHS method is less than or equal to the variance from the SRS method: [19]

$$\mathrm{Var}(\mathrm{E}(\mathbf{X}))_{\mathrm{LHS}} \leq \mathrm{Var}(\mathrm{E}(\mathbf{X}))_{\mathrm{SRS}}. \tag{33}$$

An example of applying the LHS can be found, for instance, in Ref. [21].

In statistical inference analysis, also known as inductive statistics, the researcher infers the properties of an assumed underlying population or distribution. This implies the assumption that the sample is from a larger population. The properties of only the observed sample, in turn, are dealt with descriptive statistics. In the pursue of general safety limits we are naturally applying the inductive statistics. Presenting the uncertainty analysis' results is straightforward and involves mainly acquiring point estimates (Sec. 2.2.5) and interval estimates (Sec. 2.2.6). The point estimates are the best estimates for specific parameters while the interval estimates are intervals under which the true (always unknown) value of the parameter falls with a certain probability. In uncertainty analysis the means and the standard deviations are the most interesting point estimates while the tolerance and possibly the confidence intervals are employed as the interval estimates. Furthermore, the results of a repeated measurement from an unknown distribution can be summarized visually with an estimated PDF or an empirical CDF. The visual presentation is often preferable to the first two moments since some information is necessarily lost when condensing the output distribution into just point and interval estimates, see Sec. 2.2.4.

Further processing of the results is easy if it can be assumed that the output data are approximately normally distributed. Pearson's chi-square test can be used to test the goodness of fit, i.e., whether there is a significant deviation from an assumed underlying theoretical distribution, see Sec. 2.2.7. However, due to the probabilistic nature of the measurements, a small set of data can appear to deviate from the normal distribution even if it was sampled directly from it. Similarly, with large data sets the data may seem to match the normal distribution but in truth even small deviations become significant with a large number of observations.

2.2.1 1D random sampling from a univariate distribution

Sampling *uncorrelated* 1D parameters of the input space $\mathbf{X}$ requires generating random numbers from the distributions of the parameters. Simple methods to draw n random numbers from the normal, the truncated normal and the log-normal distribution are discussed. The ability to generate uniformly distributed (pseudo)random numbers on a finite interval is taken for granted.

Sampling from the general normal distribution $N(\mu, \sigma^2)$ can be reduced to the problem of sampling from the standard normal distribution $N(0,1)$ for Eq. (16) can simply be inverted:

$$X = \mu + \sigma Z \sim N(\mu, \sigma^2) \text{ where } Z \sim N(0,1). \tag{34}$$

Also the generation of log-normally distributed samples relies heavily on sampling the standard normal distribution. The $N(0,1)$ distributed sample can converted to the "log-space" with a transformation

$$X = e^{\mu+\sigma Z} \text{ where } \begin{cases} X \sim \ln N(\mu, \sigma^2) \\ Z \sim N(0,1) \end{cases} \tag{35}$$

While sampling the normal distribution one can resort to the Central Limit Theorem of Sec. 2.1.1 as the most primitive method. Sampling from identical independent uniform distributions leads to an approximately normal distribution if the number of samples is large enough. This is obviously computationally expensive and therefore not a practical approach. The more sophisticated, and less brute-force, methods include inverse transform sampling [22], Box-Muller transform [23], Marsaglia polar method [24] and Ziggurat algorithm [25]. The last one is the fastest one but also overly complicated for our purposes and is thus excluded from further discussion.

The inverse transform sampling is a general method. The main idea is to obtain either analytically or via approximations the inverse of the cumulative distribution function. A random number from the distribution can then be obtained by calculating $x = F_X^{-1}(u)$ where $u \sim U(0,1)$. For the normal distribution the inverse CDF can be approximated resulting in a practical method.

The Box-Muller transform generates pairs of $N(0,1)$ distributed random numbers from uniformly distributed random numbers. Each pair is created with two uniform random numbers u_1 and u_2 employing equations

$$Z_0 = R\cos(\theta) = \sqrt{-2\ln U_1}\cos(2\pi U_2), \tag{36}$$

$$Z_1 = R\sin(\theta) = \sqrt{-2\ln U_1}\sin(2\pi U_2), \tag{37}$$

where $Z_i \sim N(0,1)$ and $U_i \sim U(0,1)$. The method can be improved by avoiding the use of the trigonometric functions by employing polar coordinates. These faster equations can be written as

$$Z_0 = \sqrt{-2\ln(U_1^2 + U_2^2)}\frac{U_1}{\sqrt{U_1^2 + U_2^2}}, \tag{38}$$

$$Z_0 = \sqrt{-2\ln(U_1^2 + U_2^2)}\frac{U_2}{\sqrt{U_1^2 + U_2^2}}, \tag{39}$$

where $U_i \sim U(-1,1)$ and applies $0 \leq U_1^2 + U_2^2 < 1$.

A random sample from the truncated normal distribution can be generated with various algorithms. In the case of the multivariate distribution, Marcov chain Monte Carlo methods such as the Gibbs sampler are useful [26]. With the univariate distribution much simpler methods are sufficient, especially, if the truncation range is not too limiting and the desired sample sizes are small. The approximate inverse transform sampling can again be used by limiting the range of the uniform distribution to meet the truncated interval. The most intuitive method, in turn, is to simply draw random numbers from the non-truncated normal distribution rejecting the ones outside the truncation interval. The approach can be inefficient with high rejection rates and/or sample sizes but it does automatically limit the support and also re-scales the probability mass to the defined interval. However, both methods require knowing the location and the scale parameter of the truncated distribution. This turns out to be a problem when they begin to deviate from the parameters of the normal distribution while trying to conserve the mean and the variance of the distribution, see Sec. 2.2.3.

2.2.2 Correlated multivariate random sampling

Consider next a collection $\mathbf{X}$ of mutually *correlated* parameters instead of independent variables. Now, the joint density function of the correlated variables cannot be expressed as the product of the individual PDF's as in Eq. (8), and the (absolute) covariance matrix $\mathbf{V}$ of Eq. (11) has non-zero off-diagonal elements. As it is, the random numbers cannot be drawn one by one and one must resort to more advanced methods. Mutually correlated normally distributed variables can be sampled with diagonalization [27, 28], Cholesky decomposition [28] and something called correlated sampling method [15]. All three will lead to the same final expression for the normal distribution but the correlated sampling is the most general method and can, at least in principle, be used with any multivariate distribution.

The covariance matrix can be transformed into a diagonal matrix $\mathbf{D}$, i.e., the data can be decorrelated, with the diagonalization:

$$\mathbf{D} = \mathbf{Q}^{\mathrm{T}}\mathbf{V}\mathbf{Q}, \tag{40}$$

where $\mathbf{Q}$ is the eigenvector matrix with the eigenvectors as columns. Now the correlated parameters $\mathbf{x}$ can be rotated to the uncorrelated coordinate system

$$\mathbf{y} = \mathbf{Q}^{\mathrm{T}}\mathbf{x}, \tag{41}$$

where the parameters can be sampled independently with the straightforward univariate methods described in Sec. 2.2.1. The shape of the multivariate normal distribution is conserved in the diagonalization, although the same result does not apply to other distributions [27]. Therefore, assuming the normal distribution, the elements of the transformed best estimate vector $\mathbf{y}$ are sampled from the normal distribution also in the "y-space". The perturbed variables can then be rotated back to the original coordinate system with the inverse transformation $\mathbf{x}_{\mathrm{perturbed}} = \mathbf{Q}\mathbf{y}$. [27, 28]

The Cholesky decomposition method is applicable to symmetric positive definite square matrices. It relies on finding the Cholesky decomposition

$$\mathbf{V} = \mathbf{A}\mathbf{A}^{\mathrm{T}}, \tag{42}$$

where $\mathbf{A}$ is a lower triangular matrix, and applying a transformation

$$\mathbf{x}_{\mathrm{perturbed}} = \mathbf{A}\mathbf{z} + \mathbf{x} \sim N(\boldsymbol{\mu}, \boldsymbol{\Sigma}), \tag{43}$$

where the elements of the column vector $\mathbf{z}$ are all $N(0, 1)$ distributed. The method can be used also with the correlation matrix $\mathbf{C}$. [28]

In the correlated sampling method the samples are similarly generated with Eq. (43) where now applies $\mathbf{A} = \mathbf{V}^{1/2} = \mathbf{Q}\mathbf{D}^{1/2}\mathbf{Q}^{\mathrm{T}}$ for the multivariate normal distribution. As expected, for the univariate case this reduces to Eq. (34). The method is equivalent to the previous two methods for the normal distribution but can be generalized for an arbitrary distribution, at least in principle, although finding the matrix $\mathbf{A}$ is a non-trivial task. For instance, the multivariate log-normal distribution can be sampled with the method without the distorting effect of the diagonalization method. [15]

Inherently positive parameters are general in applications and often negative values are outright non-physical. Unfortunately, none of the methods guarantees the positivity of the sampled values for the normal distribution, and the negative values are encountered every now and then depending on the location and the scale parameter. Multiple approaches have been suggested, for example, in Ref. [27] to deal with these cases and obtain correlated samples from the truncated normal distribution. The propositions involve often the log-normal distribution due to the incorrect interpretation of the Maximum Entropy Principle encountered in Sec. 2.2.3. Neglecting these approaches leaves, for instance, zero cut-off and re-sampling of the negative values as sound methods. The zero cut-off sets the negative values to zero distorting the sample mean from the expected value of the strived truncated normal distribution. In case of a symmetric doubly truncated distribution a symmetric cut-off does not distort the expected value, but instead creates two clear peaks to the PDF on the boundaries of the interval. A more subtle method is to re-sample the negative values but due to the correlation the whole perturbation procedure must be repeated until there are no negative values left in $\mathbf{x}_{\text{perturbed}}$.

2.2.3 Maximum Entropy Probability Distribution Function

Generating the varied input decks via random sampling requires selecting the distributions to be sampled. With the Principle of Maximum Entropy it can argued that there is an objective choice based on prior probabilities. There has been some confusion in the literature about the results of the Maximum Entropy Principle so a careful discussion is in place. We shall focus on positive variables such as the inherently positive neutron cross section data of Sec. 2.3.

The Maximum Entropy Probability Distribution (MEPD) is the probability distribution which reflects the current knowledge best without any additional assumptions. As shown by Jaynes in Ref. [29] and further discussed in Ref. [30], the entropy of a continuous distribution $f(x)$ is defined as:

$$H = -\int f(x) \ln\left(\frac{f(x)}{m(x)}\right) dx, \tag{44}$$

where $m(x)$ is the so-called prior density or "invariant measure" function to ensure invariance under change of variables. Solving the MEPD requires maximizing the entropy H with, for instance, the method of Lagrange multipliers subject to constraints:

$$1 = \int f(x)dx, \tag{45a}$$

$$G_k = \int G_k(x)dx, \quad k = 1,2,..,n, \tag{45b}$$

where the G_k are the expectation values of n different functions. The function $m(x)$ describes the complete ignorance and has been discussed in detail in Ref. [30]. A widely used [31–33] implicit assumption of $m(x) = 1$ is adopted in this Thesis.

As a demonstration, the MEPD for a known mean and a variance in the range $[0, \infty)$ is derived following the formalism of Ref. [32]. The optimization problem is clear:

$$\text{maximize} \qquad -\int_0^\infty f(x)\ln(f(x))dx \tag{46a}$$

$$\text{subject to} \qquad \int_0^\infty f(x)dx = 1 \text{ (normalization)}, \tag{46b}$$

$$\int_0^\infty xf(x)dx = m \text{ (known mean)}, \tag{46c}$$

$$\int_0^\infty (x-m)^2 f(x)dx = v^2 \text{ (known variance)}. \tag{46d}$$

The Lagrangian takes the form

$$\mathcal{L} = -\int_0^\infty f(x)\ln(f(x))dx + \lambda_0\left[\int_0^\infty f(x)dx - 1\right] + \lambda_1\left[\int_0^\infty xf(x)dx - m\right] + \lambda_2\left[\int_0^\infty (x-m)^2 f(x)dx - v^2\right], \tag{47}$$

and the Euler-Lagrange equation yields the truncated normal distribution

$$f(x) = A(\lambda_0, \lambda_1, \lambda_2)\exp\left[-\frac{1}{2}\frac{(x-m)^2}{v^2}\right], \tag{48}$$

assuming that the relative uncertainty is below one, i.e., $v^2 < m^2$. The Lagrange multipliers are fixed by the data and $\lambda_2 > 0$. With $v^2 = m^2$ the result is the exponential distribution [32] while for $v^2 > m^2$ it has been shown that there is no MEPD [33].

The conclusion is that the MEPD of a positive variable with a prescribed mean and a variance accompanying the restricted maximum uncertainty is the truncated normal distribution. Similarly it can derived that changing the interval to $(-\infty, \infty)$ leads to the normal distribution, while knowing the first two logarithmic moments, i.e., $\mathrm{E}[\ln(x)] = m_{\ln}$ and $\mathrm{E}[(\ln(x) - m_{\ln})^2] = v_{\ln}^2$, results in the log-normal distribution [32]. A persistent confusion concerning the log-normal distribution can be found from the nuclear engineering literature and since the 1990s it has been repeatedly claimed [15, 31, 34–37] that the MEPD of an inherently positive parameter with the first two moments, such as the neutron cross section data, is the log-normal distribution. Clearly, this is not the case.

Unfortunately, handling of the truncated normal distribution is not mathematically trivial and the author is not aware of any method, analytical or numerical whatsoever, enabling the calculation of the location and the scale parameter of the distribution in a general multivariate case. Apparently the only available equations have been presented by

Dowson and Wragg [33] for the univariate distribution with a semi-infinite support $[0, \infty)$:

$$H\left(\frac{\mu}{\sigma}\right) = \left(\frac{v}{m}\right)^2, \tag{49a}$$

$$\sigma = m\frac{M\left(\frac{\mu}{\sigma}\right)}{M'\left(\frac{\mu}{\sigma}\right)}, \tag{49b}$$

$$A = \frac{1}{\sigma}\frac{1}{1 - F_{N(0,1)}\left(-\frac{\mu}{\sigma}\right)}, \tag{49c}$$

where A is the normalization and $H(t)$ is defined as

$$H\left(\frac{\mu}{\sigma}\right) = \frac{M(t)M''(t)}{M'(t)^2} - 1, \tag{50}$$

and $M(t)$ is the negative reciprocal of the Mill's ratio

$$M(t) = -\frac{f_{N(0,1)}(t)}{1 - F_{N(0,1)}(t)}. \tag{51}$$

The parameters can now be solved by calculating the ratio μ/σ followed by the scale parameter σ. The location parameter μ can then be solved from the known ratio μ/σ and σ.

As it is, excluding the univariate distributions of the uncorrelated variables in the range $[0, \infty)$, the choice of the distribution is subjective in a practical sense. With the relative standard deviations above unity even the theoretical objective distribution is not clear. This leads to the slightly disappointing conclusion that, while the objective choice of the truncated normal distribution is well-founded below the uncertainty threshold, in practice the choice of the distribution is still subjective of necessity. However, with reasonable uncertainties alternative approaches can be pursued to approximate the truncated normal distribution.

Various univariate probability distributions with equal means and variances have been gathered in Fig. 3 along with a histogram and a kernel density estimate (Sec. 2.2.4) of re-sampled normally distributed data. At low uncertainties there are no visible differences but already at 30% relative standard deviation the log-normal distribution deviates from the rest. At 60% uncertainty the truncated normal distributions starts to finally diverge from the normal distribution and the re-sampling method, and at 80% uncertainty none of the other distributions resemble the truncated normal distribution. The re-sampling method does not yield the truncated distribution as much as a variant of the normal distribution because the mean and the variance were assumed to be the parameters of the truncated distribution as in a general case the parameters cannot be calculated. This approximation breaks down between 40-60% relative uncertainty [38]. Nevertheless, the re-sampling method provides a reasonable approximation before the choice becomes even more subjective.

2.2.4 Visualizing a sample from an unknown distribution

Usually processing the results of a random sampling requires some assumptions about either the underlying distribution or the data itself. However, the additional assumptions

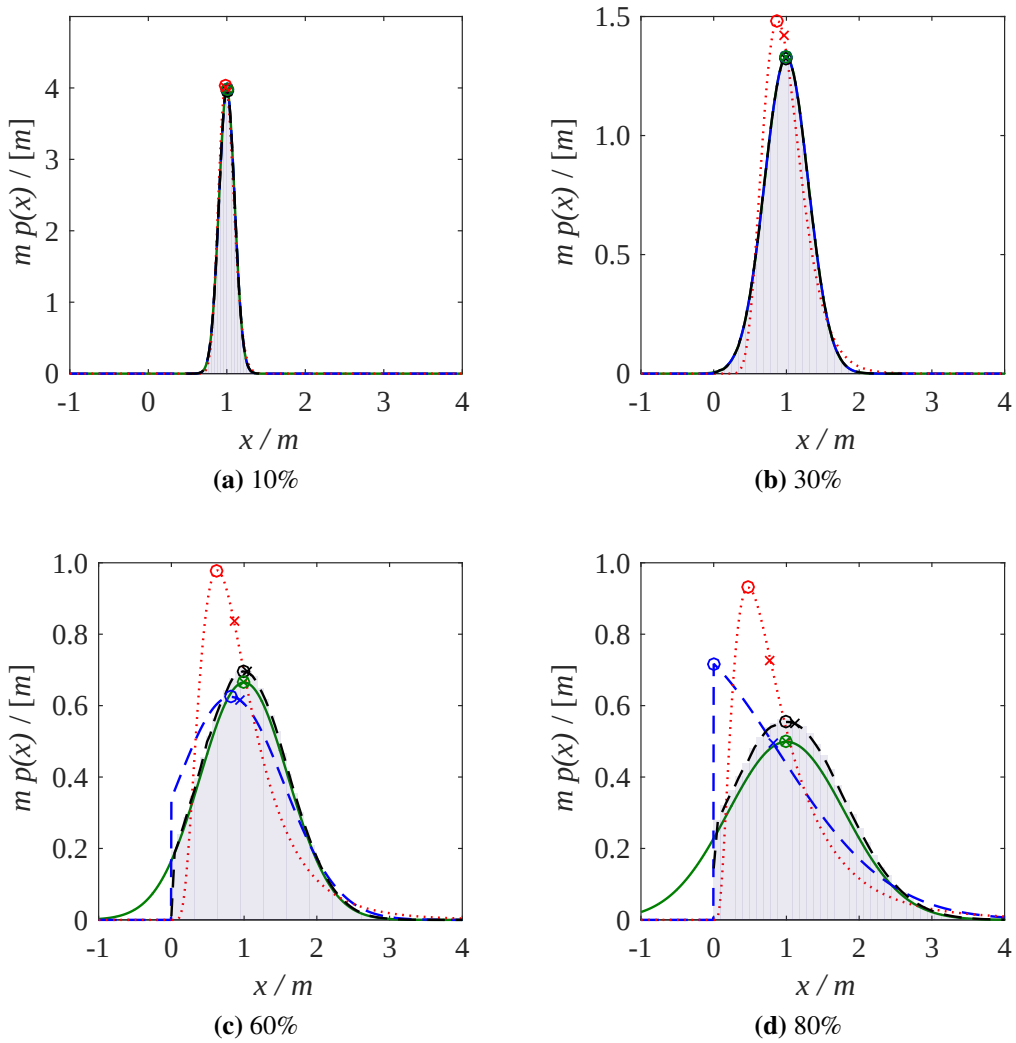

Figure 3: Comparison of univariate probability distributions with increasing relative uncertainties. A truncated normal distribution with a $[0,\infty)$ support and a log-normal distribution are drawn with the blue dashed line and the red dotted line, respectively, while the green solid line is reserved for the normal distribution. The grey histogram is the result of drawing samples from the normal distribution while re-sampling the negative values. Its kernel density estimate is represented by the black dashed curve. The distributions were defined so that, with the obvious exclusion of the sampled data and its kernel density estimate, they had equal means and variances. The modes and medians of the distributions are marked with circles and crosses, respectively.

or binning of the data can be avoided with an empirical cumulative distribution function (ECDF). Consider, once again, n independent observations $(X_1, X_2, ..., X_n)$ of the same random variable X with values $(x_1, x_2, ..., x_n)$. Now the CDF of the output distribution can be estimated with its unbiased estimator, ECDF, defined as

$$F_{\text{empirical}}(x) = \begin{cases} 0, & x < x_1, \\ i/n, & x_{(i)} \leq x \leq x_{(i+1)},\ i = 1,2,...,n-1, \\ 1, & x_{(n)} \leq x, \end{cases} \tag{52}$$

where the indices in the parentheses are the indices of the n observations in an ascending order. At each step i the value of the ECDF increases with an equal height of $1/n$. The ECDF can be applied to the visual inspection of the data but it is useful also for comparing the output distribution to some assumed theoretical distribution. For example, studying the average square difference between the two CDFs leads to the Smirnov–Cramér–Von Mises test. [10]

The results can be visualized with the empirical cumulative distribution without distorting the data with approximations or assumptions. The ECDF should therefore be favoured. Nevertheless, visualizing also the PDF is often desirable. The most common method is to plot the data as a histogram but especially with a small sample size the result is strongly dependent on the choice of the binning. A more sophisticated way is to use non-parametric (distribution-free) kernel density estimation (KDE) [39, 40].

2.2.5 Point estimates

Visualizing the result of a repeated measurement is useful but the output distribution can also be quantified by calculating the first population moment and the second central moment, i.e., the mean and the variance. Calculating the parameters of a distribution from the observations is called estimation and the found values the estimates of the parameters, denoted here with a bar $\bar{}$. The estimation is usually done with either the method of moments or the maximum-likelihood estimation. In the method of moments the unknown moments of Eq. (4) and Eq. (5), and therefore the distribution parameters, are estimated by using the sample moments as the estimates of the population moments. In this section it is assumed that the output sample has been generated with the simple random sampling and for the Latin Hypercube Sampling the given estimator of the variance is not unbiased [19].

Following Refs. [8,41], let us consider a random sample of observations $(X_1, X_2, ..., X_n)$ from a continuous distribution with a PDF f_X, a variance v^2 and an expectation value m. For simplicity the observations are one-dimensional with values $(x_1, x_2, ..., x_n)$. An estimator is unbiased if its expectation value equals the expectation value of the estimated parameter. The method of moments gives the arithmetic mean

$$m^* = \bar{X} = \frac{1}{n} \sum_{i=1}^{n} X_i, \tag{53}$$

as the unbiased estimator of the expectation value with the well-known standard deviation $v/\sqrt{n}$. The value of the estimate known as the average or the sample mean is then

$$\bar{m} = \bar{x} = \frac{1}{n} \sum_{i=1}^{n} x_i. \tag{54}$$

For the variance the unbiased estimator is

$$v^{2*} = S^2 = \frac{1}{n-1}\sum_{i=1}^{n}(X_i - \bar{X})^2, \tag{55}$$

and, as with the first moment, the sample variance is given by

$$\bar{v}^2 = s^2 = \frac{1}{n-1}\sum_{i=1}^{n}(x_i - \bar{x})^2. \tag{56}$$

The biased estimate of the standard deviation, also known as the sample standard deviation, can be calculated as

$$\bar{v} = s = \sqrt{\frac{1}{n-1}\sum_{i=1}^{n}(x_i - \bar{x})^2}. \tag{57}$$

2.2.6 Interval estimation and required sample size

The results can be analysed also with interval estimation. Three types of interval estimates are considered: the well-known confidence interval, the less-known prediction interval, and the rarest, but often the most useful of the three, the tolerance interval. Straightforward definitions of the intervals are: [41]

- Confidence interval: a parameter-specific interval due to a sampling error for population parameters such as the mean or variance
- Prediction interval: an interval under which a new data point will fall with a certain probability
- Tolerance interval: an interval comprising a certain percentage of the population with a specified probability

A suitable interval depends on the objective. The confidence interval considers only the parameters of the population. It also accounts for only the sampling error and thus the interval will approach a zero-width as the sample size increases. The prediction interval, in turn, is for predicting the behaviour of a new observation when the interval is constructed from the previous observations. Finally, the tolerance interval is appropriate for setting bounds for the whole population. It accounts for both the sampling error and the true variance of the population and therefore approaches the true uncertainty with large sample sizes. [41]

The intervals can be either parametric (distribution-dependent) or non-parametric (distribution-free) depending on whether they assume some specific underlying distribution. Here we shall consider only the intervals relevant to this study: first a parametric (normal distribution) confidence interval and then a non-parametric tolerance interval. The prediction interval is excluded from further discussion for this study is not interested in predicting any particular observation.

The justification for the confidence interval follows directly from Sec. 2.2.5. The values of the unbiased estimators vary between the samples and only the expectation value

is guaranteed to equal the estimated parameter's true value. It is therefore essential to consider the accuracy of the estimates with confidence intervals. A confidence interval includes the true value of the estimated parameter with a certain probability or confidence, often selected to be 0.95. With the confidence intervals the true value of the estimated parameter remains unknown but it is possible to say that, for example, with the said 0.95 probability the true value is within the confidence interval. [41]

The confidence interval depends on the selected underlying distribution. Following the example of Ref. [8], a general normally distributed estimator $\theta^* \sim N(\theta, \sigma_\theta^2)$ is considered. Via the standardization with Eq. (16) and the use of a standard normal table, a range covering for example 95% of the probability mass can be derived:

$$\mathrm{P}(\theta^* - 1.96\sigma_\theta \leq \theta \leq \theta^* + 1.96\sigma_\theta) = 0.95. \tag{58}$$

This is the two-sided 95% confidence interval for the expectation value θ. For instance, let us take yet again the collection of observations $(X_1, X_2, ..., X_n)$ and assuming $X \sim N(\mu, \sigma^2)$ leads us to

$$[\bar{X} - 1.96\frac{\sigma}{\sqrt{n}}, \bar{X} + 1.96\frac{\sigma}{\sqrt{n}}], \tag{59}$$

as the estimator of the 95% confidence interval of the expectation value when the parameter θ^* is replaced with the unbiased estimator of Eq. (53). Thus, with sample values $(x_1, x_2, ..., x_n)$ the confidence interval can be calculated as

$$[\bar{x} - 1.96\frac{\sigma}{\sqrt{n}}, \bar{x} + 1.96\frac{\sigma}{\sqrt{n}}]. \tag{60}$$

A confidence interval can be constructed also for the variance and, consequently, for the standard deviation. Assuming again the normal distribution $X \sim N(\mu, \sigma^2)$ and the sample $(x_1, x_2, ..., x_n)$ applies

$$\frac{(n-1)S^2}{\sigma^2} \sim \chi^2(\nu),\ \nu = n - 1, \tag{61}$$

as explained in Sec. 2.1.1 for the sum of squares of independent $N(0, 1)$ distributed random variables. For a two-sided confidence interval with a confidence level $1 - \alpha$ it follows

$$\mathrm{P}\left(\chi^2_{1-\alpha/2} \leq \frac{(n-1)S^2}{\sigma^2} \leq \chi^2_{\alpha/2}\right) = 1 - \alpha, \tag{62}$$

which, in turn, results in the estimate of the confidence interval $1 - \alpha$:

$$\frac{n-1}{\chi^2_{\alpha/2}}s^2 \leq \sigma^2 \leq \frac{n-1}{\chi^2_{1-\alpha/2}}s^2,\ \nu = n - 1, \tag{63}$$

where the s^2 is defined by Eq. (56).

Calculating a suitable tolerance interval for the output parameters is found to be less straightforward. The GRS method applies a traditional coverage approach first suggested by Wilks [17, 18] and later extended to the multivariate case by Wald [42]. A second,

newer, bracketing methodology was developed by Nutt and Wallis [43]. The results of the two approaches are found to be generally conflicting.

Let us consider first the coverage approach. The goal is to calculate the minimum sample size n for a continuous multivariate joint density function $f_{\mathbf{X}}$ so that $100\alpha\%$ of the population, i.e., of the indefinitely large sample, is within the tolerance interval with a confidence level $\beta < 1$. Or in terms of an equation, find the minimum sample size so that a condition

$$\mathrm{P}\left(\int_{L_p}^{M_p} \dots \int_{L_1}^{M_1} f(t_1,\dots,t_p)dt_1\dots dt_p \geq \alpha\right) = \beta, \tag{64}$$

applies. Here p is the number of the output parameters and $[L_i, M_i]$ the tolerance interval of a variable x_i. The approach was summarised and further extended to correlated output parameters by Guba *et al.* [44] with the minimum and the maximum of the sample as the interval boundaries. For instance, with values $\alpha = \beta = 0.95$ the minimum sample size would promise that 95% of the total population is within the tolerance interval, or in other words, 95% of the total population has been covered with the confidence level of 95%. It was proposed that for p output variables depending on each other the equation for a two-sided tolerance limit can be written as

$$\sum_{i=0}^{n-2p} \binom{n}{i} \alpha^i (1-\alpha)^{n-i} \geq \beta. \tag{65}$$

For mutually independent variables the equation reduces to the previously known results [45] of one output variable's two-sided interval

$$1 - \alpha^n - n(1-\alpha)\alpha^{n-1} \geq \beta, \tag{66}$$

and one-sided upper interval

$$1 - \alpha^n \geq \beta. \tag{67}$$

The number of the required samples increases rapidly with the coupled variable count of Eq. (65) [44]. The correlated parameters can be encountered, for example, when numerous output parameters are extracted from the same computational code. However, it should be noted that the correlated output parameters can still be considered as mutually independent if the goal is not to obtain the p-dimensional tolerance limit but just the individual tolerance limits.

As an intrinsic property of the stochastic approach, some of the new observations may be outside the tolerance interval. With high minimum coverage and confidence level these occurrences are few but significant if they are outside the predefined safety limits. Guba *et al.* has noted [44] that in the statistical approach the safety is not deterministic in nature but rather characterized by the parameters α and β. The system is considered safe if the largest element of the sample is within the safety limits. Usually this means that the largest element must be below some upper limit set by technological considerations. According to the IAEA a $\alpha/\beta = 95/95$ limit, leading directly to a sample size of $n \geq 93$ for the one-dimensional two-sided tolerance interval of Eq. (66), is sufficient for the regulatory purposes [1].

The coverage approach has been criticized mainly by Wallis in Ref. [46] as well as in his following publications [43, 47] where he formulated the bracketing approach partially in cooperation with Nutt. He argued that using a single probability for the multivariate case allows a trade-off between the ranges of the variables and, thus, it could not be ensured that the univariate ranges of Eq. (64) are truly been looked over with the desired coverage and confidence levels. The bracketing approach can be expressed as

$$\int_{-\infty}^{\infty}\int_{L_i}^{M_i}\int_{-\infty}^{\infty} f(t_1,...t_i,...,t_p)dt_1...dt_i...dt_p \geq \beta_i, \text{ for each i,} \tag{68}$$

with each variable having its own coverage and probability. With just one variable the bracketing and the coverage approach yield the same equations (67,66) but otherwise they conflict. The criticism of Wallis has been countered by the proponents of the coverage approach in Ref. [48] while the bracketing approach has been criticised in Refs. [49, 50], which, in turn, have been countered by Nutt and Wallis in Refs. [51, 52]. The main argument of the critics has been that the bracketing approach mixes the coverage α with a probability while α should be understood only as a fraction of the distribution. To the author's best knowledge and understanding, the criticism of the bracketing method has been justified and at any rate the coverage approach is the current norm.

2.2.7 Chi-square test for normality

The parametric confidence intervals of Sec. 2.2.6 assumed the normal distribution. Therefore, the use of the resulting equations requires normally distributed data. This property can be tested with the widely used chi-square (χ^2) test [8]. The test yields a p-value answering to the question: "At what probability such deviation from the theoretical distribution would be observed if the studied parameter follows the theoretical distribution?" The test begins by specifying a null hypothesis H_0 for calculating the p-value and an alternative hypothesis H_1 to be favoured if the null hypothesis does not apply. Testing for normality would use the hypotheses:

- H_0: The observed parameter is normally distributed
- H_1: The observed parameter is not normally distributed

A significance level α, the probability to reject the null hypothesis even if it is true, is selected before conducting the test. The calculated p-value can be directly compared to the significance level, often selected to be 5%, and the null hypothesis is accepted if the p-value is higher than the significance level. In other words, with a high enough p-value it is concluded that the deviation from the theoretical distribution is not statistically significant, i.e., the deviation is deemed to be due to chance alone. Correspondingly, in the statistically significant case of $p < \alpha$ the null hypothesis is rejected in favour of the alternative hypothesis.

The test is performed by dividing the sample into k cells so that each of the cells has a certain number of observations O_i and a theoretical expected frequency E_i. The value of the test-statistics is then defined as

$$\chi_0^2 = \sum_{i=1}^{k} \frac{(E_i - O_i)^2}{E_i}, \tag{69}$$

where the χ_0^2 is asymptotically χ^2 distributed if the null hypothesis applies. There are certain limitations to the use of the test varying by literature source. Here we adopt the conditions of Ref. [8] given as

- The observations are statistically independent
- The number of observations is sufficient ($n \geq 50$)
- $E_i \geq 2$ for every cell i
- At maximum 20% of the E_i are below 5

2.3 Neutronics and nuclear data

The general stochastic approach can be applied directly to nuclear engineering. This section includes a short introduction to the basic concepts but does not even attempt to give a comprehensive view of the whole area of nuclear engineering. Most of the reactor physics' concepts are simply neglected and the focus is on the neutron cross section data. A reader who is novice in nuclear engineering is directed to Ref. [53] or any other introductory level textbook.

2.3.1 Introduction to reactor physics

Following the example of Ref. [53], consider the interaction of an incident neutron with a nucleus. The interaction probability is characterized by microscopic cross sections σ which can be understood as inherently positive energy dependent continuous random variables. The microscopic cross section is defined as

$$\sigma(E) = \frac{\text{Number of reactions/nucleus/second with energy E}}{\text{Number of incident neutrons/cm}^2\text{/second with energy E}} = [\text{m}^2],$$

and, with the units of area, one of its interpretations is the effective cross-sectional area of the nucleus, hence the name. In nuclear engineering the cross sections are traditionally given in barns (1b = 10^{-28} m^2). The microscopic cross sections are reaction-wise and may have summation rules related to them. The total neutron cross section σ_t is the sum of its partial reactions which, in turn, are the sum of their respective partial reactions:

$$\sigma_\text{t}(E) = \sigma_\text{s}(E) + \sigma_\text{a}(E) = \sigma_\text{e}(E) + \sigma_\text{in}(E) + \sigma_\text{f}(E) + \sigma_\gamma(E) + \ldots \tag{70}$$

This neutron cross section hierarchy is illustrated in Fig. 4. On the macro-scale the interaction probability depends naturally also on the (time-dependent) atomic density N_at. The macroscopic cross section, defined as the interaction probability per travelled unit length, for a reaction x is given by

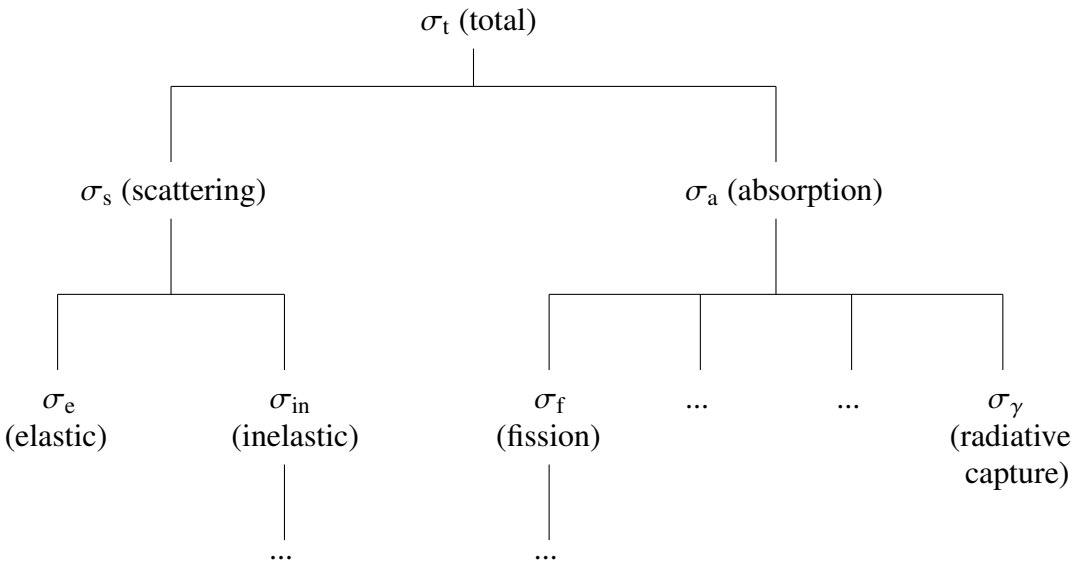

Figure 4: Neutron cross section hierarchy as explained in Ref. [53]

$$\Sigma_x(\mathbf{r},E,t) = N_{at}(\mathbf{r},t)\sigma_x(E) = [\mathrm{m}^{-1}]. \tag{71}$$

The equation can be also generalized for a homogeneous mixture of nuclide species i

$$\Sigma_x(\mathbf{r},E,t) = \sum_i \Sigma_{x,i}(\mathbf{r},E,t) = \sum_i N_{at,i}(\mathbf{r},t)\sigma_x(E). \tag{72}$$

Consider next an arbitrary (infinitesimal) volume dV about $\mathbf{r}$, an energy interval dE about E and a unit vector $\hat{\mathbf{\Omega}}$ within interval $d\hat{\mathbf{\Omega}}$. Now, an angular neutron density gives the number of neutrons in the volume element dV with the energy E and the direction $\hat{\mathbf{\Omega}}$ at a time t

$$n(\mathbf{r},E,\hat{\mathbf{\Omega}},t)dV\,d\hat{\mathbf{\Omega}}dE. \tag{73}$$

The scalar neutron density can be obtained by integrating over the full solid angle

$$n(\mathbf{r},E,t) = \int_{4\pi} n(r,\hat{\mathbf{\Omega}},E,t)d\hat{\mathbf{\Omega}}, \tag{74}$$

and the total neutron density by adding an integral over energy

$$n(\mathbf{r},t) = \int_{4\pi}\int_E n(\mathbf{r},\hat{\mathbf{\Omega}},E,t)dE\,d\hat{\mathbf{\Omega}}. \tag{75}$$

A quantity known as a neutron flux is useful for calculating the physical reaction rates. With the help of the neutron speed v, the angular neutron flux

$$\psi(\mathbf{r},\hat{\mathbf{\Omega}},E,t) = vn(r,\hat{\mathbf{\Omega}},E,t) = [\mathrm{m}^{-2}\mathrm{s}^{-1}], \tag{76}$$

and its scalar counterpart

$$\phi(\mathbf{r},E,t) = \int_{4\pi} \psi(\mathbf{r},\hat{\mathbf{\Omega}},E,t)d\hat{\mathbf{\Omega}} = vn(\mathbf{r},E,t), \tag{77}$$

allow writing the reaction rate of a reaction x as

$$R_{\mathrm{x}}(t) = \int_V \int_{\hat{\mathbf{\Omega}}} \int_E \Sigma_{\mathrm{x}}(\mathbf{r},E,t)\psi(\mathbf{r},\hat{\mathbf{\Omega}},E,t)dEd\hat{\mathbf{\Omega}}dV \tag{78}$$

$$= \int_V \int_E \Sigma_{\mathrm{x}}(\mathbf{r},E,t)\phi(\mathbf{r},E,t)dEdV. \tag{79}$$

The angular neutron flux does not have a clear physical interpretation but it relates the six-dimensional phase space neutron density to the physical reaction rates. The scalar flux, in turn, can be thought as the total distance travelled by the whole neutron population per unit time and volume. [53]

The flux, and therefore the reaction rates, can be obtained by solving the neutron transport equation describing the neutron balance

$$\underbrace{\frac{1}{v}\frac{\partial}{\partial t}\psi(\mathbf{r},\hat{\mathbf{\Omega}},E,t)}_{\text{time-rate of change}} + \underbrace{\hat{\mathbf{\Omega}}\cdot\nabla\psi(\mathbf{r},\hat{\mathbf{\Omega}},E,t)}_{\text{streaming term}} + \underbrace{\Sigma(\mathbf{r},E)\psi(\mathbf{r},\hat{\mathbf{\Omega}},E,t)}_{\text{total removal term}} = \underbrace{q(\mathbf{r},\hat{\mathbf{\Omega}},E,t)}_{\text{source term}}, \tag{80}$$

where the source term consists of a scattering source S, an external source Q and a fission source F. Neither the derivation nor the solution algorithms are discussed here but both topics have been covered for example in Ref. [53]. It suffices to say that the equation can be solved with both highly accurate continuous energy Monte Carlo methods and faster, but less accurate, deterministic methods. In the deterministic methods the continuous energy-dependence is discretized into energy groups. The scalar flux and the cross sections can then be condensed into groupwise parameters while preserving the reaction rate. The groupwise flux of an energy group g is given by

$$\phi_g(\mathbf{r},t) = \int_{E_g}^{E_{g-1}} \phi(\mathbf{r},E,t)dE, \tag{81}$$

with the group cross section being the flux-volume-weighted average [53]

$$\Sigma_{\mathrm{x},g}(t) = \frac{\int_V \int_{E_g}^{E_{g-1}} \Sigma_{\mathrm{x}}(\mathbf{r},E,t)\phi(\mathbf{r},E,t)dEdV}{\int_V \int_{E_g}^{E_{g-1}} \phi(\mathbf{r},E,t)dEdV}. \tag{82}$$

The scattering source describes the scattering to the neutron density phase space element from the other energies and directions. It can be written with a double-differential scattering cross section:

$$S(\mathbf{r},\hat{\mathbf{\Omega}},E,t) = \int_{4\pi} \int_E \Sigma_{\mathrm{s}}(\mathbf{r},\hat{\mathbf{\Omega}}' \rightarrow \hat{\mathbf{\Omega}},E' \rightarrow E)\psi(\mathbf{r},\hat{\mathbf{\Omega}}',E',t)d\hat{\mathbf{\Omega}}'dE'. \tag{83}$$

The fission source, in turn, can be written with the help of the scalar flux

$$F(\mathbf{r},E,t) = \frac{1}{4\pi}\int_0^\infty \chi(E)\nu\Sigma_\mathrm{f}(\mathbf{r},E')\phi(\mathbf{r},E',t)dE'. \tag{84}$$

as the fission neutrons are emitted isotropically. Here $\chi(E)$ is the fission spectrum describing the probability for the fission neutron to be emitted with an energy dE about E while ν is the total average fission neutron yield per fission. Finally, the external source term does not depend on the flux and describes the effect of possible external sources.

The problem of solving the neutron transport equation can be modified into a steady-state problem by scaling the fission source term with an eigenvalue $1/k$. The k can be identified as the multiplication factor defined as

$$k = \frac{\text{Number of neutrons in generation } i+1}{\text{Number of neutrons in (preceding) generation } i}, \tag{85}$$

with three different regimes: sub-critical $k < 1$, critical $k = 1$ and supercritical $k > 1$. The neutron count, and therefore the chain reaction, is stable when the system is critical. In a sub-critical system, in turn, the chain reaction will eventually die out while in a supercritical system the chain reaction will grow. The departure from the steady-state is measured with reactivity in per cent milles (pcm). [53]

2.3.2 Evaluated nuclear data and multigroup covariance data

Nuclear data such as the cross sections, fission product yields, resonance parameters, angular distributions and thermal scattering laws are conventionally stored in nuclear data libraries (NDL). The data are generally in Evaluated Nuclear Data Format (ENDF-6) [54] followed most importantly by three major nuclear data libraries: ENDF/B from the United States [55], European JEFF [56] and Japanese JENDL [57]. The nuclear data libraries contain evaluations, i.e., experimentally and theoretically produced recommended data sets, for each material. The ENDF-6 format conveys only the expected values and the second moments of the quantities. The probability distributions of the stored quantities have not been specified any further with the format manual explicitly stating that the format does not fix the distributions' shapes. [54]

The ENDF-format allows attaching covariance data to the nuclear data tapes. In this Thesis we shall refer to the files containing one or more ENDF materials as "tapes" following the tradition of the ENDF-format [54]. In essence they are a simply regular binary or ASCII files. The tapes are grouped into materials which are further subdivided into files with certain MF numbers. Currently the covariance data are supported for [54]

- MF = 31: Average number of neutrons per fission ν
- MF = 32: Resonance parameters
- MF = 33: Neutron cross sections
- MF = 34: Angular distributions of secondary particles
- MF = 35: Energy distributions of secondary particles

- MF = 40: Production of radioactive nuclei

but in this Thesis we restrict ourselves only on the neutron cross section covariances.

Although originally in a rather complicated ENDF-format, the covariance data are conventionally processed into a more useful multigroup format. In the multigroup format the energy grid of each cross section is divided into energy groups with their own best estimate, variance and interlinking correlations. The multigroup data are visualized in Fig. 5 for the radiative capture cross section σ_γ of ^{235}U. Other important nuclear data formats are the pointwise PENDF format for neutron cross sections with a linear-linear interpolation between the data points and the likewise pointwise ACE format for continuous energy nuclear data libraries employed by Monte Carlo codes [5].

There has been a clear progress in reporting the nuclear data covariances but especially the older libraries are lacking in the covariance data. The low-fidelity covariance project [58] has met this need by producing an almost complete set of low-fidelity data for the covariance files of the ENDF/B-VII.0 evaluation. One of the goals of the project was to allow the identification of the most sensitive nuclides as leaving some of the considered nuclides without uncertainties would have risked neglecting possible high-impact uncertainty sources.

As the name implies, the low-fidelity covariances are based on more or less crude approximations with the aim for completeness instead of high-fidelity. Hence, the libraries with good high-fidelity covariance data coverage are the most useful for the purposes of uncertainty and sensitivity analysis. The covariance data of the latest versions of the three major nuclear data libraries, namely ENDF/B-VII.1, JEFF-3.2 and JENDL-4.0u, have been compared recently in Ref. [59]. It was noted that the JEFF-3.2 had a poor covariance coverage for nuclear fuel materials such as ^{235}U. The high-fidelity covariance data readily present in the latest JENDL and ENDF/B libraries 4.0u and VII.1 had a generally good coverage but the Japanese library lacked the uncertainty estimates for multiple structural materials such as zirconium and tin. However, the shortage of the covariance data is much more pressing, e.g., for the preceding ENDF/B library VII.0 which has almost no covariances. Vanhanen and Pusa suggested in Ref. [59] that the low-fidelity data could be used to supplement the evaluated nuclear data covariances when there are no high-fidelity covariances present. Similar suggestions have been made at least in Ref. [60] and Ref. [61] with an emphasis on relative, rather than absolute, covariance data.

There is also a third major type of covariance data, namely the relative covariance libraries of the SCALE-package available from the NEA Data Bank in a COVERX format. The SCALE-5.1 package contains four 44-group cross section covariance matrix libraries [62]

- 44GROUPV5COV, Basic ENDF/B-V Covariance Library
- 44GROUPV5REC, Recommended ENDF/B-V Covariance Library
- 44GROUPV6COV, Basic ENDF/B-VI Covariance Library
- 44GROUPV6REC, Recommended ENDF/B-VI Covariance Library

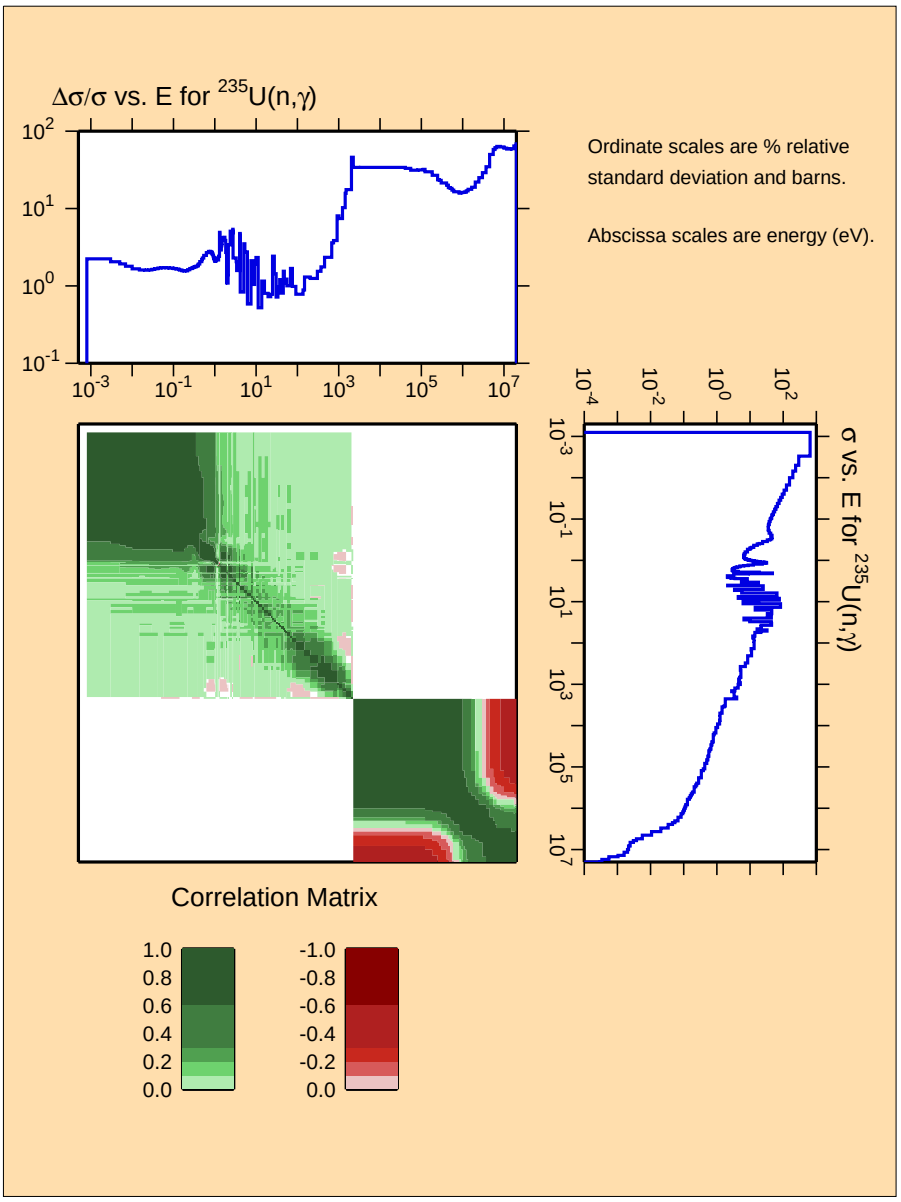

Figure 5: Multigroup best estimate and covariance data for the radiative capture of ^{235}U based on ENDF/B-VII.1

and the more extensive ZZ-SCALE6.0/COVA-44G covariance library of SCALE6.0 merged from various sources [60]. The good coverage comes with the assumption that the relative uncertainties can be generalized to all cross section libraries even if they originate from a different source.

2.3.3 Perturbing nuclear data

The conventional method for introducing uncertainty stochastically to the nuclear data has been to perturb the multigroup microscopic cross sections with the data of the SCALE covariance libraries [63–65]. In this approach groupwise perturbation factors P_g are generated from the covariance data and applied to the processed multigroup cross sections

$$\sigma_{g,\text{perturbed}} = P_g \cdot \sigma_g. \tag{86}$$

The methodology originates from the OECD/NEA UAM-LWR benchmark [61, 66] discussed more in Sec. 3. The multigroup cross sections have been perturbed also with the covariance data of the evaluated nuclear data libraries [67]. The SCALE covariance library with the multigroup perturbation yields around 0.5% relative standard deviation for the effective multiplication factor, although the literature values have been varying [68]. The result accounts for the uncertainties of the neutron cross sections, the average fission neutron yield and the average fission spectrum.

An alternative approach based on the ACE-formatted pointwise nuclear data has also been proposed [7, 65]. Instead of perturbing the multigroup cross sections, the perturbation is directed to the pointwise data. The multigroup covariance data with the respective multigroup best estimate cross sections are again used for computing the set of multiplicative perturbation factors. However, in this method the factors are applied to the pointwise nuclear data:

$$\sigma_{g,\text{perturbed}} = P_g \cdot (\sigma_{E_1}, \sigma_{E_2}, ..., \sigma_{E_n}) = (P_g\sigma_{E_1}, P_g\sigma_{E_2}, ..., P_g\sigma_{E_n}), \tag{87}$$

so that $(E_1, E_2, ..., E_n) \in g$. Thus, the method assumes a full within-group correlation. A method for the statistical perturbation has been developed also for the SCALE code system in Ref. [69]. In this Thesis, a novel variant of the pointwise approach is presented for the nuclear data random sampling, see Sec. 3.2.2.

In the nuclear data perturbation both the spectral decomposition [63] and a "Cholesky-like" decomposition [65] have been used. The general symmetric covariance square matrix is positive *semidefinite* rather than positive *definite* so a generalized inverse and a pseudodeterminant are required in the Cholesky decomposition, hence the "Cholesky-like" decomposition. Also shifting between the two method depending on the matrix properties has been proposed [7]. Both the simple random sampling [7] and the Latin Hypercube Sampling [67] has already been applied in nuclear engineering.

2.3.4 Neutronics of a pin cell

The deterministic DRAGON lattice code was the main tool in the reactor physics calculations of this research, although the Monte Carlo code Serpent was also used to a small extent. For Monte Carlo neutronics the reader is directed to Ref. [70] while we take a practical view on the DRAGON code and the deterministic calculations.

A nuclear fuel pin cell can be modelled in various ways in addition to the obvious selection of the calculation methods. The physical approach is to model a square cell with specular (mirror-like) boundary conditions where the neutrons obey the law of reflection on

the cell boundaries. An approximate, but computationally cheaper, option is to convert the Cartesian cell into a 1D system of concentric cylinders and thereby reduce the dimensions of the problem. This annular cell is commonly achieved via circularization performed with the well-known Wigner–Seitz approximation in which the amount of moderator and the cell area are conserved by scaling the cell pitch a into an area-equivalent cylinder radius $a/\sqrt{\pi}$. [71, 72] Other circularization methods include the Askew and the Sanchez cylinderizations [4, 73]. In the annular cell white (isotropic) boundary conditions are applied instead of the specular boundaries for the reflection with an isotropic angular distribution ensures the return of the reflected neutrons to the fuel also without them undergoing scattering [71, 72].

The DRAGON code supports a variety of calculation methods for solving the neutron transport equation. In Ref. [68] a method of collision probabilities and a rather similar interface current method were discussed and compared with the ultimate conclusion of recommending the collision probabilities. A detailed presentation of the both well-known techniques can be found in Refs. [71–73]. In practice, the method of collision probabilities is supported by DRAGON's EXCELT module while the interface current calculations are performed with the SYBILT module.

Self-shielding modelling can be done with either the SHI module (equivalence in dilution method) or the USS module (subgroup approach) of the DRAGON code. The former module employs the generalized Stamm'ler method with an option of extending it with the Livolant-Jeanpierre normalization scheme, the Nordheim distributed self-shielding model and the Riemann integration method. The latter module supports both physical (USS SUBG) and mathematical (USS PTSL) probability tables. [4] The model extensions have been described briefly, for example, in Ref. [74]. The spatial model can be further improved by introducing radial mesh splitting [71, 75]. As discussed in Ref. [68] improving the self-shielding model becomes easily a bottle-neck for the processing time of DRAGON but, in return, it greatly improves the accuracy of the code.

2.4 Nuclear fuel behaviour and technical parameters

The FINIX code was used as the fuel behaviour code in this Thesis. Currently it is still in active development and lacks phenomena arising at high burn-ups including fuel swelling and cladding creep, though this is not a problem when considering fresh fuel. Other assumptions of the code are a small axial heat transfer compared to the radial heat transfer and perfectly cylindrical pellets with no axial dependence, i.e., the fuel pellet and the cladding have the same central axis.

The uncertain parameters in the fuel behaviour can generally be handled as mutually independent [76]. In this study the fuel behaviour parameters refer to technical parameters, such as the geometrical parameters of the fuel rod, and the material parameters, such as the thermal conductivity of the fuel. As covered in Sec. 2.2.1, drawing samples from the univariate distributions is simple. A more complicated task is to determine the connection between the fuel behaviour parameters and the parameters used in the reactor physics calculations. The most important couplings are the densities and the effective temperatures of the material regions.

Table 1: Fuel behaviour parameters perturbed in Ref. [76] with their best estimates (nominal values) and uncertainties. The third column indicates whether the parameter is available for perturbation in the FINIX code.

Parameter	Value	In FINIX
Cladding outer diameter	(10.92 ± 0.06) mm	Yes
Cladding thickness	(0.673 ± 0.025) mm	Yes
Pellet outer diameter	(9.40 ± 0.02) mm	Yes
Fuel enrichment	(4.85 ± 0.003) atom-%	Yes
Density (% of the theoretical)	(93.8 ± 1.6) %	Yes
Density (ρ_{theo} = 10 970 kg/m^3)	(10 290 ± 176) kg/m^3	Yes
Coolant pressure	(15.51 ± 0.31) MPa	Yes
Coolant inlet temperature	(561 ± 3) K	Yes
Coolant mass flux	(3460 ± 69) kg/(m^{2}s)	Yes
Fuel thermal conductivity	±10 %	Yes
Fuel thermal expansion	±15 %	Yes
FGR diffusion coefficient	+200%/ − 67%	No
Fuel swelling	±20 %	No
Cladding creep	±30 %	No
Cladding axial growth	±50 %	No
Cladding corrosion	±40 %	No
Cladding H concentration	±80 ppm	No
Cladding thermal conductivity	±5 W/mK	Yes
Cladding thermal expansion	±30 %	Yes
Gas thermal conductivity	±0.02 W/mK	Yes
Coolant heat transfer	±5 %	Yes
Linear power	±5 %	Yes

The fuel behaviour uncertainty has been studied in Ref. [76] where the authors presented the fuel behaviour parameters of Tab. 1 with their respective uncertainties. For generating perturbed input values, the study applied the truncated normal distribution with a symmetric 2.5% cut-off while approximating the parameters of the distribution with the nominal value and the uncertainty, i.e., with the parameters of the corresponding normal distribution. This was, of course, a necessity because as explained in Sec. 2.2.3 there are no equations for computing the parameters for the doubly truncated supports. However, as noted in Sec. 2.2.3 with reasonable uncertainties, such as encountered in Tab. 1, the approximation is perfectly valid.

2.4.1 Material densities

The fuel behaviour code FINIX computes a continuous density profile assuming the conservation of mass but does not take a stand on the moderator density. The density of

the helium in the gas gap, in turn, can be calculated with correlations found also from the FINIX code. For the density of pure helium ρ_{He} applies the gas law of helium [77]:

$$\frac{p \cdot 10^5}{2077.3 \cdot \rho_{\mathrm{He}} T} = Z, \tag{88}$$

where Z is the compressibility factor given by

$$Z = 1 + 0.4446 \frac{p}{T^{1.2}}, \tag{89}$$

with p and T as the pressure (in bars) and the temperature of the helium gas, respectively. The final equation for the density in the SI units is thus

$$\rho_{\mathrm{He}} = 48.14 \cdot 10^{-5} \frac{p}{T} \left(1 + 0.4446 \cdot 10^{-5} \frac{p}{T^{1.2}}\right)^{-1}. \tag{90}$$

In the normal conditions of a PWR reactor assuming ideal gas behaviour would introduce only a 1% error compared to Eq. (90) [68].

The density calculations of the water coolant can be based on the 2007 version of the IAPWS-IF97 formulation for industrial use [78]. For compressed liquid the specific volume v is given by

$$v(\pi, \tau) = \pi \gamma_\pi \frac{RT}{p}, \tag{91}$$

where R is the specific gas constant of ordinary water (0.461 526 $\mathrm{kJ\,kg^{-1}\,K^{-1}}$) and

$$\gamma_\pi = \sum_{i=1}^{34} -n_i I_i (7.1 - \pi)^{I_i - 1} (\tau - 1.222)^{J_i}, \tag{92}$$

with parameters $\pi = p/p^*$ and $\tau = T^*/T$, and reference state constants $p^* = 16.53$ MPa, $T^* = 1386$ K. The coefficients I_i, J_i and n_i have been provided in Ref. [78]. The reader should be aware that in some sources such as Ref. [79] the coefficients may be incorrect. The density is the inverse of the specific volume

$$\rho_{\mathrm{water}} = \frac{1}{v}. \tag{93}$$

Eq. (91) is valid in a parameter regime

$$273.15\,\mathrm{K} \leq \mathrm{T} \leq 623.15\,\mathrm{K},\ p_{\mathrm{s}}(T) \leq p \leq 100\,\mathrm{MPa}, \tag{94}$$

where $p_{\mathrm{s}}(T)$ is the saturation pressure.

2.4.2 Effective temperatures

The cylindrical coordinates (r, θ, z) are a natural choice as the coordinate system of a cylindrical fuel rod. The fuel behaviour code FINIX assumes a negligible axial heat transfer and a radial symmetry removing the dependence on z and θ. The resulting time-dependent 1D heat conduction equation can thus be written as

$$C_{\mathrm{V}}(T)\frac{\partial T}{\partial t} - \frac{1}{r}\frac{\partial}{\partial r}\left[\lambda(T) r \frac{\partial T}{\partial r}\right] - s(r) = 0, \tag{95}$$

where C_{V}, λ and s are the volumetric heat capacity, the thermal conductivity and the heat source term [80]. FINIX solves the equation in the fuel and the cladding regions numerically with a built-in finite element method solver yielding a node-wise linearly interpolated temperature profile. For example, with a constant heat source and conductivity the temperature follows a simple parabolic profile.

Unfortunately, typical reactor physics codes do not model the temperature profile but require effective homogenized temperatures [81]. Especially the fuel temperature has to be considered carefully due to the Doppler broadening of the resonance peaks for it should be ensured that the reaction rates are preserved as well as possible. A simple volume-averaged temperature calculated from the continuous temperature profile is therefore not necessarily the best choice for describing the neutronics accurately.

The different effective temperature models have been studied and compared by de Kruijf in Ref. [81]. Formulas for calculating the effective fuel temperatures are mainly based on parabolic radial temperature profiles. This assumption has the advantage of being able to write the effective temperature in a simple form with the centreline and the surface temperature such is the case with the Arnold and Dannels' model [82]

$$T_{\mathrm{f,eff}} = T_{\mathrm{s}} + 0.35(T_{\mathrm{c}} - T_{\mathrm{s}}), \tag{96}$$

which, however, has been considered dubious due to the lack of theoretical background [81].

A more elegant way to calculate the effective temperature is to utilize weight factors w_i for each node-wise temperature T_i so that the fuel temperature can be written as:

$$T_{\mathrm{f,eff}} = \sum_i w_i T_i. \tag{97}$$

Fuel behaviour codes can provide the temperature for each of the nodes but calculating the required weight factors is a more complicated task. The problem has been approached, for instance, by using the volume averaged temperature as the effective temperature, i.e., applying volume weights in the Eq. (97), or by employing the chord weighting method [81]. In the latter method chords are set-up spanning the fuel region so that the different lengths and angles are covered. The chords have a temperature distribution dependent on the chord length and angle.

A more simpler model can be derived [81] from the chord weighting method by assuming that the effective fuel temperature of each chord equals the average temperature of the chord. In the event of high resonance absorption, equal weights can be assigned to the chords with the absorption focusing on the pellet's surface. Assuming as well a linear absorption with respect to the fuel temperature yields ultimately the formula

$$T_{\mathrm{f,eff}} = \int p(Y)\overline{T(Y)}dY, \tag{98}$$

known as the Rowland's model [83]. In the equation Y, $p(Y)$ and $T(Y)$ are the diametral projection of the chord, the chord length distribution and the effective temperature of the chord Y, respectively. The effective temperature of each chord is given by

Table 2: Weight factors of the Rowland model for ten equi-volume zones of a cylinder as reported in Ref. [81]

Zone i (inner to outer)	Weight w_i
1	0.079560
2	0.081176
3	0.084304
4	0.087240
5	0.090726
6	0.094994
7	0.100461
8	0.107987
9	0.119917
10	0.153034

$$\overline{T(Y)} = \frac{1}{Y}\int_0^Y T(y)dy, \tag{99}$$

with $T(y)$ as the temperature distribution of the chord's projection. For example, dividing the fuel pellet into 10 equi-volume zones gives the weight factors w_i presented in Tab. 2 for the Eq. (97). For the parabolic temperature profile the equation simplifies into [81]

$$T_{\mathrm{f,eff}} = T_{\mathrm{s}} + \frac{4}{9}(T_{\mathrm{c}} - T_{\mathrm{s}}). \tag{100}$$

The case of low absorption is less complicated for one arrives at the volume averaged temperature

$$T_{\mathrm{f,eff}} = \frac{\int_V T(r)dV}{\int_V dV}, \tag{101}$$

by simply assuming again the absorption to be linear with the fuel temperature and an isotropic neutron distribution [81]. This is the result reported also by Dresner [84]. The low resonance absorption case, i.e., the volume averaged model, has been found useful in fast reactors [81]. The cladding and the gas gap of a thermal reactor are regions of low neutron absorption, and can be approximated with the volume averaging leading to $T_{\mathrm{c,eff}}$ and $T_{\mathrm{g,eff}}$. Finally, the temperature of the moderator $T_{\mathrm{m,eff}}$ is often assumed to be fixed.

3 Implementing CFENSS-SRS for pointwise neutron cross sections and univariate fuel parameters

The novel CFENSS-SRS (**C**oupled **F**uel B**e**haviour and **N**eutronics **S**tochastic **S**ampling with **S**imple **R**andom **S**ampling) tool is based on perturbing the PENDF format microscopic neutron cross section data and univariate fuel parameters. The tool applies the GRS stochastic approach of Sec. 2.2 to quantify the uncertainty of the output space with the simple random sampling. As a demonstration, the method was implemented close to the framework of the OECD/NEA UAM-LWR Phase I benchmark case "Exercise I-1: TMI-1 PWR" [61] originally intended for studying just the stand-alone neutronics. First, we start by introducing the specifications of the benchmark before moving on to processing and perturbing the nuclear data. The section is concluded by coupling the nuclear data perturbation system to the fuel behaviour uncertainty.

3.1 OECD/NEA UAM-LWR benchmark

The OECD/NEA UAM-LWR (Uncertainty Analysis in Modelling for Design, Operation and Safety Analysis of LWRs) benchmark [61] was launched to supplement the best estimate calculations with an uncertainty and sensitivity analysis. The benchmark includes three phases with three to four exercises in each. The Phase I deals with the neutronics (cell, lattice and core neutronics), the Phase II with the full core calculations (fuel physics, thermal hydraulics and time-dependent neutronics) and the Phase III simulating the whole system (core multi-physics). In this Thesis we worked close to the framework of the neutronics phase, and more specifically, its first exercise for the Three Mile Island 1 Pressurized Water Reactor (TMI-1 PWR), although we did not limit ourselves to the pure neutronics. The structure of the Phase I is as follows:

- Exercise I-1: "Cell Physics" focused on multigroup microscopic cross section libraries and their uncertainties.
- Exercise I-2: "Lattice Physics" focused on few-group macroscopic cross section libraries and their uncertainties.
- Exercise I-3: "Core Physics" focused on core steady-state stand-alone neutronics calculations and their uncertainties.

The exact specifications of the TMI-1 exercise are presented in Tab. 4 for both hot zero power (HZP) and hot full power (HFP) reactor conditions. Assumptions of the pin cell exercise include an infinite domain, fresh fuel, no soluble boron, a steady-state simulation (no fuel depletion or fission product build-up) and no thermal expansion of solid structures (the densities and the geometries are conserved). The specifications allow two models for the pin cell geometry: the square pin cell with the specular boundary conditions and the circularized annular pin cell with the isotropic boundary conditions. Although a fast and simple approximation, the cylindrical model has been discarded as too inaccurate already in the preceding work of Ref. [68].

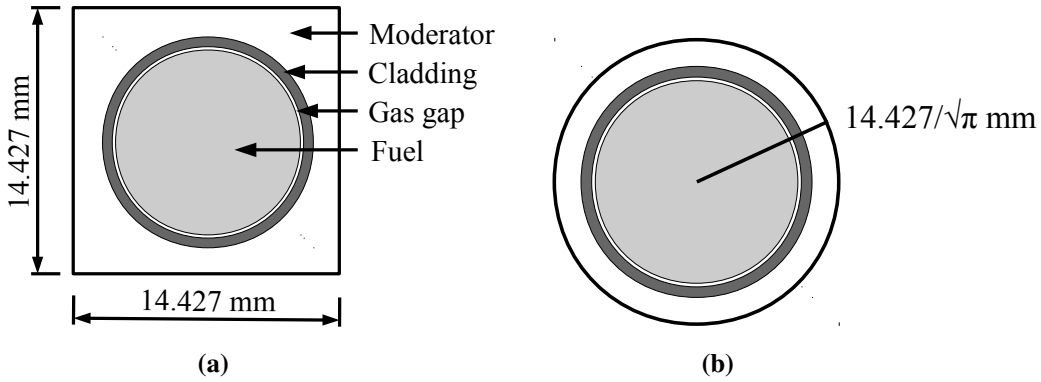

Figure 6: Illustration of (**a**) the Cartesian and (**b**) the annular pin cell geometries of the TMI-1 pin cell exercise. The schematics are not to scale.

Table 3: Nuclides and materials present in the OECD/NEA UAM-LWR TMI-1 PWR benchmark (fresh fuel). Notation "-0" refers to natural concentrations. [61]

^{1}H	^{4}He	^{16}O	Cr-0	Fe-0
Zr-0	Sn-0	^{234}U	^{235}U	^{238}U

The studied materials are mainly elements in their natural isotopic compositions and even the Zircaloy-4 of the cladding is mainly natural zirconium with only small percentages of other elements, see Tab. 3. The weight fractions of the individual isotopes in the natural mixtures can be calculated from their respective isotopic compositions [85] and atomic masses [86]. The resulting weight percentages and a detailed list of the nuclides can be found from Appendix B.

3.2 CFENSS-SRS perturbation system

Numerous computer codes were used to realise the statistical CFENSS-SRS perturbation system summarized for multigroup libraries in Fig. 7. The covariances of the nuclear data were processed with an in-house C++ code ECTS 0.93 beta (Evolved Covariance Tool Set) developed by Risto Vanhanen. The code utilized a slightly modified NJOY2012.50 for processing the covariances on the ENDF tapes to the multigroup format. A Python 2.7 code was written to process the libraries with a slightly modified NJOY99.396, perturb them accordingly (Sec. 3.2.2), and ultimately run the neutronics calculations with the lattice code DRAGON 5.0.1 ev200 (Sec. 3.2.3). The fuel behaviour code FINIX 0.15.6 provided the neutronics calculations with the densities, the geometries and the effective temperatures of the pin cell. Following the convention of the GRS method, the number of the perturbed input spaces was based on the non-parametric tolerance limits of Sec. 2.2.6. The computer used to perform the calculations was Ubuntu 14.04/Intel® Core™2 Quad Processor Q9550 @ 2.83 GHz.

Table 4: Specifications of the OECD/NEA UAM-LWR benchmark Exercise I-1 for a TMI-1 PWR pin cell. The isotopes of the cladding are present in their natural concentrations with the exception of oxygen (only ^{16}O is accounted for as stated in Tab. 3). [61]

Parameter	Value
Unit cell pitch [mm]	14.427
Fuel pellet diameter [mm]	9.391
Fuel pellet material	UO_2
Fuel density [g/cm^3]	10.283
Fuel enrichment [w/0]	4.84
U-234 [w/0]	0.0054
Cladding outside diameter [mm]	10.928
Cladding thickness [mm]	0.673
Cladding material	Zircaloy-4
Element	wt%
O	0.125
Cr	0.100
Fe	0.210
Zr	98.115
Sn	1.450
Cladding density [g/cm^3]	6.55
Gap material	^4He
Moderator material	H_2O
Fuel temperature [K]	
HZP	551
HFP	900
Gas gap temperature [K]	
HZP	551
HFP	900
Cladding temperature [K]	
HZP	551
HFP	600
Moderator temperature [K]	
HZP	551
HFP	562
Moderator density [g/cm^3]	
HZP	0.766
HFP	0.7484
Reactor power [MW_{th}]	
HZP	2.772
HFP	2772
Fuel rods per fuel assembly	208
Assemblies in the core	177
Rods in reactor	36816
Active core length [m]	3571.20

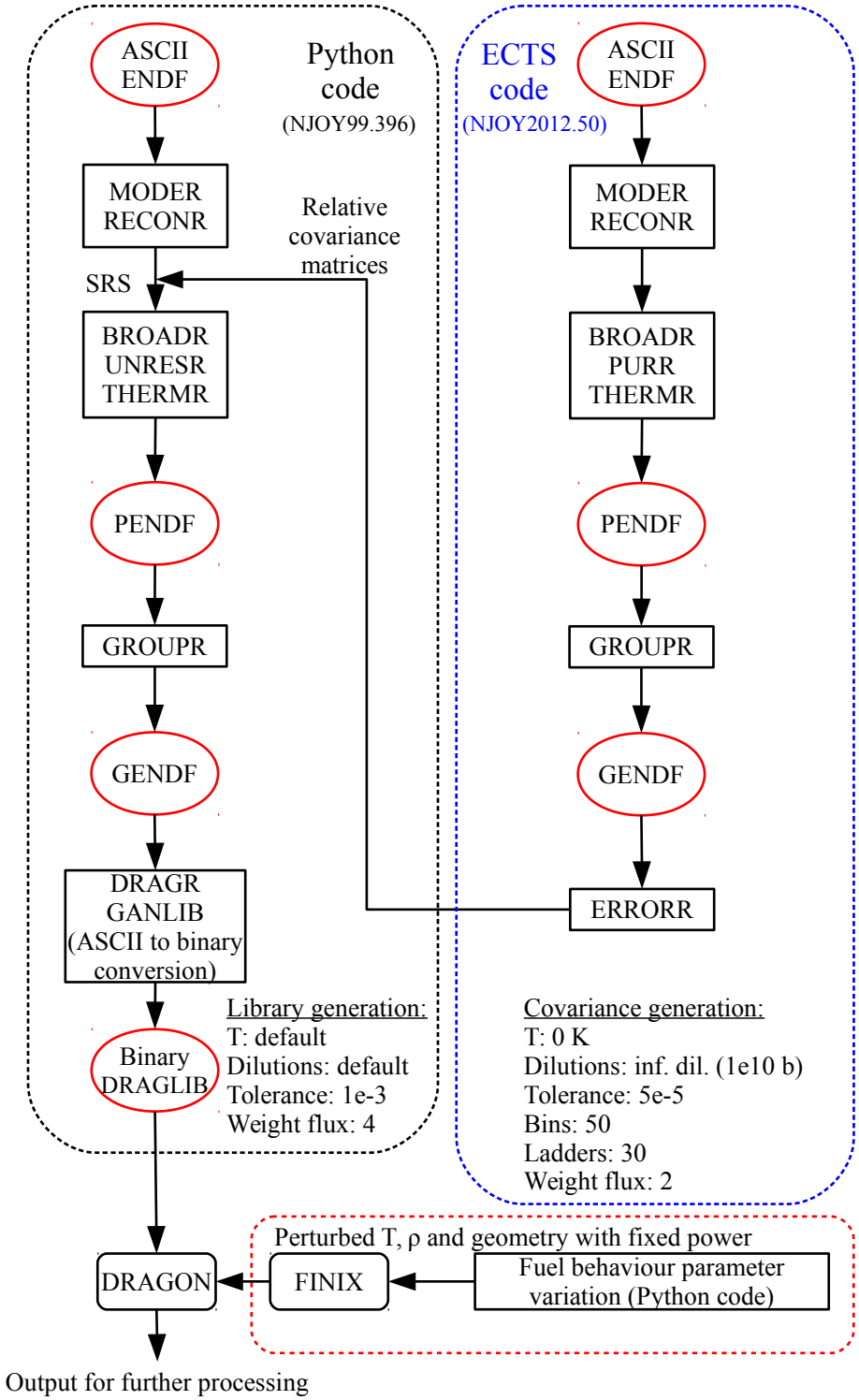

Figure 7: Statistical CFENSS-SRS perturbation system for combined FINIX-DRAGON runs with multigroup nuclear data libraries. The covariance generation is performed only once but the perturbation is done hundreds of times. The presented system yields the collection of the output vectors $(\mathbf{y}_1, \mathbf{y}_2, \ldots, \mathbf{y}_n)$ encountered in Fig. 2.

3.2.1 Nuclear data processing

The nuclear data library and the multigroup covariance library generation flowchart is presented in Fig. 7. The nuclear data libraries were generated with an extensively modified PyNjoy Python class [87] and open-source Python scripts provided along with the DRAGON code package. The original Python scripts were converted into suitable functions and integrated into the main Python code. These functions controlled the library processing by calling the modules of the NJOY99 code via the PyNjoy class. The older NJOY99, as opposed to the newer NJOY2012, had to be used for the library generation because the DRAGON code required its own DRAGLIB library format. The conversion to this format was performed with a slightly modified DRAGR module supported at the time only by NJOY99. The NJOY2012 compatible DRAGR version was released only after the library processing system was already in place.

The best estimates obtained with the latest NDLs varies around 200 pcm at maximum [68] which did not exclude any of the libraries as a poor choice for the study. Thus, the decision was based on the completeness of the high-fidelity covariance data with the ENDF/B-VII.1 NDL having the best coverage for the relevant nuclides. The nuclides were processed in series starting from the evaluated ASCII format ENDF tapes containing the nuclear data of the NDL. The tapes were first converted into a blocked binary format (MODER) before processing them into the pointwise PENDF format (RECONR). Unlike in the existing literature (see Sec. 2.3.3), the perturbation of the cross sections (Sec. 3.2.2) was done right after the RECONR module when the cross sections were still at 0 K. The Doppler broadening (BROADR), the unresolved resonances (UNRESR) and the thermal scattering (THERM) were all modelled after the perturbation step so that the uncertainty would propagate also through these models. The deterministic UNRESR module was selected instead of the probabilistic PURR module for processing the unresolved resonances because it has been judged suitable for multigroup calculations regardless of its approximations [5] while being considerably faster. Finally, the PENDF tapes were converted into the groupwise GENDF format (GROUPR) before further processing them into the ASCII DRAGLIB format with the DRAGR module. The equality module of GANLIB [88] was used to convert the DRAGLIB from the ASCII format into the binary format expected by DRAGON, see Appendix B.

The CFENSS-SRS tool was equally adept at generating the continuous energy ACE format libraries. This required only replacing the deterministic UNRESR module with the probabilistic PURR module to create the probability tables required by the Monte Carlo codes. Then the processed PENDF tapes could be fed directly to the ACE module of NJOY. Disabling the perturbation step it was also possible to construct pure ACE format NDLs for benchmarking the deterministic best estimate calculations of the DRAGON code with the Serpent code. The original mixed libraries of the Monte Carlo code have been gathered from multiple sources and would not have allowed comparable results.

A detailed list of the used NJOY processing parameters is provided in Tab. 5 but the explicit definitions of the parameters are outside our scope. Refer to the NJOY2012 manual [5] for the specific models, approximations and parameters of NJOY. The temperature and the dilution settings used in the library processing were provided by the default settings of the original Python scripts. The applied weight flux $1/E$ + *fission spectrum* + *thermal*

Table 5: Processing parameters of NJOY99/2012 for the NDL and the covariance library generation. All non-listed parameters were set as the defaults of the original Python code or the NJOY codes.

Parameter	NDL (NJOY99)	Covariances (NJOY2012)
Tolerance	$1 \cdot 10^{-3}$	$5 \cdot 10^{-5}$
Temperature	Nuclide dependent set of temperatures	0 K
Background	Nuclide dependent set of backgrounds	Inf. dil. ($1 \cdot 10^{10}$ b)
Equiprobable angles	16	16
Thermal cut-off	4.0 eV	4.0 eV
Legendres	1 to 3, nuclide dependent	1 to 3, nuclide dependent
Bins/ladders	-/-	50/30
Weight flux	1/E + fission spectrum + thermal Maxwellian (4)	Constant (2)

Maxwellian is suitable for thermal reactors [5]. The limitations of the tolerance parameter and the number of angles are discussed in Sec. 4.1.3. Both the nuclear data and the corresponding covariances were processed into a slightly modified XMAS-172 group structure [89] designed for the purposes of LWR analysis [71]. The lower and upper boundaries of the energy grid were 10^{-5} eV and 20 MeV, i.e., one energy grid point was added as the upper boundary. The functionality of the library processing system was tested successfully by generating unperturbed best estimate libraries and comparing them to the open source DRAGLIBs available at the DRAGON download site [90].

Perturbing the continuous energy cross section data as postulated in Sec. 2.3.3 requires covariances for the energy-interval-based averages. The multigroup covariances, i.e., the covariances between the multigroup-averaged quantities, can be interpreted as these covariances when a constant weight flux is used. The process was again started from the ENDF tapes containing the point covariances and ultimately computing the multigroup covariances with the ERRORR module. The tolerance parameter was set as tight as possible within the technical limitations of the code.

With processing the covariance data were reduced to the major reactions by removing possible redundant covariances. The cross-material neutron cross section covariances were neglected and only the intra-material neutron cross section covariances were utilized, while all other possible parameters such as the angular distributions, the resonance parameters and the energy grid were assumed to be exact. Lumped covariances were not present for any of the benchmark's nuclides. The covariance matrices were modified to achieve the nearest positive-semidefinite covariance matrix in the sense of the Frobenius norm, see Sec. 2.1. The inverse of the standard deviations was applied as the weight of the Frobenius norm. The achieved average best estimates and the positive eigenvalues with their corresponding eigenvectors were transferred to the nuclear data sampling in an in-house binary format.

The benchmark's specifications instruct using the same SCALE-6.0 covariance library ZZ-SCALE6.0/COVA-44G for the different nuclear data libraries. The assumption is that the relative covariances can be generalized for several libraries. [61] However, we did not restrict ourselves purely to the ZZ-SCALE6.0/COVA-44G library but a second covariance library was constructed by supplementing the ENDF/B-VII.1 evaluation with the low-fidelity covariances where no high-fidelity data were present. In practical terms, the low-fidelity covariances were introduced to the evaluation tapes with a Python script. It is notable that neither of the covariance libraries was "pure" but assembled from various sources.

3.2.2 Nuclear data random sampling

A novel method was developed for introducing the uncertainty to the cross section data. The goal was to account for a larger share of the nuclear data libraries' processing chain than before. Utilizing the covariance data of the ENDF tapes directly would have required extensive knowledge of the ENDF-6 format, see also Ref. [5]. We propose that the uncertainties can be introduced via the multigroup covariances. Similar to the already existing perturbation methods, new multigroup cross sections were random sampled one independent covariance block at a time. These blocks can be easily identified from the Fig. 5 where the full covariance matrix contains actually two independent covariance matrices on the low and high neutron energy. However, instead of directly replacing the old multigroup cross sections, the new values were divided with the best estimate average cross sections to obtain the interval specific scale factors $P_g(\Delta E)$ of Eq. (87). The simple random sampling (SRS) was selected over the LHS due to its simplicity, and because the required sample sizes were possible to reach even with the SRS method.

As noted in Sec. 2.3.3, a similar method for perturbing the pointwise-energy nuclear data has been described in Ref. [7]. However, the existing literature did not influence the Thesis' methodology as the author was unaware of it up to the moment the perturbation system was already in place and running. As opposed to the method presented here, the previous work varied the ACE-formatted data generated by NJOY's ACE module following the PURR module. Furthermore, the stochastic sampling method employed the zero cut-off instead of the re-sampling tactic. The previous work, however, confirmed the validity of the general methodology by benchmarking it against the multigroup perturbation method. cccc In the CFENSS-SRS methodology the PENDF data were modified right after the RECONR processing, i.e., the microscopic neutron cross sections to be modified were pointwise data at 0 K with a linear-linear interpolation. This allowed propagating the uncertainties through a large portion of the processing chain. Both the unresolved and the resolved resonances could have been handled better by perturbing the resonance parameters directly but this was well outside the scope of the Thesis. The longer processing chain improved the propagation of the uncertainties but, naturally, it also increased the processing time of each library sample. Optimizing the library generation time is discussed in Sec. 4.1.3.

Over the perturbation the cross section data must remain consistent and obey the summation rules of Fig. 4. Consequently, three rules were imposed on the microscopic cross sections, and thereby on the sampling algorithm, to retain the consistency within the PENDF data:

1. A parent reaction was perturbed if it had covariances while none of the recursive constituting reactions had covariances (or if it had no partial reactions to begin with).

2. A partial reaction was scaled if the parent reaction had covariances while none of the recursive constituting reactions had covariance matrices.

3. A parent reaction was summed/rebuilt from the partial reactions if any of the recursive constituting reactions had covariances (and the reaction was readily present on the tape).

The rules imply that the covariance data of the constituting partial reactions were taken into account recursively. The pointwise data were modified only for compelling reasons such as introducing the perturbation, the aim for consistency, or an occasional incorrect blocked binary format produced by the NJOY99 code. For instance, previously non-existing redundant pointwise data were not added to the tapes even though it would have been possible, hence the parentheses in the third rule.

Nuclide ^{235}U from the ENDF/B.VII.1 library and Fig. 4 can be used to demonstrate these rules. The nuclide has covariances, *inter alia*, for the elastic scattering and the fission cross sections but not for their respective parent reactions nor the constituting partial reactions. The total neutron cross section and the partial reactions of the fission reaction do, however, have cross section best estimate data. Thus, the tape carries redundant cross section data which much follow the summation rules. Let us first take a look at the simpler case of the elastic scattering. The reaction has covariance matrices while its (non-existent) partial reactions lack them so it will be perturbed accordingly and, consequently, the data of the total neutron cross section are recalculated under the summation rules to retain the consistency. Similarly, the partial reactions of the fission reaction fail in covariances and are therefore scaled under the summation rules when the fission cross section is perturbed. The partial reactions must be scaled as opposed to simply removing them for they are required in processing the angular distributions not present for the parent reaction.

The interval specific scale factors were used to scale the microscopic pointwise cross sections relatively, see also Eq. (87). The relative scaling preserved the shape of the data, e.g., the $1/v$–behaviour seen in Fig. 8, within each energy interval in contrast to absolute scaling. The scaling slightly distorted the average cross sections because on the boundaries of the energy intervals the neighbouring intervals affected the data. This was due to the linear interpolation between the adjacent data points with varying scale factors. The discontinuities followed directly from the approach to apply the covariance data. The deviations were small between positively correlated energy intervals with small uncertainties while strong negative correlations with large uncertainties yielded somewhat larger discontinuities. At all events the effect was estimated to be negligible for it was limited to the relatively few energy boundaries (171 boundaries as opposite to tens of thousands of pointwise cross section values). A negligible effect was also caused by rounding and biasing of the PENDF data when alternating between the data formats during the perturbation process.

We shall continue using the capture cross section of ^{235}U as an example. The result of a single average cross section perturbation is presented in Fig. 8. The sampling was performed with the covariance data of Fig. 5. Following the energy-dependent relative

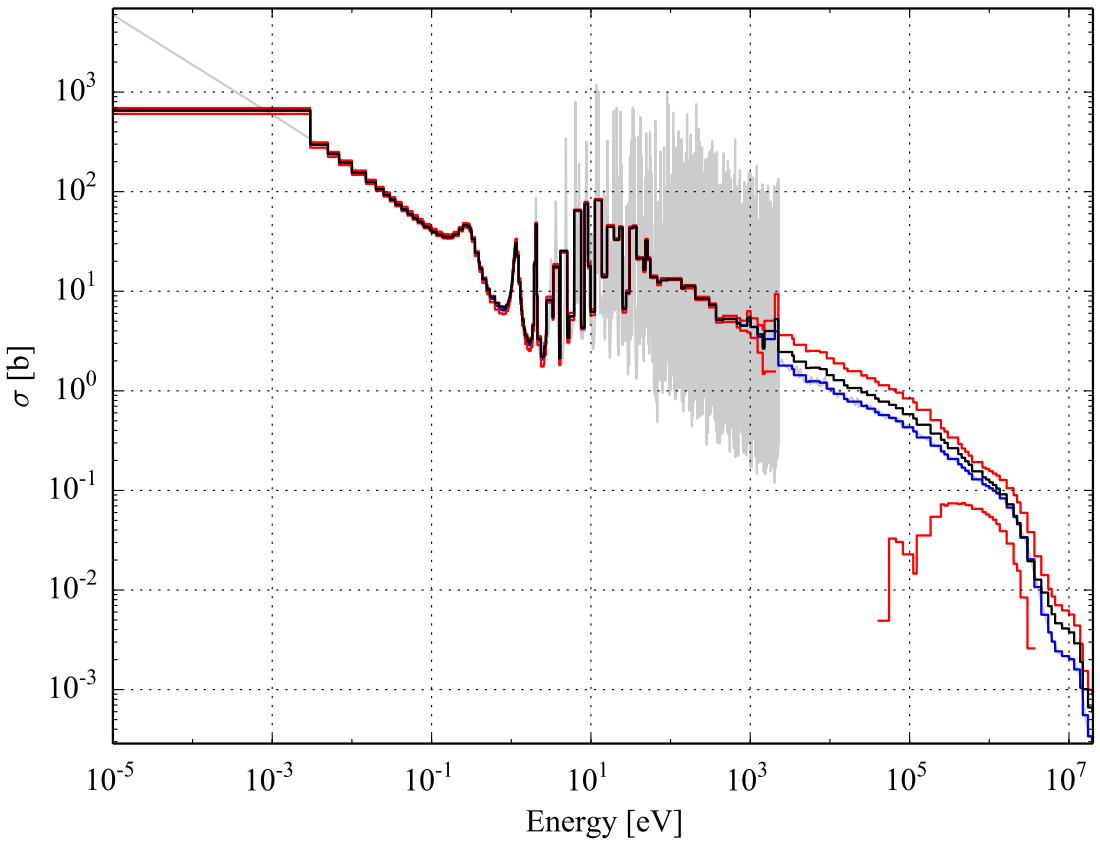

Figure 8: Nuclear data random sampling for the capture cross section of ^{235}U. The red curves bound a 95% normal distribution confidence interval on both sides of the blue best estimate average curve. The black curve represents the perturbed average cross sections while the whitened background curve is for the pointwise data. Occasionally the lower red curve disappears by dropping to negative values and outside the used scale. Comparison to Fig. 5 identifies these energy intervals as the high uncertainty regions.

standard deviations the groupwise confidence intervals vary from strict to rather loose ones. The sampled average cross sections were used to calculate the groupwise scaling factors P_g for perturbing the whitened pointwise cross sections. An interesting remark of abilities of this approximative method is that the whole energy scale from the low to high energies can be covered with a relative ease. A similar random sampling and perturbation step was performed for all suitable reactions on every simulation run.

The MEPD providing the objective choice for the random sampling of the average cross sections with relative uncertainties below 100% would have been the truncated normal distribution. For the ENDF/B-VII.1 NDL so high reaching uncertainties tend to be found from the high energy region where such uncertainties are not a rarity even for the major cross sections of important nuclides such as the ^{238}U or ^{235}U. Luckily, in thermal reactors the energetic neutrons are of lesser importance. The high uncertainties are also often related to small best estimate cross section values so that their absolute significance is lower than the relative uncertainty alone would imply. Selecting the sampling distribution

separately for every covariance block on the basis of the maximum uncertainty is hardly practical. Therefore, the truncated normal distribution was set as the pursued sampling distribution for all cross section data.

Due to the lack of a suitable method for the correlated random sampling of the truncated samples, the sampling was based on the correlated sampling of a normal distribution while re-sampling the negative values. For instance, in Fig. 8 the red lower boundary of the 95% confidence interval is below zero near 10^4 eV and again around 10^7 eV owing to the high relative uncertainties. As it is, with a non-negligible probability the random sampling would yield negative cross sections when drawing the samples from the normal distribution.

In practice, the matrix $\mathbf{A}$ of Eq. (43) was not calculated perfectly. With absolute covariance matrices this lead to a small number of positive and negative values close to zero ($|\Delta\sigma| \leq O(10^{-13})$ b) in the column vector $\mathbf{Az}$ when the corresponding elements in the best estimate vector $\mathbf{x}$ were zeros. This was caused by the errors being multiplied with the random numbers of the vector $\mathbf{z}$. Combined with the summation this caused false-positives to appear in the $\mathbf{x}_{\text{perturbed}}$ when searching for the non-physical negative values for the re-sampling. The problem was averted simply by scaling the equation for relative covariance matrices or, in the case of the absolute covariance matrices, by correcting the sampled values to zero whenever the corresponding elements of $\mathbf{x}$ were zero. The introduced error was negligible in both cases. Furthermore, the small errors also implied that the diagonalization was numerically accurate enough with the used matrix dimensions.

3.2.3 FINIX-DRAGON coupling and perturbation of fuel behaviour

FINIX and DRAGON were connected together to allow deterministic neutronics calculations with an improved model for the fuel behaviour. As shown in Fig. 7 the connection was done via the geometry parameters such as the fuel pin radius, and the temperature and the density profile. This allowed accounting for, e.g., the thermal expansion of the solid structures. It was decided to use a single material region for each of the four main pin cell sections: the fuel, the gas gap, the cladding and the moderator, and couple the codes via the densities and the effective temperatures of the regions. These were handled as discussed in Sec. 2.4.1 and Sec. 2.4.2. The effective temperature of the fuel was calculated with the parabolic Rowland model based on the results of Sec. 4.1.1. The single region fuel pellet is common in reactor physics calculations [71] but the accuracy of the simulation was nevertheless improved by employing the radial splitting directive available in DRAGON for the fuel and the cladding regions.

Coupling the lattice code to the fuel behaviour code shifted the effective multiplication factor and the other responses due to a distinct temperature profile compared to the benchmark's specifications. To avert this, the power form factor of the pin cell was selected carefully so that with the best estimate values the FINIX code produced the 900 K fuel temperature within the accuracy of $O(10^{-7}$ K) or less than 0.1 pcm. The coolant temperature was fixed to the 562 K by the input but the cladding ($T_c = 600\,\text{K} \rightarrow 589\,\text{K}$) and the gas gap ($T_g = 900\,\text{K} \rightarrow 662\,\text{K}$) temperatures were also shifted. Despite significant shifts in an absolute sense, to the neutronics the impact of the deviations was only around 2 pcm and, hence, negligible.

Table 6: Model settings for the DRAGON and FINIX codes

DRAGON parameter	Type/value/model
Geometry type	Cartesian square cell
Boundary conditions	Specular (mirror-like)
Fuel nodes	25
Gas gap nodes	1
Cladding nodes	10
Tracking module (nangl, dens)	EXCELT (12, 20.0)
Self-shielding module	SHI
Livolant-Jeanpierre	Yes
Nordheim distributed model	Yes
Riemann integration method	Yes
FINIX parameter	**Type/value**
Simulation mode	Steady-state
Pellet radial nodes	40
Cladding radial nodes	40
FINIX-DRAGON interface	
$T_{\mathrm{f,eff}}$	Rowland parabolic Eq. (100)
$T_{\mathrm{g,eff}}$ and $T_{\mathrm{c,eff}}$	Volume averaged Eq. (101)
$T_{\mathrm{m,eff}}$	Constant (benchmark specifications)
Rod power	Scaled to achieve $T_{\mathrm{f}} = 900\,\mathrm{K}$

The perturbation of the fuel parameters was based on the work of Ikonen and Tulkki discussed in Sec. 2.4. All of the parameters of Tab. 1 were perturbed within the technical limitations of the FINIX code with the notable exception of the rod power fixed to achieve the desired temperature profile. Applying a suitable power form factor as described earlier was justifiable because the Thesis considered a small arbitrary segment of the fuel rod and, hence, there was no compelling reason to favour one rod power over another.

The settings of the DRAGON code were based on the previous study [68] and the results of Sec. 4.1.2. The parameters are listed in Tab. 6 along with all relevant FINIX settings. The nodalizations were selected so that the responses were converged and numerically stable. Default values were applied for all parameters not mentioned in the list. Ultimately, the DRAGON lattice code was directed to compute the one-group constants along with the effective multiplication factor. The post-processing of the results was performed with a Python script relying on Python's scientific computing package NumPy and plotting library matplotlib [91].

4 Statistical uncertainty and sensitivity analysis results

The results of this Thesis can be roughly divided into two distinctive parts. First, we shall cover the results enabling the practical implementation of the CFENSS-SRS system. These include studies of, *inter alia*, the modelling and discretization options as well as the numerical stability. It was confirmed that the numerical behaviour of the calculation system did not depend on the perturbed input spaces. The result was vital so that the output uncertainties could be fully attributed to the perturbed input data. The constant parameters did, however, have a significant impact on the best estimates and, thus, one of the goals was to achieve the best possible accuracy with a reasonable computational time. In the second subsection the results of the actual uncertainty analysis and a rough code based sensitivity analysis are presented. Various sampling methodologies and covariance libraries are compared. All reported results are for the ENDF/B-VII.1 NDL.

4.1 Results of the CFENSS-SRS system

Comprehensive studies leading to the selection of the DRAGON parameters of Tab. 6 have been previously presented in Ref. [68]. There it was found that, depending on the choice of tracking parameters of the EXCELT module, the k_{eff} varies systematically around 200 pcm. To conclude the parameter selection studies, the effective temperature models, the numerical behaviour of DRAGON and the processing time optimization of the NDL generation were all studied extensively. Without accurate best estimate results the reliability of the uncertainty and sensitivity analysis could be rightly challenged.

4.1.1 Temperature models for the FINIX-DRAGON interface

As explained in Sec. 4.1.1, there are several models with varying degrees of complexity for computing the effective temperature of a region, especially the fuel temperature. In this research the moderator temperature was fixed while the effective temperature of the cladding was taken as the average temperature for it corresponded to the low resonance absorption case discussed in Sec. 2.4.2. Considering the nuclear fuel the literature implied that the outcomes of the models would differ [81] and, hence, test runs were performed for the pellet's temperature both in the HZP and the HFP conditions of the UAM-LWR benchmark without any perturbation. The Arnold and Dannels' model, the Rowland's model with the weight factors, the Rowland's model with the parabolic r^2 approximation and the volume weighted average were compared by calculating the effective multiplication factor with the different temperature profiles.

In the HZP conditions the results were close to each other: the fuel temperatures and the effective multiplication factors were within 0.1 degrees and 0.1 pcm of each other. Consequently, these results did not give any implication on which model to select but they confirmed that all four models predict correctly at least the effective temperature of the constant (flat) HZP profile around 551.4 K. The results for two different pellet axial nodalizations in the HFP conditions are presented in Tab. 7. The weighted model of Rowland used the pre-calculated weight factors listed in Tab. 2. The corresponding weight factors were not computed for the 16 nodes' case.

Table 7: Effective temperature model results for the temperature and the k_{eff} variation in the HFP reactor conditions. The parabolic Rowland model was used as the reference level in the related neutronics calculations.

Model	T_{eff} with 10 zones [K]	T_{eff} with 16 zones [K]
Rowland–parabolic	963.9	960.7
Rowland–weighted	938.7	-
Arnold and Dannels	916.3	913.8
Volume weighted	964.6	964.8
	k_{eff} with 10 zones [K]	Δk_{eff} [pcm] with 10 zones
Rowland–parabolic	1.395475	0.0
Rowland–weighted	1.396313	83.8
Arnold and Dannels	1.391764	168.8
Volume weighted	1.395340	-13.5

Contrary to the HZP case, the results of the four models differ in the HFP conditions. Based on the literature discussed in Sec. 4.1.1, the weighted Rowland model should be selected especially if the temperature profile deviates from the parabolic profile to a significant extent. However, this work considered only the steady-state situation in which the temperature profile is nearly parabolic according to both the literature [71, 81] and a visual inspection of the node-wise interpolated profile from FINIX. The use of the weight factors would have demanded additional computational and human resources as the practical implementation of the weight factors is a nontrivial task. Hence, the more simpler parabolic model was selected but, as a result, the capabilities of the continuous radial temperature profile provided by FINIX were not fully harnessed. The approximation decreased the k_{eff} best estimate around 80 pcm and while not a negligible impact it is still less than the ~200 pcm variation of the EXCELT module.

4.1.2 Convergence tests for FINIX and DRAGON

Convergence test were performed for both the FINIX and the DRAGON code to ensure the numerical stability with the different nodalizations and the perturbed input data. The fuel behaviour code supports also very dense radial discretizations. In Fig. 9 the effective temperature of the fuel is calculated with the parabolic Rowland's model while tightening the nodalization. While visually the temperature appears to converge after a couple hundred nodes, it actually takes up to ~350 000 fuel pellet nodes before the slowly decreasing curve finally acquires fluctuations. The convergence test was repeated for the cladding nodalization with similar results, although this time with an increasing temperature behaviour. The dense nodalizations do not cause in any way a significant increase in the total computational time but nonetheless such high nodalizations are hardly sensible. It was decided to use 40 cladding and fuel pellet nodes leading to a systematic discretization error of a negligible 1 pcm.

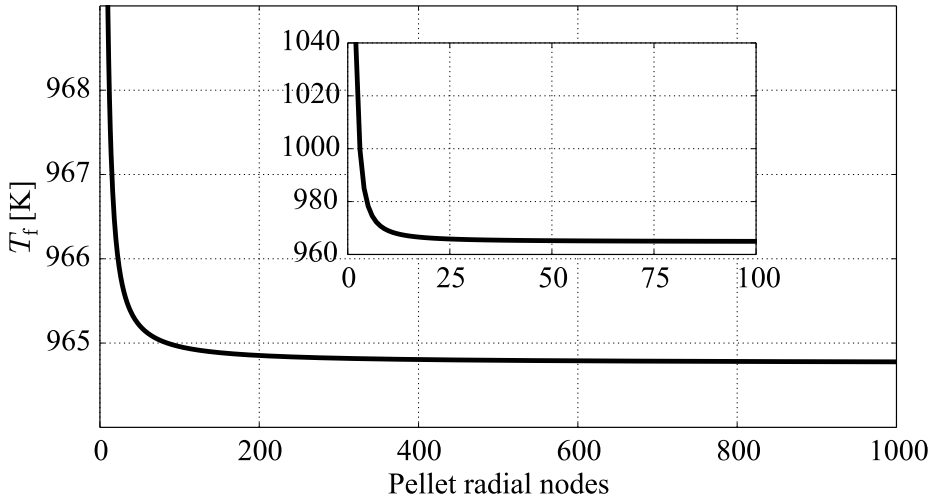

(a)

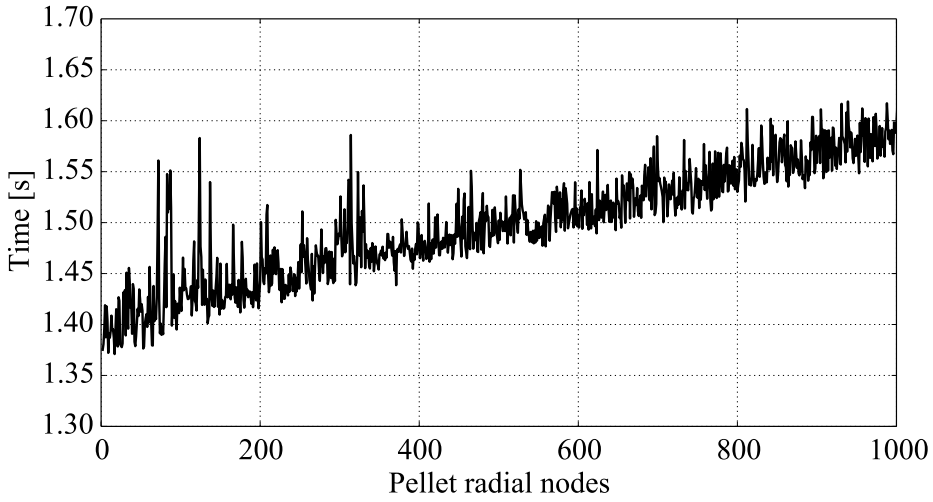

(b)

Figure 9: Convergence test results for the fuel pellet radial discretization in FINIX with two radial cladding nodes: **(a)** the effective pellet temperature and **(b)** the processing time of the FINIX code as a function of the pellet radial nodalization.

Tracking discretization convergence tests have been performed for the DRAGON code earlier in Ref. [68]. Here those studies were further extended to confirm the stability of DRAGON's numerical behaviour with the perturbed nuclear data libraries. An example of the results is shown in Fig. 10 where the k_{eff} has been calculated for different tracking discretization combinations (dens, nangl) with the EXCELT tracking module and the specular boundary conditions. The visual inspection was supplemented by calculating the maximum variation and Pearson's correlation coefficient for the two sets of data, and performing a statistical test with the null hypothesis of uncorrelated samples, see Tab. 8. The tests were repeated with similar results for the EXCELT module with the isotropic

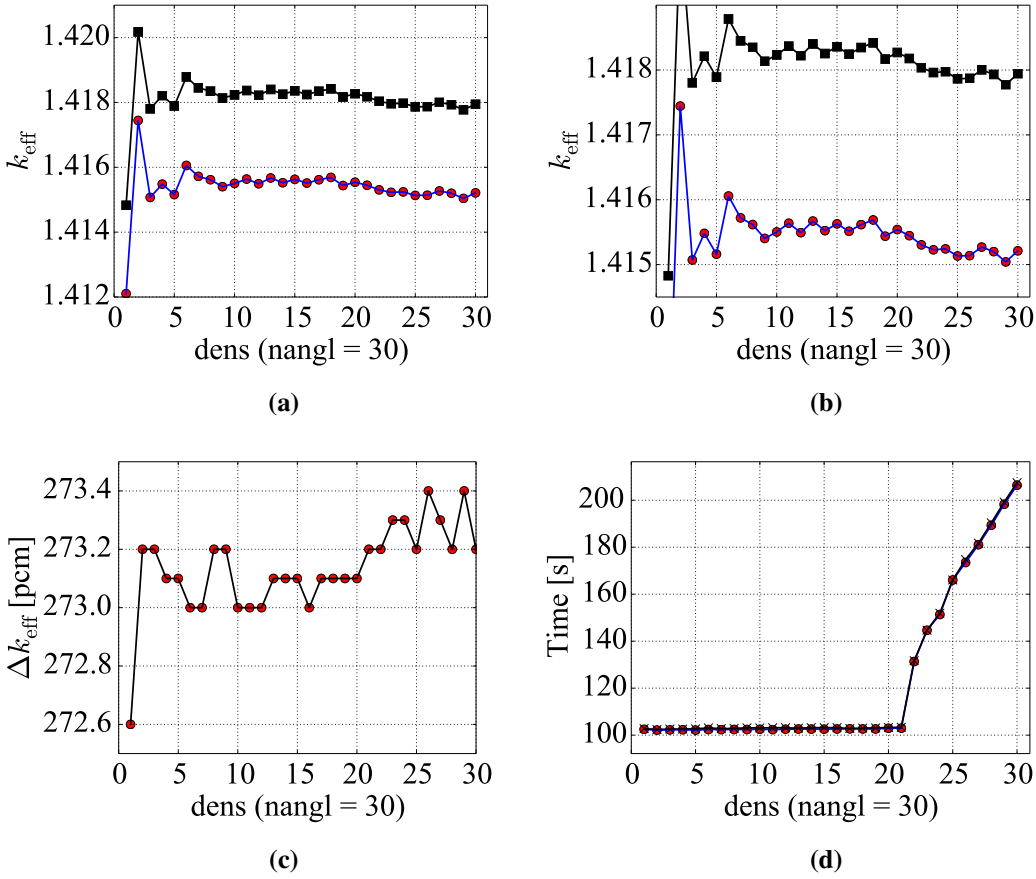

Figure 10: Convergence test for DRAGON with the EXCELT module and specular boundary conditions. (**a**) The effective multiplication factor with two perturbed NDLs, (**b**) a zoomed in picture, (**c**) the difference and (**d**) the computational time. The parameters "dens" and "nangl" control the tracking line density and the number of angles.

Table 8: Maximum variations and correlation coefficients of the numerical stability tests

Tracking module/BC	Max. variation [pcm]	ρ
EXCELT/specular	0.4	0.999998
EXCELT/isotropic	2	0.999997
SYBILT/isotropic	-	0.999990

boundary conditions and for the SYBILT module with the annular pin cell geometry. The p-values did not support the uncorrelation hypothesis and with the high correlation coefficients we can conclude that the numerical behaviour of DRAGON is not affected by the perturbation of the library data. Thus, we reach the vital conclusion that the lattice code does not introduce any stochastic uncertainty to the calculations but only slightly shifts the output distribution.

Table 9: Optimization results of the nuclear data library processing. The k_{eff} calculations were performed on the UAM-LWR benchmark in the HFP conditions with the Cartesian cell geometry and the EXCELT tracking module.

Tolerance	Angles	Time [h]	Δk_{eff} [pcm]	Comments
$5 \cdot 10^{-5}$	16	5.0	-0.8	
$5 \cdot 10^{-5}$	24	5.2	-0.8	
$1 \cdot 10^{-4}$	24	3.0	0.0	
$5 \cdot 10^{-4}$	24	3.2	-1.8	Anomaly, the test run was performed under heavy parallel computation
$1 \cdot 10^{-3}$	16	1.6	0.0	Open source, reference
$1 \cdot 10^{-3}$	16	1.5	-11.4	Bootstrapping on
$1 \cdot 10^{-3}$	24	1.8	-4.7	

4.1.3 Run time optimization of the nuclear data library processing

The computational time of a single simulation run is dominated by the generation of the DRAGLIB library with the NJOY99 code, taking around an hour and a half at minimum as opposite to the 20 minutes of the DRAGON run and the one second required by the FINIX code. The reasonable processing time was reached with a series of test runs. The tolerance, number of equi-probable scattering angles and the bootstrapping option of the BROADR module were varied to determine their impact on both the processing time and the accuracy of the code. Other settings of NJOY99 were set as presented in Tab. 5.

The results are summarized in Tab. 9. The minimum tolerance is greatly limited by the processing time while the number of angles has its own smaller impact. Using looser settings does not, however, have a great effect on the results when the settings of the open source DRAGLIBs are used as a reference level. The bootstrap approximation does not greatly decrease the run time but it has a significant impact on the effective multiplication factor. For confirmation, the calculations were repeated by employing the SYBILT module with similar results. Ultimately, and perhaps unsurprisingly, the settings of the open source DRAGLIBs used as the reference values are found to be the optimal settings in the trade-off between the accuracy and the required CPU resources. The processing time of the libraries could certainly be further decreased with a better knowledge of, for instance, the necessary minimum coverage of the temperature and the dilution parameters used in the input of the NJOY code.

4.2 Uncertainty and sensitivity analysis results

The uncertainty analysis methodologies of the nuclear engineering literature are varying in almost every aspect: the used covariance data, the selected sampling method (SRS/LHS), the varied parameters (pointwise or multigroup) and controlling the unphysical negative values of the inherently positive parameters. This leads rather predictably to discrepancies in the results and motivated the study of the different methodologies. In literature, as well as in this Thesis, the effective multiplication factor is certainly the most studied

Table 10: Deterministic and Monte Carlo best estimate results for the effective multiplication factor and the $\nu\Sigma_f$ in fuel. A deterministic best estimate simulation was performed on both the benchmark's HFP temperature profile (UAM-LWR HFP) and the corresponding profile provided by the FINIX code (FINIX HFP). The Monte Carlo results are accompanied by their statistical errors.

Code/temperature profile	k_{eff}	$\nu\Sigma_f$ [cm^{-1}]
DRAGON/UAM-LWR HFP	1.409553	0.100380
FINIX-DRAGON/FINIX HFP	1.408579	0.098227
Serpent/UAM-LWR HFP	1.413660 ± 0.00014	0.098628 ± 0.00012

response but also other responses such as the one-group constants can be considered. As a demonstration the one-group $\nu\Sigma_f$ for the fuel was selected as a secondary response.

The first runs performed with the CFENSS-SRS computational system were dedicated for best estimate analysis. Both the UAM-LWR benchmark's HFP temperature profile and the corresponding temperature profile from FINIX discussed in Sec. 3.2.3 were studied. The calculations yielded the results shown in Tab. 10 with the deterministic results being complemented by a Serpent Monte Carlo run. The Monte Carlo run was performed with a pure ENDF/B-VII.1 ACE-formatted nuclear data library rather than the readily available impure nuclear data libraries of the Serpent code. The ACE-library was generated with the tools available in the CFENSS-SRS code. The agreement between the deterministic runs is good as can be expected from the small differences in the temperature profiles. The Monte Carlo result computed with the input file of Appendix C shows that the total modelling error of the DRAGON code is around 400 pcm. The fluctuations originating from the tracking parameter selection of DRAGON is ~200 pcm so the deterministic and the Monte Carlo results are clearly different. However, such differences have been encountered also in the literature [68].

Next, we shall turn our focus on the actual uncertainty and sensitivity analysis. The two-sided tolerance intervals were employed to determine the sufficient sample size as no real safety limits were involved. The $\alpha/\beta = 95/95$ rule ($n \geq 93$) deemed sufficient by IAEA was not used as such, but the sampling was continued even after this limit until the mean and the standard deviation were converged within a reasonable accuracy. The convergence was reached usually after 300 simulations but perturbing just the fuel behaviour parameters required exceptionally 1000 simulation runs. This exception was not a major issue in regard of the computational time as the most time consuming task was perturbing, and then rebuilding, the nuclear data library.

The distribution-free sample parameters of the uncertainty analysis results are presented in Tab. 11. Six different "methods" or cases were studied varying the covariance libraries, the involved codes and the extent of the perturbation step. The method 1 applies the implemented CFENSS-SRS methodology to its full extent while, for example, the second method applied the code coupling but not the neutronics perturbation. The methods from 3 to 6 used the UAM-LWR benchmark's HFP temperature profile while the methods 1 and 2 applied the corresponding profile computed with the FINIX code. As expected, perturbing the fuel behaviour parameters alongside the nuclear data library increases the

Table 11: Sample mean $\bar{m}$ and relative sample standard deviation $\bar{v}_{\mathrm{rel}}$ for the studied methods with respective sample sizes n. The keywords F, D, E, S, a, r, rs and zc refer to sampling the fuel behaviour parameters, perturbing the nuclear data library, the ENDF/B-VII.1 covariance library supplemented with the low-fidelity covariances, the SCALE6.0 covariance library, absolute covariance matrices, relative covariance matrices, and the resampling and the zero cut-off strategies, respectively. For instance, "F + D" refers to a combined FINIX-DRAGON run with the perturbation of both the fuel behaviour parameters and the nuclear data library. The notation "E/rs (r)", in turn, implies perturbing the NDL with the pure relative ENDF-VII.1 high-fidelity covariance library supplemented with the low-fidelity data while resampling the negative values. Combined these are the CFENSS-SRS method (method 1).

Method	Covariance	Response	n	$\bar{m}$ [unit]	$\bar{v}_{\mathrm{rel}}$ [%]
1)	F + D, E/rs (r)	k_{eff}	407	1.408534	0.484
		$\nu\Sigma_{\mathrm{f}}$		$0.098\,\mathrm{cm}^{-1}$	1.444
2)	F, E/rs (r)	k_{eff}	1000	1.408507	0.265
		$\nu\Sigma_{\mathrm{f}}$		$0.098\,\mathrm{cm}^{-1}$	1.086
3)	D, E/rs (r)	k_{eff}	415	1.410155	0.389
		$\nu\Sigma_{\mathrm{f}}$		$0.100\,\mathrm{cm}^{-1}$	0.891
4)	D, S/rs (r)	k_{eff}	402	1.409933	0.374
		$\nu\Sigma_{\mathrm{f}}$		$0.100\,\mathrm{cm}^{-1}$	0.867
5)	D, S/rs (a)	k_{eff}	300	1.409616	0.387
		$\nu\Sigma_{\mathrm{f}}$		$0.100\,\mathrm{cm}^{-1}$	0.801
6)	D, S/zc (r)	k_{eff}	276	1.409597	0.356
		$\nu\Sigma_{\mathrm{f}}$		$0.100\,\mathrm{cm}^{-1}$	0.830

total relative uncertainty. The $\nu\Sigma_{\mathrm{f}}$ reveals somewhat larger relative uncertainties compared to the effective multiplication factor. Other one-group constants, for instance, the one-group absorption and scattering cross sections, were also considered confirming the validity of the results to be presented but otherwise they are excluded from further analysis.

The parametric normal distribution confidence intervals of the responses are given in Tab. 12. As explained in Sec. 2.1.1, with large sample sizes the distribution approaches the normal distribution regardless of the underlying distribution of the individual runs. The χ^2 normality test was performed on the samples to check whether the they could be modelled with the normal distribution applying the two sample moments. Of the two confidence intervals, the standard deviation's holds a greater importance as it narrows down the possible (probable) range of the population standard deviation. Considering the effective multiplication factor the zero cut-off leads to a much lower p-value, and hence a deviation from the normal distribution, than the re-sampling strategy. With the conventional 5% significance level the deviation cannot be attributed to the statistics alone and, thereby, the zero cut-off approach distorts the output distribution. As it is, the confidence intervals

Table 12: Parametric confidence intervals for the means and the relative standard deviations of the studied methods alongside their χ^2 normality test p-values. The notation follows Tab. 11.

Method	Covariance	Response	p	$\Delta\bar{m}$ [unit]	$\Delta\bar{v}_{\mathrm{rel}}$ [%]
1)	F + D, E/rs (r)	k_{eff}	0.93	66 pcm	0.453; 0.520
		$\nu\Sigma_{\mathrm{f}}$	0.87	$1.4 \cdot 10^{-4}$ cm^{-1}	1.351; 1.550
2)	F, E/rs (r)	k_{eff}	0.07	23 pcm	0.254; 0.277
		$\nu\Sigma_{\mathrm{f}}$	0.18	$6.6 \cdot 10^{-5}$ cm^{-1}	1.040; 1.135
3)	D, E/rs (r)	k_{eff}	0.38	53 pcm	0.364; 0.417
		$\nu\Sigma_{\mathrm{f}}$	0.84	$8.6 \cdot 10^{-5}$ cm^{-1}	0.834; 0.956
4)	D, S/rs (r)	k_{eff}	0.46	52 pcm	0.350; 0.402
		$\nu\Sigma_{\mathrm{f}}$	0.45	$8.5 \cdot 10^{-5}$ cm^{-1}	0.811; 0.931
5)	D, S/rs (a)	k_{eff}	0.45	62 pcm	0.358; 0.420
		$\nu\Sigma_{\mathrm{f}}$	0.25	$9.1 \cdot 10^{-5}$ cm^{-1}	0.741; 0.870
6)	D, S/zc (r)	k_{eff}	0.01	NaN	NaN
		$\nu\Sigma_{\mathrm{f}}$	0.97	$9.8 \cdot 10^{-5}$ cm^{-1}	0.766; 0.906

of the normal distribution are invalid for the zero cut-off case ($p \leq 5\%$). For the second response the situation is the opposite with perfectly valid confidence intervals.

Eyeing the results of the methods 2 and 3 reveals that the impact of the fuel behaviour parameters to the relative uncertainty of k_{eff} is somewhat smaller than that of perturbing the nuclear data library but still significant. The methods 3 and 4 were used for comparing the nuclear data covariance libraries with the extended ENDF/B-VII.1 covariance library yielding a slightly higher relative uncertainties than the ZZ-SCALE6.0/COVA-44G covariance library from SCALE6.0. The methods 4 and 5, in turn, were introduced to study switching between the relative and absolute covariance matrices while the methods 4 and 6 were used for comparing the zero cut-off strategy to the re-sampling method. The spread of the relative uncertainties resulting from these nuclear data uncertainty propagation experiments was small for the effective multiplication factor as well as the one-group $\nu\Sigma_{\mathrm{f}}$.

The first method is the actual CFENSS-SRS method while the third method is comparable to the nuclear data perturbation studies available in the literature. The convergence of the sample moments of the CFENSS-SRS method is shown in Fig. 11. Increasing the number of simulations would continue decreasing the confidence intervals of the moment estimates towards zero. The sample mean stabilizes fast while the relative sample standard deviation converges after 300 simulation runs. The k_{eff} convergence results of the other methods are provided in Appendix A.

The final output distributions of the first and the third method are shown in Fig. 12. An example of the $\nu\Sigma_{\mathrm{f}}$ distribution is provided for comparison. Both the empirical cumulative distribution functions and the kernel density estimates follow closely the corresponding normal distributions as can be expected from the p-values of Tab. 12. The distributions are approximately symmetrical around the closely located best estimates and sample means.

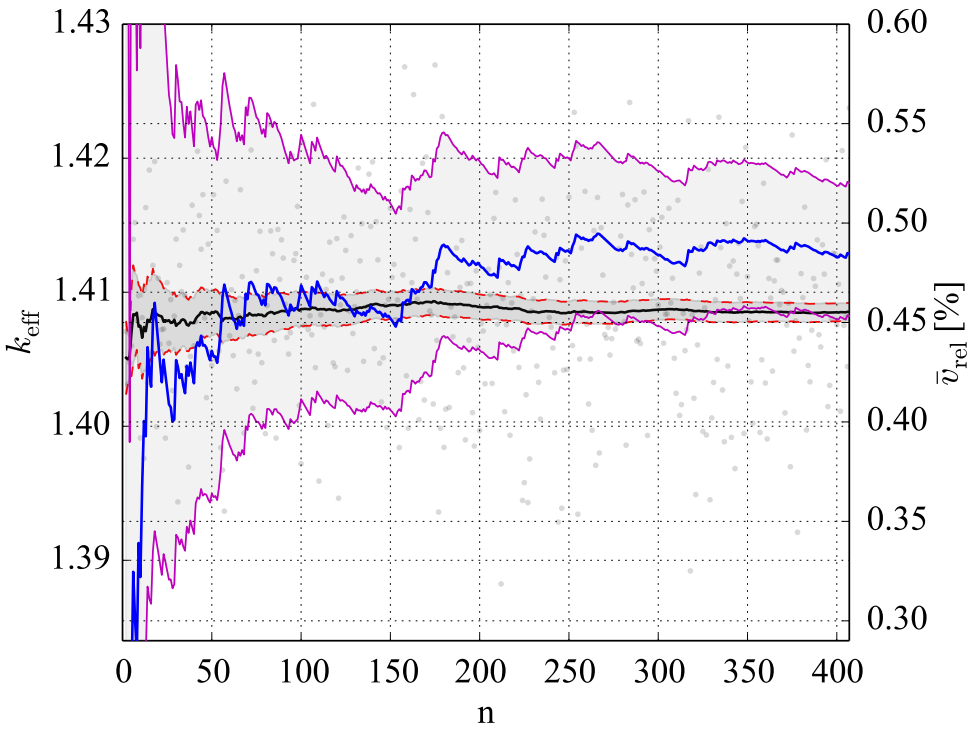

Figure 11: Convergence results for the sample mean and the relative sample standard deviation of the CFENSS-SRS method (method 1). The mean is drawn with a solid black line bounded by two dashed red lines illustrating the 95% confidence interval. The relative standard deviation and its 95% confidence interval are drawn with solid blue and purple lines, respectively. The results of the individual simulations are whitened on the background.

Plotting the kernel density estimates and the relative uncertainties of all six method together for studying the effect of the code coupling yields Fig. 13. The curves show the widening of the continuous probability distributions as the relative standard deviation increases. The bar graph underlines the differences in the perturbation methods. These are discussed more in Sec. 5.

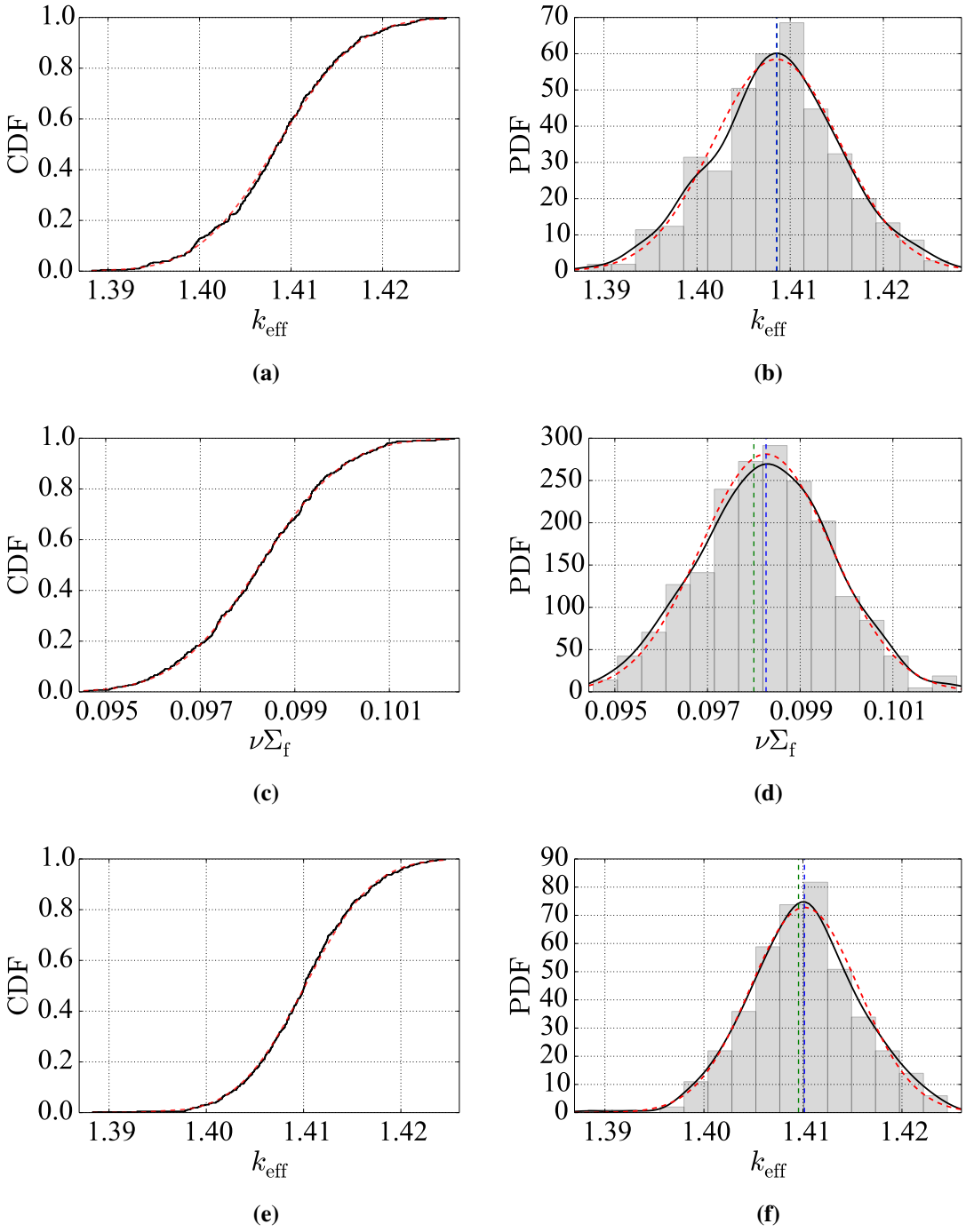

Figure 12: Empirical cumulative distribution functions and their normal distribution fits for **(a)** the k_{eff} and **(c)** the $\nu\Sigma_{\mathrm{f}}$ of the method 1 and **(e)** the k_{eff} of the third method. The subfigures **(b)**, **(d)** and **(f)** present the respective kernel density estimates of the probability distribution functions accompanied by 15 bin histograms. The ECDFs and the KDEs are drawn with solid black lines while dashed red lines are reserved for the fitted normal distribution. The partly overlapping green and blue dashed vertical lines of **(b)**, **(d)** and **(f)** mark the best estimate and the sample mean.

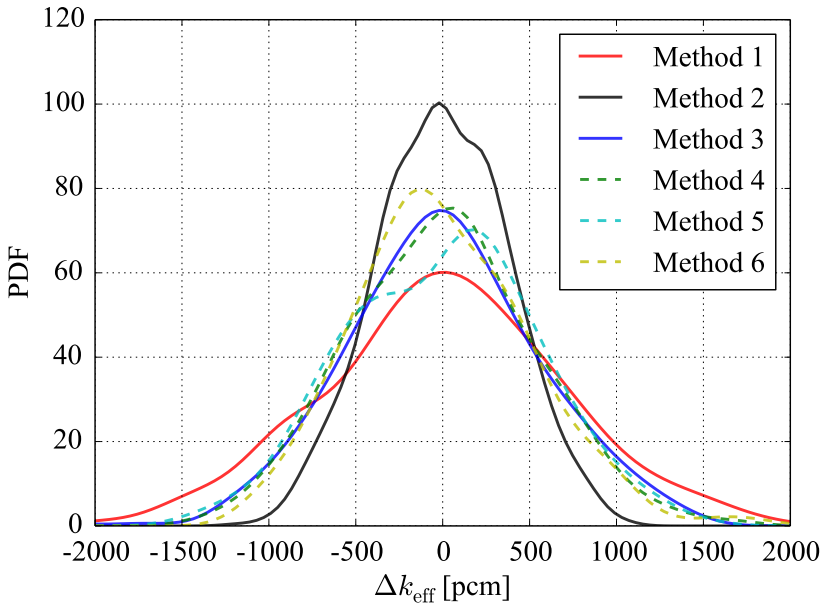

(a)

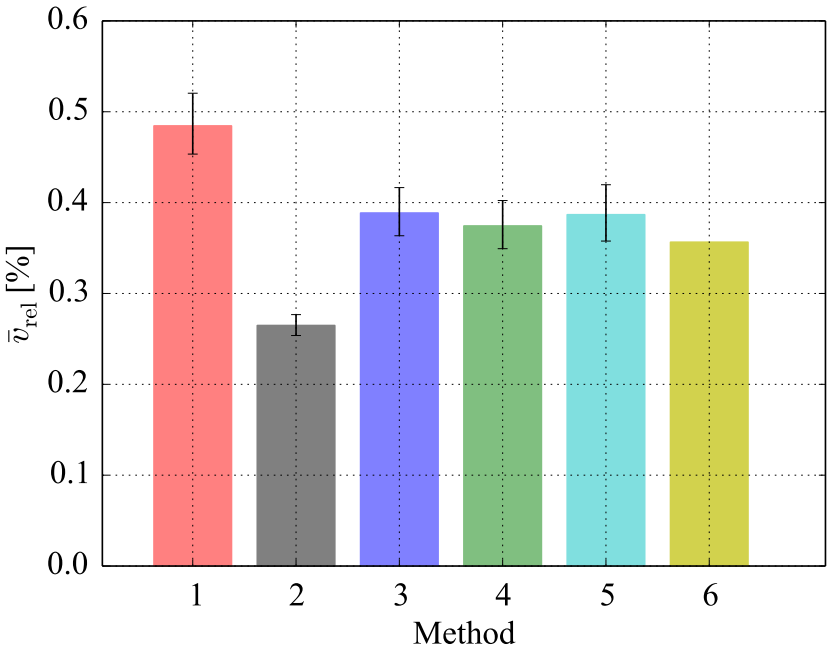

(b)

Figure 13: Impact of the code coupling to the output uncertainty of the effective multiplication factor. In **(a)** the KDEs of the six methods are presented, while in **(b)** the corresponding relative standard deviations with their 95% confidence intervals are given as a bar graph. The KDEs have been centralized around the sample means.

5 Discussion

The main goal of this Thesis was to reveal whether the fuel behaviour and the neutronics uncertainties could be handled separately and simply summed in quadrature to reach the total combined uncertainty. The statistics of the results was sufficient for asserting with a good confidence that this can indeed be done. Considering the effective multiplication factor, the bar graph of Fig. 13 highlights that the first three methods are outside each other's confidence intervals, implying that the differences are not due to chance alone but are the direct consequences of the perturbations. Assuming the relative standard deviations of the methods 2 and 3 to be independent and adding them with the well-known quadrature formula for the propagation of errors

$$\Delta k_{\text{eff,tot}} = \sqrt{\sum_i \Delta k_{\text{eff},i}^2}, \tag{102}$$

yields the total uncertainty of the method 1, i.e., the full CFENSS-SRS method, within the accuracy of the confidence interval. The result applied also to other responses. Therefore, such coupled perturbation systems as presented in this study are perhaps no longer a necessity and the uncertainty components could be studied separately. However, the relatively large confidence intervals ask for higher sample sizes to confirm the result. In any case, the fuel behaviour and the neutronics must still be coupled to obtain the output uncertainty attributed to the fuel behaviour in the neutronics responses.

The different nuclear data perturbation strategies were studied with the methods 3, 4, 5 and 6. The differences in the relative library uncertainties are so small that the acquired statistics is still insufficient for a detailed analysis as the confidence intervals overlap. For instance, both the relative and the absolute covariance matrices yielded similar response uncertainties as did the comparison between the two covariance libraries. With the current spread in the relative standard deviations more than 1000 simulation runs would be required before strong assertions could be made regarding the differences between the methods. The only clear deviation is the distorting effect of the zero cut-off approach on the effective multiplication factor's distribution shape limiting the further parametric analysis. The different covariance libraries should be studied more as, for example, in Ref. [21] the ENDF/B-VII.1 and the JENDL-4.0 covariance libraries were found to differ greatly.

The kernel density estimates of Fig. 13 show similar approximately symmetrical output distributions. Even the small bend in the curve of the fifth method can still be attributed to the statistics alone with the reasonably high p-value. Only the positive skewness related to the zero cut-off approach in the method 6 stands out. The skewness is more noticeable when the distribution is plotted separately, see Fig. A2. It appears that the zero cut-off approach should not be used for the undesired negative values due to the strong distorting impact but instead, for instance, sampled again as done in the CFENSS-SRS method. The approach will nevertheless remain inevitably approximate while the generalized sampler for the correlated multivariate truncated normal distribution is not available.

The propagated uncertainty is in all cases larger than the maximum ~200 pcm impact from most of DRAGON's parameters discussed in Sec. 4.1. Thus, it appears that the accuracy of the deterministic best estimate results are currently restricted by the precision

of the nuclear data and the fuel behaviour parameters. At the least this applies to the DRAGON code as long as the code's user is reasonably experienced in selecting the suitable submodels and their parameters.

The uncertainty analysis yields considerably lower relative uncertainties for the effective multiplication factor than the ~0.5% generally encountered in the literature. Based on Ref. [92] and a private communication with Maria Pusa, the total contribution of the average total fission neutron production and the fission spectrum from ^{235}U and ^{238}U to a total relative uncertainty of 0.512% is around 42.5 %. Assuming the same fraction being neglected in this Thesis yields 0.484% as the expected total nuclear data library uncertainty with the $\bar{\nu}_{\mathrm{rel}}$ = 0.389% of the method 3 from Tab. 11. Taking into account also the 95% confidence interval of the computed relative uncertainties results in an interval [0.452, 0.518]. The result asserts that the obtained low relative uncertainties for the nuclear data library are likely due to simply neglecting the uncertainties of the average total fission neutron yield and the fission spectrum.

6 Conclusions and future guidelines

In the course of this study, a novel CFENSS-SRS (**C**oupled **F**uel B**e**haviour and **N**eutronics **S**tochastic **S**ampling with **S**imple **R**andom **S**ampling) methodology was successfully developed and implemented for the combined perturbation of the nuclear fuel parameters and the nuclear data library. The method relied on the statistical approach in the uncertainty analysis. One-dimensional truncated normal distributions were applied for perturbing the fuel behaviour parameters while a correlated sampling method was used for perturbing the correlated neutron cross section data. The conventional multigroup approach was not employed but the neutron cross sections were perturbed already in the pointwise linearly interpolated format before further processing. The approach allowed propagating the introduced uncertainties through a large portion of the nuclear data library processing chain. The occasionally encountered unphysical negative values of the inherently positive neutron cross sections were re-sampled as opposed to setting them to zero. The whole nuclear data sampling process was based on relative covariance matrices rather than absolute ones. The tool was originally built for the high-fidelity covariance data readily available in the ENDF/B-VII.1 nuclear data library supplemented by low-fidelity covariances for completeness, but also the SCALE6.0 covariance library was experimented with.

The CFENSS-SRS methodology is currently lacking in the nuclear data uncertainties as only the neutron cross section data were perturbed. However, also the average fission neutron yield and, to a lesser extent, the fission spectrum have their own considerable impact on the nuclear data library uncertainty. The CFENSS-SRS should be improved by implementing their perturbation to the code system before moving to further research objectives. The nuclear data sampling methodology could be improved also by gathering more statistics for comparing the effects of the different sampling strategies such as the zero cut-off approach relative to the re-sampling of the occasional negative values of inherently positive parameters. However, it was concluded that the impact of the choices in the methodology is in any case low compared to accounting for the high-impact nuclear data parameters. Thus, the first task of the immediate future would be adding a support for perturbing the average total fission neutron yield and the fission spectrum. This could be followed by a more demanding task of perturbing also the resonance parameters directly.

The nuclear data random sampling was far more complicated than perturbing the nuclear fuel parameters with the approximated one-dimensional truncated normal distribution. The fuel behaviour perturbation could be improved by employing more accurate uncertainties, by acquiring a method for the random sampling a general truncated normal distribution, or by utilizing the full capabilities of the FINIX code via a more extensive use of the continuous temperature and density profiles. The importance of these improvements is nevertheless secondary to advancing the nuclear data perturbation.

The results of the uncertainty analysis presented in Sec. 4.2 were in a good agreement with the literature. The results were supplemented by a rough code based sensitivity analysis supporting the hypothesis that the two parameter groups can be perturbed separately. As a conclusion, the total combined uncertainty could be computed by simply summing the fuel behaviour and the neutronics uncertainty components in quadrature. Additionally, it was revealed that currently the accuracy of the deterministic DRAGON code is limited by the nuclear data uncertainties, rather than the parameter choices of the code's submodels.

The conclusion may be extended also to other deterministic lattice codes, thus encouraging the development of more advanced uncertainty propagation methods over more accurate deterministic codes.

A natural continuity of the Thesis would be applying the CFENSS-SRS methodology to the Monte Carlo neutronics to gain more accurate best estimates. The CFENSS-SRS tool is based on perturbing the pointwise nuclear data and is thus perfectly capable of generating perturbed nuclear data libraries also for the Monte Carlo codes, unlike the conventional multigroup approach. Introducing the stochastic neutronics introduces additional uncertainty to the responses but this can be easily removed. The time-consuming Monte Carlo neutronics could be used just for obtaining the best estimate values while the uncertainty propagation could be done with the faster deterministic codes. If successful, the uncertainty distribution could ultimately be simply shifted to peak at the MC best estimate value without a notable loss in accuracy but with great savings in the processing time. Without the need for the highly accurate best estimate results, the deterministic lattice codes would have short processing times per simulation run. The approach would require limiting the nuclear data library processing time as well as confirming that the uncertainty distribution is not distorted by, for instance, a sparser discretization in the neutronics.

Initial results suggest that the relative uncertainties obtained from the DRAGON code and the Serpent code are equal so the approach appears viable. The Serpent calculations were performed by Aarno Isotalo while the author modified the CFENSS-SRS code suitable for generating the perturbed ACE libraries. Aalto University School of Science "Science-IT" project provided the required computer resources.

Finally, it is proposed that the development of the random sampling method for the general multivariate truncated normal distribution should be considered. The multivariate log-normal distribution has received ample attention due to the improperly interpreted Principle of Maximum Entropy regarding the inherently positive variables with the first two known moments. Ultimately the efforts lead to the development of an equivalent method for the multivariate log-normal distribution. Such a sampler would be useful for uncertainty analysis in the fields of both nuclear fuel behaviour and neutronics, not mentioning the other research areas applying the truncated distribution.

References

[1] "Best Estimate Safety Analysis for Nuclear Power Plants: Uncertainty Evaluation," tech. rep., International Atomic Energy Agency (IAEA), 2008. Safety Reports Series No. 52.

[2] J. C. Helton and D. E. Burmaster, "Guest editorial: treatment of aleatory and epistemic uncertainty in performance assessments for complex systems," *Reliability Engineering & System Safety*, vol. 54, no. 2–3, pp. 91–94, 1996.

[3] T. Ikonen, J. Kättö, and H. Loukusa, "FINIX - Fuel behavior model and interface for multiphysics application - Code documentation for version 0.15.6," tech. rep., VTT, 2015. VTT-R-02988-15.

[4] G. Marleau, A. Hébert, and R. Roy, "A user guide for DRAGON version5, IGE-335," tech. rep., Institut de génie nucléaire, École Polytechnique de Montréal, 2014.

[5] R. E. MacFarlane *et al.*, *The NJOY Nuclear Data Processing System, Version 2012*. Los Alamos National Laboratory, 2012.

[6] H. Glaeser, "GRS Method for Uncertainty and Sensitivity Evaluation of Code Results and Applications," *Science and Technology of Nuclear Installations*, vol. 2008, 2008. Article ID 798901, 7 pages.

[7] T. Zhu, *Sampling-Based Nuclear Data Uncertainty Quantification for Continuous Energy Monte Carlo Codes*. PhD thesis, École Polytechnique Fédérale de Lausanne, 2015.

[8] P. Laininen, *Todennäköisyys ja sen tilastollinen soveltaminen*. Otatieto, 1998. In Finnish.

[9] D. L. Smith and N. Otuka, "Experimental Nuclear Reaction Data Uncertainties: Basic Concepts and Documentation," *Nuclear Data Sheets*, vol. 113, no. 12, pp. 3006–3053, 2012. Special Issue on Nuclear Reaction Data.

[10] F. James, *Statistical Methods in Experimental Physics*. World Scientific Publishing, 2 ed., 2006.

[11] R. Vanhanen, "Computing Positive Semidefinite Multigroup Nuclear Data Covariances," *Nuclear Science and Engineering*, vol. 179, no. 4, pp. 411–422, 2015.

[12] R. Vanhanen, "Computing More Consistent Multigroup Nuclear Data Covariances," *Nuclear Science and Engineering*, vol. 181, no. 1, pp. 60–71, 2015.

[13] W. C. Horrace, "Some results on the multivariate truncated normal distribution," *Journal of Multivariate Analysis*, vol. 94, no. 1, pp. 209–221, 2005.

[14] G. Žerovnik *et al.*, "Transformation of correlation coefficients between normal and lognormal distribution and implications for nuclear applications," *Nuclear Instruments and Methods in Physics Research Section A: Accelerators, Spectrometers, Detectors and Associated Equipment*, vol. 727, pp. 33–39, 2013.

[15] G. Žerovnik, A. Trkov, and I. A. Kodeli, "Correlated random sampling for multivariate normal and log-normal distributions," *Nuclear Instruments and Methods in Physics Research Section A: Accelerators, Spectrometers, Detectors and Associated Equipment*, vol. 690, pp. 75–78, 2012.

[16] "Report of the Uncertainty Methods Study for Advanced Best Estimate Thermal Hydraulic Code Applications – Volume 1," Tech. Rep. 2, NEA, 1998.

[17] S. S. Wilks, "Determination of Sample Sizes for Setting Tolerance Limits," *The Annals of Mathematical Statistics*, vol. 12, no. 1, pp. 91–96, 1941.

[18] S. S. Wilks, "Statistical Prediction with Special Reference to the Problem of Tolerance Limits," *The Annals of Mathematical Statistics*, vol. 13, no. 4, pp. 400–409, 1942.

[19] M. D. McKay, R. J. Beckman, and W. J. Conover, "A Comparison of Three Methods for Selecting Values of Input Variables in the Analysis of Output from a Computer Code," *Technometrics*, vol. 21, no. 2, pp. 239–245, 1979.

[20] J. C. Helton and F. J. Davis, "Latin hypercube sampling and the propagation of uncertainty in analyses of complex systems," *Reliability Engineering & System Safety*, vol. 81, no. 1, pp. 23–69, 2003.

[21] A. Hernández-Solíz, *Uncertainty and sensitivity analysis applied to LWR neutronic and thermal-hydraulic calculations*. PhD thesis, Chalmers University of Technology, 2012.

[22] M. E. Muller, "An Inverse Method for The Generation of Random Normal Deviates on Large-Scale Computers," *Mathematics of Computation*, no. 2, pp. 167–174, 1958.

[23] G. E. P. Box and M. E. Muller, "A Note on the Generation of Random Normal Deviates," *The Annals of Mathematical Statistics*, vol. 29, no. 2, pp. 610–611, 1958.

[24] G. Marsaglia and T. A. Bray, "A Convenient Method for Generating Normal Variables," *SIAM Review*, vol. 6, no. 3, pp. 260–264, 1964.

[25] G. Marsaglia and W. W. Tsang, "A Fast, Easily Implemented Method for Sampling from Decreasing or Symmetric Unimodal Density Functions," *SIAM Journal on Scientific and Statistical Computing*, vol. 5, no. 2, pp. 349–359, 1984.

[26] Y. Li and S. K. Ghosh, "Efficient Sampling Methods for Truncated Multivariate Normal and Student-*t* Distribution Subject to Linear Inequality Constraints," *Journal of Statistical Theory and Practice*, vol. 9, no. 4, pp. 712–732, 2015.

[27] G. Žerovnik, *Use of covariance matrices for estimating uncertainties in reactor calculations*. PhD thesis, University of Ljubljana, 2012.

[28] R. U. Seydel, *Tools for Computational Finance*. Springer, 5 ed., 2012.

[29] E. T. Jaynes, "Information Theory and Statistical Mechanics," *Physical Review*, vol. 106, no. 4, pp. 620–630, 1957.

[30] E. T. Jaynes, "Prior Probabilities," *IEEE Transactions on Systems Science and Cybernetics*, vol. 4, no. 3, pp. 227–241, 1968.

[31] F. H. Fröhner, "Assigning Uncertainties to Scientific Data," *Nuclear Science and Engineering*, vol. 126, no. 1, pp. 1–18, 1997.

[32] J. N. Kapur, *Maximum-Entropy Models in Science and Engineering*. Wiley, 1989.

[33] D. C. Dowson and A. Wragg, "Maximum-Entropy Distributions Having Prescribed First and Second Moments," *IEEE Transactions on Information Theory*, vol. 19, no. 5, pp. 689–693, 1973.

[34] D. L. Smith *et al.*, "Large errors and severe conditions," *Nuclear Instruments and Methods in Physics Research Section A: Accelerators, Spectrometers, Detectors and Associated Equipment*, vol. 488, no. 1–2, pp. 342–361, 2002.

[35] D. L. Smith *et al.*, "An Approach for Dealing with Large Errors," tech. rep., Argonne National Laboratory, 2001. ANL/NDM-154.

[36] G. Žerovnik, R. Capote, and A. Trkov, "On random sampling of correlated resonance parameters with large uncertainties," *Nuclear Instruments and Methods in Physics Research Section A: Accelerators, Spectrometers, Detectors and Associated Equipment*, vol. 723, pp. 89–98, 2013.

[37] G. Žerovnik *et al.*, "Random Sampling of Correlated Parameters – a Consistent Solution for Unfavourable Conditions," *Nuclear Data Sheets*, vol. 123, pp. 185–190, 2015. Special Issue on International Workshop on Nuclear Data Covariances April 28 - May 1, 2014, Santa Fe, New Mexico, USA.

[38] A. Taavitsainen and R. Vanhanen, "On the maximum entropy distributions of inherently positive nuclear data." Working paper, 2016.

[39] M. Rosenblatt, "Remarks on Some Nonparametric Estimates of a Density Function," *The Annals of Mathematical Statistics*, vol. 27, no. 3, pp. 832–837, 1956.

[40] E. Parzen, "On Estimation of a Probability Density Function and Mode," *The Annals of Mathematical Statistics*, vol. 33, no. 3, pp. 1065–1076, 1962.

[41] T. P. Ryan, *Modern Engineering Statistics*. Wiley, 2007.

[42] A. Wald, "An Extension of Wilks' Method for Setting Tolerance Limits," *The Annals of Mathematical Statistics*, vol. 14, no. 1, pp. 45–55, 1943.

[43] W. T. Nutt and G. B. Wallis, "Evaluation of nuclear safety from the outputs of computer codes in the presence of uncertainties," *Reliability Engineering & System Safety*, vol. 83, no. 1, pp. 57–77, 2004.

[44] A. Guba, M. Makai, and L. Pál, "Statistical aspects of best estimate method–I," *Reliability Engineering & System Safety*, vol. 80, no. 3, pp. 217–232, 2003.

[45] S. S. Wilks, *Mathematical Statistics*. New Jersey: Princeton University Press, 1947.

[46] G. B. Wallis, "Contribution to the paper 'Statistical aspects of best estimate method-1' by Attila Guba, Mihakly Makai, Lenard Pal," *Reliability Engineering & System Safety*, vol. 80, no. 3, pp. 309–311, 2003.

[47] G. B. Wallis, "Evaluating the probability that the outputs of a computer code with random inputs will meet a set of evaluation criteria," *Reliability Engineering & System Safety*, vol. 91, no. 7, pp. 820–827, 2006.

[48] M. Makai and L. Pál, "Reply to contribution of Graham B. Wallis," *Reliability Engineering & System Safety*, vol. 80, no. 3, pp. 313–317, 2003.

[49] M. Makai, "Comment on "Evaluating the probability that the output of a computer code with random inputs will meet a set of evaluation criteria" by G.B. Wallis [Reliab Eng Syst Saf 2006;91:820–7] ," *Reliability Engineering & System Safety*, vol. 92, no. 7, pp. 992–993, 2007.

[50] Y. Orechwa, "Comments on 'Evaluation of nuclear safety from the outputs of computer codes in the presence of uncertainties' by W.T. Nutt and G.B. Wallis," *Reliability Engineering & System Safety*, vol. 87, no. 1, pp. 133–135, 2005.

[51] G. B. Wallis and W. T. Nutt, "Reply to "Comments on 'Evaluation of nuclear safety from the outputs of computer codes in the presence of uncertainties' by W.T. Nutt and G.B. Wallis," by Y. Orechwa," *Reliability Engineering & System Safety*, vol. 87, no. 1, pp. 137–145, 2005.

[52] G. B. Wallis, "Reply to M. Makai's comments on my paper "Evaluating the probability that the output from a computer code with random inputs will meet a set of evaluation criteria" [Reliab Eng Syst Saf 2006; 91:820–27]," *Reliability Engineering & System Safety*, vol. 92, no. 6, pp. 841–843, 2007.

[53] J. J. Duderstadt and L. J. Hamilton, *Nuclear Reactor Analysis*. Wiley, 1976.

[54] *ENDF-6 Formats Manual*, 2012. Report BNL-90365-2009 Rev.2 – Revision 85.

[55] M. B. Chadwick *et al.*, "ENDF/B-VII.1 Nuclear Data for Science and Technology: Cross Sections, Covariances, Fission Product Yields and Decay Data," *Nuclear Data Sheets*, vol. 112, no. 12, pp. 2887–2996, 2011. Special Issue on ENDF/B-VII.1 Library.

[56] "The JEFF-3.1.1. Nuclear Data Library," tech. rep., OECD/NEA Data Bank, 2009. JEFF Report 22.

[57] K. Shibata *et al.*, "JENDL-4.0: A New Library for Nuclear Science and Engineering," *Journal of Nuclear Science and Technology*, vol. 48, no. 1, pp. 1–30, 2011.

[58] R. Little *et al.*, "Low-fidelity Covariance Project," *Nuclear Data Sheets*, vol. 109, no. 12, pp. 2828–2833, 2008. Special Issue on Workshop on Neutron Cross Section Covariances June 24-28, 2008, Port Jefferson, New York, USA.

[59] R. Vanhanen and M. Pusa, "Survey of prediction capabilities of three nuclear data libraries for a PWR application," *Annals of Nuclear Energy*, vol. 83, pp. 408–421, 2015.

[60] "ZZ-SCALE6/COVA-44G: A 44-group cross section covariance matrix library retrieved from the SCALE-6 package," 2012. Code Package USCD1236/03.

[61] K. Ivanov *et al.*, "Benchmarks for Uncertainty Analysis in Modelling (UAM) for the Design, Operation and Safety Analysis of LWRs - Volume I: Specification and Support Data for Neutronics Cases (Phase I)," 2013. NEA/NSC/DOC(2013)7.

[62] "ZZ-SCALE5.1/COVA-44G: A 44-group cross section covariance matrix library retrieved from the SCALE-5.1 package," 2007. Code Package USCD1236/01.

[63] I. Panka, A. Keresztúri, and C. Maráczy, "Selected examples on multiphysics researches at KFKI AEKI – Results for Phase I of the OECD/NEA UAM benchmark," in *Proceedings of the Twentieth Symposium of Atomic Energy Research*, September 2010.

[64] L. Mercatali, K. Ivanov, and V. H. Sanchez, "SCALE Modeling of Selected Neutronics Test Problems within the OECD UAM LWR's Benchmark," *Science and Technology of Nuclear Installations*, vol. 2013, 2013. Art. ID 573697, 11 pages.

[65] W. W. Wieselquist, T. Zhu, A. Vasiliev, and H. Ferroukhi, "PSI Methodologies for Nuclear Data Uncertainty Propagation with CASMO-5M and MCNPX: Results for OECD/NEA UAM Benchmark Phase I," *Science and Technology of Nuclear Installations*, vol. 2013, 2013. Art. ID 549793, 15 pages.

[66] R. N. Bratton, M. Avramova, and K. Ivanov, "OECD/NEA Benchmark for Uncertainty Analysis in Modelling (UAM) for LWRs – Summary and Discussion of Neutronics Cases (Phase I)," *Nuclear Engineering and Technology*, vol. 46, no. 3, pp. 313–342, 2014.

[67] A. Hernández-Solíz, C. Demaziére, and C. Ekberg, "Uncertainty and sensitivity analyses applied to the DRAGONv4.05 code lattice calculations and based on JENDL-4 data," *Annals of Nuclear Energy*, vol. 57, pp. 230–245, 2013.

[68] A. Taavitsainen, "Coupled FINIX-DRAGON Calculation Chain for an LWR Pin Cell Case." Special Assignment, Aalto University School of Science, 2015.

[69] M. L. Williams *et al.*, "A Statistical Sampling Method for Uncertainty Analysis with SCALE and XSUSA," *Nuclear Technology*, vol. 183, no. 3, pp. 515–526, 2013.

[70] J. Leppänen, *Serpent - a Continuous-energy Monte Carlo Reactor Physics Burnup Calculation Code*. VTT, 2015.

[71] D. Cacuci, ed., *Handbook of Nuclear Engineering - Vol. I: Nuclear Engineering Fundamentals*. Springer Science & Business Media, 2010.

[72] C. Demaziére, *Modelling of Nuclear Reactors*. Chalmers University of Technology, Department of Applied Physics, Division of Nuclear Engineering, 2015.

[73] A. Hébert, *Applied Reactor Physics*. Presses internationales Polytechnique, 2009.

[74] T. Reysset, "Development and qualification of advanced computational schemes for pressurized water reactors and creation of specific interfaces towards GRS full-core tools," Master's thesis, École Polytechnique de Montréal, 2009.

[75] D. Ćalić, M. Kromar, and A. Trkov, "Use of Monte Carlo and Deterministic Codes for Calculation of Plutonium Radial Distribution in a Fuel Cell," in *Proceedings of the 20th International Conference Nuclear Energy for New Europe*, September 2011.

[76] T. Ikonen and V. Tulkki, "The importance of input interactions in the uncertainty and sensitivity analysis of nuclear fuel behavior," *Nuclear Engineering and Design*, vol. 275, pp. 229–241, 2014.

[77] H. Petersen, "The Properties of Helium: Density, Specific Heats, Viscosity, and Thermal Conductivity at Pressures from 1 to 100 bar and from Room Temperature to about 1800 K," tech. rep., Danish Atomic Energy Commission Research Establishment Risö, 1970. Risö Report No. 224.

[78] "Revised Release on the IAPWS Industrial Formulation 1997 for the Thermodynamic Properties of Water and Steam," tech. rep., International Association for the Properties of Water and Steam, 2007.

[79] "Thermophysical properties database of materials for light water reactors and heavy water reactors," tech. rep., International Atomic Energy Agency, 2006. IAEA-TECDOC-1496.

[80] T. Ikonen, "Finix - fuel behaviour model and interface for multiphysics applications - code documentation for version 0.13.9," tech. rep., VTT, 2013. VTT-R-06563-13.

[81] W. J. M. De Kruijf, *Reactor Physics Analysis of the Pin-Cell Doppler Effect in a Thermal Nuclear Reactor*. PhD thesis, Delft University of Technology, 1994.

[82] W. H. Arnold and R. A. Dannels, "The Doppler coefficient of $U^{238}O_2$," *Transactions of the American Nuclear Society*, no. 3, pp. 229–230, 1960.

[83] G. Rowlands, "Resonance absorption and non-uniform temperature distributions," *Journal of Nuclear Energy. Parts A/B. Reactor Science and Technology*, vol. 16, no. 4, pp. 235–236, 1962.

[84] L. Dresner, "Some Remarks on the Effect of a Nonuniform Temperature Distribution on the Temperature Dependence of Resonance Absorption," *Nuclear Science and Engineering*, vol. 11, no. 1, pp. 39–42, 1961.

[85] M. Berglund and M. E. Wieser, "Isotopic compositions of the elements 2009 (IUPAC Technical Report)," *Pure and Applied Chemistry*, vol. 83, no. 2, pp. 397–410, 2011.

[86] G. Audi *et al.*, "The NUBASE2012 evaluation of nuclear properties," *Chinese Physics C*, vol. 36, no. 12, pp. 1157–1286, 2012.

[87] A. Hébert, "A PyNjoy tutorial," tech. rep., Institut de génie nucléaire, École Polytechnique de Montréal, 2014. IGE-305.

[88] A. Hébert and R. Roy, "The GANLIB version 5 developer's guide," tech. rep., Institut de génie nucléaire, École Polytechnique de Montréal, 2012. IGE-313.

[89] E. Sartori, "OECD/NEA Data Bank: Standard Energy Group Structures of Cross Section Libraries for Reactor Shielding, Reactor Cell and Fusion Neutronics Applications: VITAMIN-J, ECCO-33, ECCO-2000 and XMAS," tech. rep., 1990. JEF/DOC-315 Revision 3.

[90] "Draglib Download Page." `http://www.polymtl.ca/merlin/libraries.htm`. Online; Updated 08-April-2014, Accessed 5-June-2015.

[91] J. D. Hunter, "Matplotlib: A 2D graphics environment," *Computing In Science & Engineering*, vol. 9, no. 3, pp. 90–95, 2007.

[92] M. Pusa, "Incorporating sensitivity and uncertainty analysis to a lattice physics code with application to CASMO-4," *Annals of Nuclear Energy*, vol. 40, no. 1, pp. 153–162, 2012.

[93] R. Roy, "The CLE-2000 Tool-box," tech. rep., Institut de génie nucléaire, École Polytechnique de Montréal, 1999. IGE-163.

A Additional uncertainty analysis results

The effective multiplication factor results omitted in Sec. 4.2, i.e., the methods from 2 to 6, are presented here. The empirical cumulative distribution functions are shown in Fig. A1, the kernel density estimates of the probability distributions in Fig. A2 and the convergence results in Fig. A3. As an interesting remark the relative standard deviation of the second method do not converge until around 1000 simulations are performed. The convergence of the $\nu\Sigma_f$ is generally slightly faster than the convergence of the effective multiplication factor.

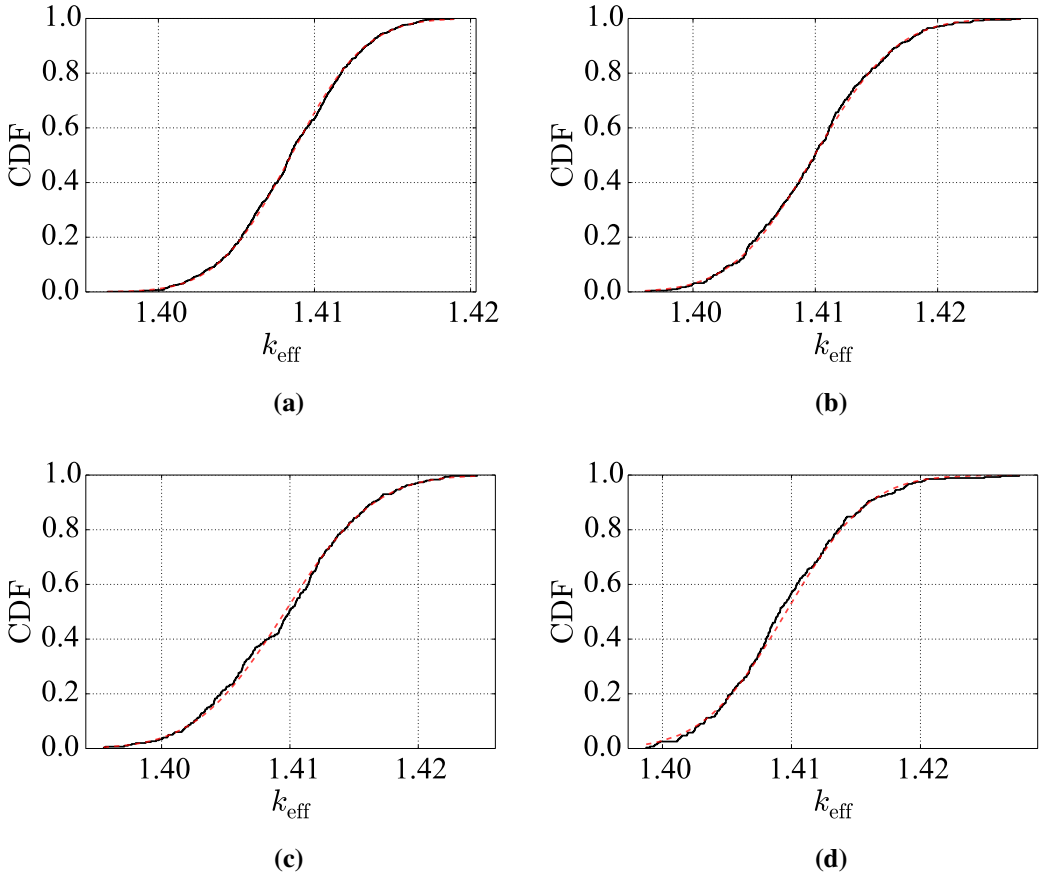

Figure A1: Empirical cumulative distribution functions and fitted normal distributions for methods **(a)** 2, **(b)** 4, **(c)** 5 and **(d)** 6. The black and red lines represent the ECDFs approximated with the fitted normal distributions.

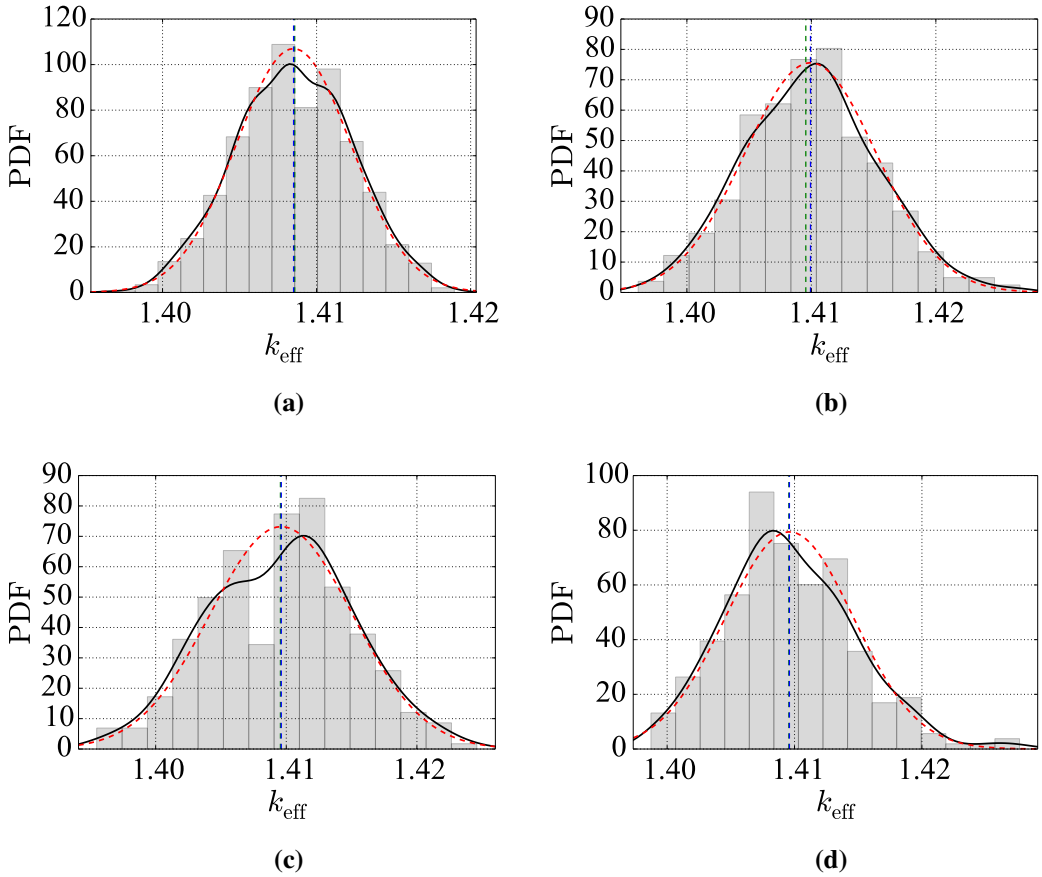

Figure A2: Kernel density estimates of the probability distribution functions and fitted normal distributions for methods **(a)** 2, **(b)** 4, **(c)** 5 and **(d)** 6. The KDEs and the fitted normal distributions are drawn with black and red lines, respectively, while blue and green dashed lines mark the locations of the sample means and best estimates. In **(a)**, **(c)** and **(d)** the sample mean and the best estimate are practically equal.

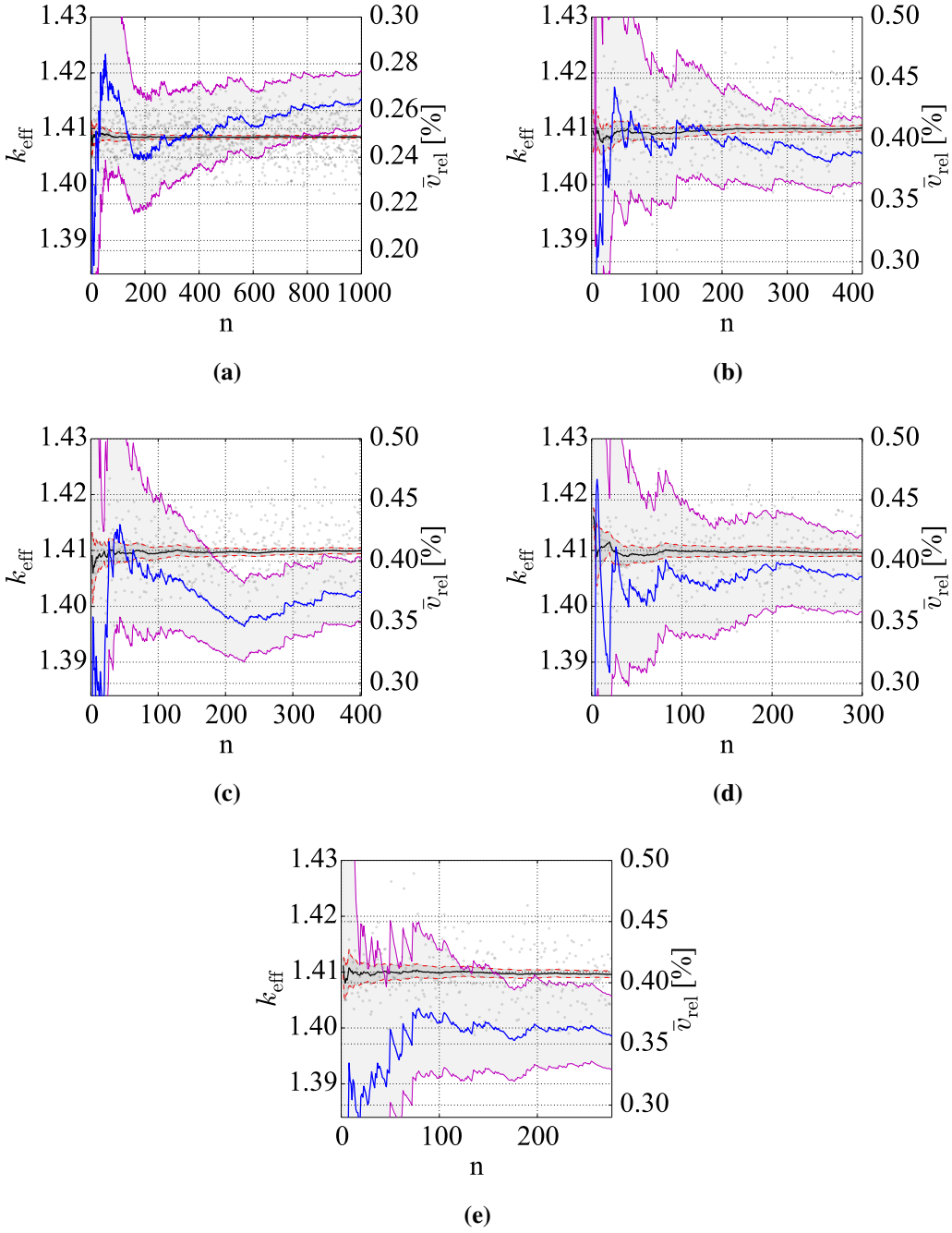

Figure A3: Convergence results for methods **(a)** 2, **(b)** 3, **(c)** 4, **(d)** 5 and **(e)** 6 along with the whitened individual simulations on the background. The means and the relative standard deviations are drawn with solid black and blue lines, respectively. The boundaries of the corresponding 95% confidence intervals are marked with red dashed lines and purple solid lines. The confidence intervals of the sixth method are strictly speaking invalid but they are shown here to demonstrate the scale.

B DRAGON HFP input file examples

The input files of DRAGON are written in CLE-2000 language [93] in which commands can be written up to column 72. The comments begin with an asterisk (*) while the CLE-2000 commands are terminated with a semicolon (;). Two input file examples are provided: an input for calculating the effective multiplication factor and the one-group constants for the OECD/NEA UAM-LWR benchmark TMI-1 pin cell exercise in the hot full power reactor conditions of FINIX, and the ASCII to binary conversion for the DRAGLIB. In the former, the material mixtures begin with a keyword "MIX" followed by an identifier number, temperature [K], density [g/cm^3] and a list of the comprising isotopes. The nuclei are defined with an alias name, a library name, a weight percentage (%) and number 1 (if the nuclei accounts for self-shielding).

```
*----
*  FINIXDRAGONPC
*  Benchmark TMI-1 PWR HFP
*----
*  Define STRUCTURES and MODULES used
*----
LINKED_LIST
  PINCELL DISCR LIBRARY LIBRARY2 CP CALC OUT ;
SEQ_BINARY
  TRKSPC ;
MODULE
  LIB: GEO: EXCELT: SHI: ASM: FLU: EDI: DELETE: END: ;
*----
*  Microscopic cross sections from draglibendfb7r1
*----
LIBRARY := LIB: ::
  NMIX 4 CTRA APOL
  MIXS LIB: DRAGON FIL: DRAGLIB
  *-- Fuel
  MIX 1 900.000000 10.044271
    U234     = U234   0.004760 1
    U235     = U235   4.275140 1
    U238     = U238   83.867309 1
    O16F     = O16   11.852791
  *-- Gas gap
  MIX 2 661.830039 0.002245
    He4     = He4   100.000000
  *-- Cladding
  MIX 3 589.256806 6.519739
    C_O16     = O16   0.125000
    Cr50     = Cr50   0.004174
    Cr52     = Cr52   0.083699
```

```
    Cr53     = Cr53   0.009674
    Cr54     = Cr54   0.002453
    Fe54     = Fe54   0.011856
    Fe56     = Fe56   0.192993
    Fe57     = Fe57   0.004537
    Fe58     = Fe58   0.000614
    Zr90     = Zr90   49.750307
    Zr91     = Zr91   10.970128
    Zr92     = Zr92   16.952409
    Zr94     = Zr94   17.553857
    Zr96     = Zr96   2.888299
    Sn112     = Sn112   0.013259
    Sn114     = Sn114   0.009182
    Sn115     = Sn115   0.004772
    Sn116     = Sn116   0.205842
    Sn117     = Sn117   0.109665
    Sn118     = Sn118   0.348798
    Sn119     = Sn119   0.124758
    Sn120     = Sn120   0.477154
    Sn122     = Sn122   0.068941
    Sn124     = Sn124   0.087629
  *-- Moderator
  MIX 4 562.000000 0.748371
    O16M     = O16   88.808513
    H1H2O     = H1_H2O   11.191487
  ;
*----
*  Geometry PINCELL : Cartesian cell with an embedded annular region
*----
PINCELL := GEO: :: CARCEL 3
  X- REFL X+ REFL MESHX 0.000000 1.442700
  Y- REFL Y+ REFL MESHY 0.000000 1.442700
  RADIUS 0.000000 0.474107 0.479342 0.546839 SPLITR 25 1 10
  MIX 1 2 3 4 ;
*----
*  Self-shielding calculation: SHI
*  Transport calculation: EXCELT
*  Flux calculation for K no leakage
*----
DISCR TRKSPC := EXCELT: PINCELL ::
  MAXR 37 TRAK TSPC 12 20.000000 ;
LIBRARY2 := SHI: LIBRARY DISCR TRKSPC :: EDIT 1 LJ LEVEL 2 ;
CP := ASM: LIBRARY2 DISCR TRKSPC ;
CALC := FLU: CP LIBRARY2 DISCR ::
  TYPE K ;
```

```
OUT := EDI: LIBRARY2 DISCR CALC ::
  EDIT 4 COND MERG MIX MICR ALL SAVE ;
DISCR TRKSPC CP := DELETE: DISCR TRKSPC CP ;
ECHO "DRAGONPC completed" ;
END: ;
QUIT "LIST" .
```

Converting a DRAGLIB from the ASCII format to the binary (XSM) format requires applying the equality module (:=) of GANLIB [88] available with the DRAGON package:

```
*----
*  DRAGLIB conversion, from ASCII export to XSM binary
*----
XSM_FILE DRGLIB ;
SEQ_ASCII EXPORT ;
MODULE UTL: END: ;
*
DRGLIB := EXPORT :: EDIT 10 ;
UTL: DRGLIB :: DIR ;
END: ;
```

C Serpent HFP input file

Serpent input file used for computing the Monte Carlo best estimate for the Exercise-I (TMI-1 PWR) of the OECD/NEA UAM-LWR benchmark in the hot full power reactor conditions. The input file was written by Aarno Isotalo.

```
% layer boundaries
surf 101 cyl 0.0 0.0 0.474107
surf 102 cyl 0.0 0.0 0.479342
surf 103 cyl 0.0 0.0 0.546839

surf 1000 sqc 0.0 0.0 0.72135   % assembly pitch

% dummy universes so that we can generate group constants for the regions
cell 201 1 fuel -101
cell 202 2 gap   101 -102
cell 203 3 clad       102 -103
cell 204 4 mod             103  -1000

% top level geometry
cell 301 0 fill 1 -101
cell 302 0 fill 2  101 -102
cell 303 0 fill 3       102 -103
cell 304 0 fill 4            103 -1000
cell 300 0 outside                1000

set bc 3

% --- materials

mat fuel -10.044271 tmp 900
    92234.09c   -0.004760
    92235.09c   -4.275140
    92238.09c  -83.867309
     8016.09c  -11.852791

mat gap -0.002245  tmp 661.830039
    2004.05c -1

mat clad -6.519739  tmp 589.256806
     8016.05c   -0.125000
    24050.05c   -0.004174
    24052.05c   -0.083699
    24053.05c   -0.009674
    24054.05c   -0.002453
```

```
     26054.05c   -0.011856
     26056.05c   -0.192993
     26057.05c   -0.004537
     26058.05c   -0.000614
     40090.05c  -49.750307
     40091.05c  -10.970128
     40092.05c  -16.952409
     40094.05c  -17.553857
     40096.05c   -2.888299
%    50112.05c   -0.013259
%    50114.05c   -0.009182
     50115.05c   -0.004772
     50116.05c   -0.205842
     50117.05c   -0.109665
     50118.05c   -0.348798
     50119.05c   -0.124758
%    50120.05c   -0.477154
     50120.05c   -0.499595
     50122.05c   -0.068941
     50124.05c   -0.087629

mat mod -0.748371 tms 562.000000 moder lwtr 1001
      8016.05c  -88.808513
      1001.05c  -11.191487

% --- Library data:

set acelib "/home/aisotalo/usva/sss/libraries/endfb7r1_485_poi_noExe5/sss_endfb
therm lwtr 0 hh2o.05t hh2o.06t
set ures 1

% --- Neutron population and criticality cycles:

set nbuf 5
%set pop 5000 25 5
set pop 20000 2500 20

plot 3 500 500

% --- macroscopic absorption cross-section in fuel

det FuelFlux    dm fuel
det FuelTotCap  dm fuel  dr -2 fuel  dt 3 FuelFlux
det FuelTotFis  dm fuel  dr -6 fuel  dt 3 FuelFlux
```

```
% --- B1 calculation

set fum cas70

% --- Group constant and adf generation

set dbrc 4.000E-7 2.100E-4 92238.00c 92235.00c
set nfg 1
set gcu 0 1 2 3 4
set coefpara 1
INF_FLX
INF_KINF
INF_REP_TIME
INF_PROMPT_LIFE
INF_TOT
INF_CAPT
INF_FISS
INF_NSF
INF_KAPPA
INF_INVV
INF_NUBAR
INF_ABS
INF_REMXS
INF_RABSXS
INF_CHIT
INF_CHIP
INF_CHID
INF_TRANSPXS
INF_DIFFCOEF
B1_KINF
B1_KEFF
B1_REP_TIME
B1_PROMPT_LIFE
B1_B2
B1_ERR
B1_FLX
B1_FISS_FLX
B1_TOT
B1_CAPT
B1_FISS
B1_NSF
B1_KAPPA
B1_INVV
B1_NUBAR
B1_ABS
```

```
B1_REMXS
B1_RABSXS
B1_CHIT
B1_CHIP
B1_CHID
B1_TRANSPXS
B1_DIFFCOEF
IMP_KEFF
ANA_KEFF
BETA_EFF
LAMBDA

branch case1 % --- nominal
coef 1 0
1 case1
```